SYSTEMATIC INVESTIGATION OF INTRAMOLECULAR THROUGH-SPACE CHARGE TRANSFER IN NAPHTHALENE-BASED SYSTEMS WITH VARIOUS DONOR AND ACCEPTOR MOIETIES

THESIS SUBMITTED TO
THE GRADUATE SCHOOL OF ENGINEERING AND SCIENCE
OF BILKENT UNIVERSITY
IN PARTIAL FULFILLMENT OF THE REQUIREMENTS FOR
THE DEGREE OF
MASTER OF SCIENCE
IN CHEMISTRY

By

Gizem YILDIZ

August 2025

SYSTEMATIC INVESTIGATION OF INTRAMOLECULAR THROUGH-SPACE CHARGE TRANSFER IN NAPHTHALENE-BASED SYSTEMS WITH VARIOUS DONOR AND ACCEPTOR MOIETIES

By Gizem YILDIZ

August 2025

We certify that we have read this thesis and that in our opinion it is fully adequate, in scope and in quality, as a thesis for the degree of Master of Science.

Yunus Emre TÜRKMEN (Advisor)

Bilge BAYTEKİN

Halil İ. OKUR

Fahri ALKAN

Salih ÖZÇUBUKÇU

Approved for the Graduate School of Engineering and Science:

Orhan ARIKAN

Director of the Graduate School

ABSTRACT

SYSTEMATIC INVESTIGATION OF INTRAMOLECULAR THROUGH-SPACE CHARGE TRANSFER IN NAPHTHALENE-BASED SYSTEMS WITH VARIOUS DONOR AND ACCEPTOR MOIETIES

Gizem YILDIZ

M.Sc. in Chemistry

Advisor: Asst. Prof. Yunus Emre Türkmen

August 2025

Charge transfer (CT) is the transition between two states with different charge densities, which involves electron donor-acceptor moieties, and the distribution of charges is the key aspect of such excited states. Our group has recently designed a novel scaffold that facilitates intramolecular through-space charge transfer, incorporating a naphthalene spacer, benzofuran as an electron-donating moiety, and various ynone groups as electron-accepting moieties. This scaffold exhibits a CT band in the visible region in its UV-Vis and fluorescence spectra.

In this work, we aim to investigate how electronic structures, spatial positioning, and electron density differences influence charge transfer behavior by synthesizing a range of substrates with varying electron-donating and electron-accepting groups. For this purpose, we utilize Sonogashira and Suzuki coupling reactions to synthesize the various target compounds and examine the charge transfer properties. The photophysical properties of the synthesized complexes were analyzed with the help of two main spectroscopic techniques, UV-Vis and fluorescence spectroscopy.

Keywords: Charge transfer, electron donor-acceptor moieties, intramolecular through-space charge transfer, naphthalene spacer, benzofuran.

ÖZET

ÇEŞİTLİ VERİCİ VE ALICI KISIMLAR İÇEREN NAFTALİN BAZLI SİSTEMLERDEKİ İNTRAMOLEKÜLER UZAY-İÇİ YÜK TRANSFERİNİN SİSTEMATİK ARAŞTIRMASI

Gizem YILDIZ

Kimya Bölümü, Yüksek Lisans

Tez Danışmanı: Dr. Yunus Emre Türkmen

Ağustos 2025

Yük transferi, farklı yük yoğunluklarına sahip iki hal arasındaki geçiştir ve electron verici-alıcı grupları içerir; yüklerin dağılımı bu uyarılmış hallerdeki kilit unsurudur. Grubumuz yakın zamanda naftalin bağlayıcı grubu, elektron verici grup olarak benzofuran ve elektron alıcı grup olarak alkinon gruplarını içeren, intramoleküler uzay-içi yük transferini sağlayan bir iskelet tasarladı. Bu iskelet, UV-Vis ve floresans spektrumlarında görünür bölgede bir yük transferi bandı sergilemiştir.

Bu çalışmada, çeşitli elektron verici ve electron alıcı grupları kullanarak bir grup substrat sentezleyerek elektronik yapının, uzamsal konunlanmasının ve elektron yoğunluğu farklarının yük transferi davranışlarını nasıl etkilediğini araştırmayı amaçlıyoruz. Bu amaçla, Sonogashira ve Suzuki eşleme reaksiyonlarından faydalanarak çeşitli hedef bileşikler sentezledik ve yük transferi özelliklerini gözlemledik. Sentezlenen komplekslerin fotofiziksel özellikleri iki ana spektroskopi tekniği olan UV-Vis ve floresans spektroskopisi yardımıyla analiz edildi.

Anahtar Kelimeler: Yük transferi, elektron verici-alıcı kısımlar, intramoleküler uzay-içi yük transferi, naftalin bağlayıcı grubu, benzofuran.

ACKNOWLEDGEMENT

First and foremost, I would like to express my gratitude to my advisor, Yunus Emre Türkmen, for guiding me on this journey and for trusting and supporting me. I will always remember the opportunity he gave me and the patience he showed me in helping me learn and grow. Thanks to him, I have learned what it means to be a good researcher.

I am also very grateful to my labmates, Merve, Suay, Badar, Kaan, Damla, and Mert, for never letting me feel like a stranger from my very first day at Bilkent and for always offering their support. You made Ankara feel like home, and working and spending time with you has been an invaluable experience that I will always cherish. And to Sena, I believe it was no coincidence that we came to Bilkent from different schools, became close friends, and are now graduating on the very same day. It feels like we were meant to meet, and I am truly glad we did.

My greatest thanks go to my family, who have supported me in all of my decisions and stood by me through every step, always showing their unconditional love. Having you is one of the greatest blessings of my life. You have taught me that learning never ends, that hard work brings fulfillment, and that sharing knowledge and all the good things in life make life more meaningful.

Lastly, Seza and Ezgi, my dearest friends, thank you for being there to lift me up every time I fell, for your endless trust and support when I felt like I couldn't make it. Even when you had no idea what I was actually doing, the way you tried to reason things out with me was incredibly sweet. In a way, we completed this master's degree together.

I dedicate this thesis to my brother Yoldaş Güney, my closest friend who has been by my side since the day I was born. I love you deeply, and just as we have shared everything since our childhood, I want us to share this as well.

LIST OF ABBREVIATIONS

ACN	Acetonitrile
APCI	Atmospheric Pressure Chemical Ionization
ATR-FTIR	Attenuated Total Reflectance Fourier Transform Infrared Spectroscopy
BCZ	Carbazole-BODIPY Dyad
BODIPY	Boron-dipyrromethene
CB[8]	Cucurbit[8]uril
CPCM	Conductor-like Polarizable Continuum Model
CT	Charge Transfer
D–A / DA	Donor–Acceptor
DCM	Dichloromethane
DFT	Density Functional Theory
DMABN	p-(*N*,*N*-Dimethylamino)benzonitrile
DMF	Dimethylformamide
DMSO	Dimethyl Sulfoxide
EDA	Electron Donor–Acceptor
EtOAc	Ethyl Acetate
FTIR	Fourier Transform Infrared Spectroscopy
HFIP	1,1,1,3,3,3-Hexafluoroisopropanol
HLCT	Hybrid Local and Charge Transfer
HOMO	Highest Occupied Molecular Orbital
HRMS	High-Resolution Mass Spectrometry
ICT	Intramolecular Charge Transfer
LC-MS	Liquid Chromatography–Mass Spectrometry
LE	Locally Excited (State)

LUMO	Lowest Unoccupied Molecular Orbital
MQ	Methoxybenzene-Quinoline Carbaldehyde (sensor system)
NMR	Nuclear Magnetic Resonance
OLED	Organic Light-Emitting Diode
PLQY	Photoluminescence Quantum Yield
Q-TOF	Quadrupole Time-of-Flight (Mass Spectrometer)
QY	Quantum Yield
Rf	Retention Factor (Thin Layer Chromatography)
TADF	Thermally Activated Delayed Fluorescence
TBCT	Through-Bond Charge Transfer
TCA	Trichloroacetic Acid
TLC	Thin Layer Chromatography
TCN	Tetracyanobenzene
TCNQ	Tetracyanoquinodimethane
TFE	2,2,2-Trifluoroethanol
THF	Tetrahydrofuran
TICT	Twisted Intramolecular Charge Transfer
TMS	Tetramethylsilane
TPA	Triphenylamine
TRZ	Triphenyltriazine
TSCT	Through-Space Charge Transfer
UV-Vis	Ultraviolet–Visible Spectroscopy
XRD	X-ray Diffraction

TABLE OF CONTENTS

1. INTRODUCTION

1.1.Light-Matter Interactions

Light is a very unique external stimulus that has effects on the properties and functions of chemical and biological systems.1 The interaction of light with matter is a fundamental issue in physical chemistry and molecular photophysics. When molecules are exposed to electromagnetic radiation, they can absorb photons whose energy corresponds to the gap between electronic energy levels. This absorption process promotes various chemical or physical changes in the matter. Understanding the nature of these transitions is highly essential to interpreting the behavior of the molecules upon excitation processes.

1.2.Excitation Process and Excited States

1.2.1. Absorption and Emission Processes

Electrons in a molecule generally reside in the singlet ground state (S_0). Upon absorption of a photon, excitation of the electrons to higher energy levels (S_N) takes place. The following relaxation of the excited electron is depicted in the Jablonski diagram, which illustrates both radiative and non-radiative pathways. Initially, the electron in higher energy levels undergoes internal conversion, which is a non-radiative process, to relax to the lowest excited singlet state (S_1). From S_1, it can return to the ground state (S_0) via radiative decay, emitting a photon in a process known as fluorescence. Alternatively, the electron may undergo intersystem crossing, a spin-forbidden but thermally accessible non-radiative process, to populate the triplet excited state (T_1). Relaxation from T_1 to S_0 is also radiative and is referred to as phosphorescence**.** Although the triplet state is typically lower in energy than the singlet excited state, phosphorescence is less probable due to the spin-forbidden nature of the $T_1 \rightarrow S_0$ transition.[2]

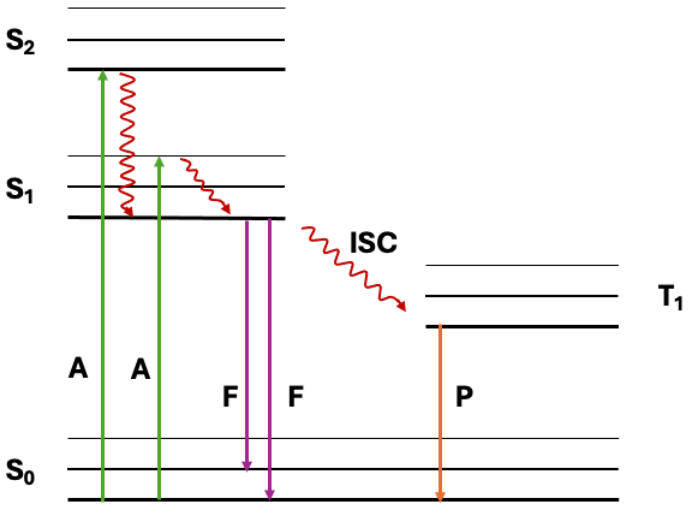

Figure 1. Jablonski Diagram (adapted from ref 3)

1.2.2. Frank-Condon Principle

Another important aspect in electronic excitation and relaxation processes that were discussed above is the movements of the nuclei. According to the Franck-Condon principle, since electronic transitions happen on a very small timescale, the location of the nuclei cannot change. So, the energy transition during absorption and emission of a photon happens vertically, in that the positions of the nuclei remain still. The probability of these vertical transitions is determined by the overlap of the initial and final vibrational electronic states, known as Franck-Condon factors. These factors explain the intensity distribution of vibronic states in the electronic spectra.[4] In particular, the systems that have major differences in their excited and ground state geometries, like CT complexes, the Franck-Condon region shifts, resulting in broad absorption bands and distinct Stokes shifts.[5,6] Stokes shift is the difference between the wavelengths of absorbed and emitted light, which is an indicator of structural changes and nonradiative processes.[7]

1.2.3. Excited States

The excitation process might occur within the same site of the molecule or between different sites of the molecule. Depending on the region where excitation happens, there are different excited states resulting from this process: Locally excited state, charge transfer state, and hybrid local and charge transfer state (HLCT).[8]

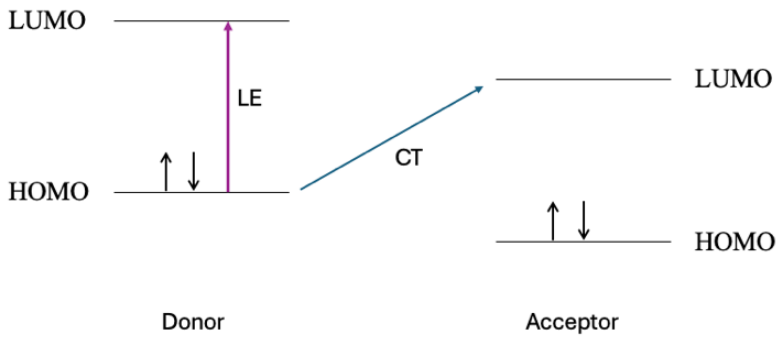

Figure 2. Schematic representation of local excitation and charge transfer

Beyond the general photophysical pathways, the character of the excited state, whether localized or charge transfer, plays a crucial role in determining the optical properties of a molecule. Electronic excitation in a molecule can occur in different regions, resulting in distinct excited-state characters. The excitation may take place within the same region of the molecule or spatially distant donor and acceptor groups.

In locally excited states, an electron moves from the highest occupied molecular orbital (HOMO) to the lowest unoccupied molecular orbital (LUMO) located on the same site of the molecule. This occurs when the energetically closest LUMO is present on the same fragment as the HOMO. Charge transfer state, however, arises when the electron is transferred from the HOMO of one site to the LUMO located on a different site, due to a smaller energy gap compared to the LE pathway. Since HOMO and LUMO in charge transfer transitions are spatially separated, the overlap between them is reduced, resulting

in a lower oscillator strength compared to the LE state. These excitations can be observed using UV-Vis absorption spectroscopy. Since the oscillator strength of CT is lower than that of LE, the CT signal will have a larger wavelength in the spectra.

The hybrid local and charge transfer (HLCT) state emerges when both LE and CT properties coexist in the excitation. This hybrid excitation is the linear combination of the two states, thus HLCT benefits from both the LE state's radiative efficiency and the CT state's charge separation advantages. Due to their tunable emission properties, the HLCT state is important for usage in optoelectronic applications.

Understanding the characteristics of charge transfer (CT) states is essential for exploring systems where intermolecular donor–acceptor interactions lead to the formation of charge transfer complexes.

1.3.Charge Transfer Complexes

Charge transfer complexes, which are also referred to as electron donor-acceptor (EDA) complexes[9] constitute an interesting and expanding area of research due to their unique and distinctive properties. The process is seen in some natural processes like photosynthesis; thus, they are valuable candidates for biological processes such as artificial photosynthesis and optoelectronic applications such as electro-optic modulators and photodetectors due to their nonlinear optical properties.[10–12] They have also been used as photocatalysts in systems exhibiting ligand-to-metal charge transfer.[13] In this system, the ligands with CT ability will be excited by photoinduction and transfer their charge to the metal that is coordinated, making the metal reactive for the substrate and facilitating the reaction. Furthermore, CT complexes are widely investigated for use as organic light-emitting diodes due to their capability to increase the performance of these materials. [14] Due to the charge transfer process, the material exhibits enhanced electrical conductivity. These complexes could be in solid crystal form, or they can be used as solutions in

different solvents. To fully understand the kinetics and thermodynamics of charge transfer processes, especially in solution-phase systems, Marcus theory offers a comprehensive theoretical framework.

1.3.1. Marcus Theory

To provide a quantitative description of electron transfer processes, the Marcus Theory is employed. It is used generally for the processes where electron transfer occurs without the formation or cleavage of chemical bonds. A key concept in Marcus Theory is the reorganization energy (λ), which refers to the energy required for the reorganization of both the solvent and the reactants to reach an equilibrium from their initial equilibrium geometry without actual transfer of electrons. The theory suggests that reorganization of the solvent and electron transfer processes occur simultaneously, not sequentially. Thus, the energy barrier for the electron transfer is lower compared to the previous theories. A very important and experimentally proven prediction of the Marcus theory is the "inverted region". According to Marcus theory, the rate of electron transfer increases as the reaction becomes more exergonic, in that ΔG becomes more negative. However, the rate of reaction starts to decrease once ΔG exceeds the magnitude of the reorganization energy. This counterintuitive phenomenon arises because the activation energy becomes larger again, despite a more favorable thermodynamic driving force. The rate reaches its maximum when ΔG equals the reorganization energy.

In Marcus theory, the solvent environment plays an important role by contributing to the reorganization energy (λ). Through its polarity and structural flexibility, the solvent reorganizes around the reactants and stabilizes charge-separated states to varying extents. Such differences in stabilization change the energy gap between ground and excited states, a phenomenon that becomes apparent as solvent-dependent shifts in absorption and emission spectra.[10,15,16]

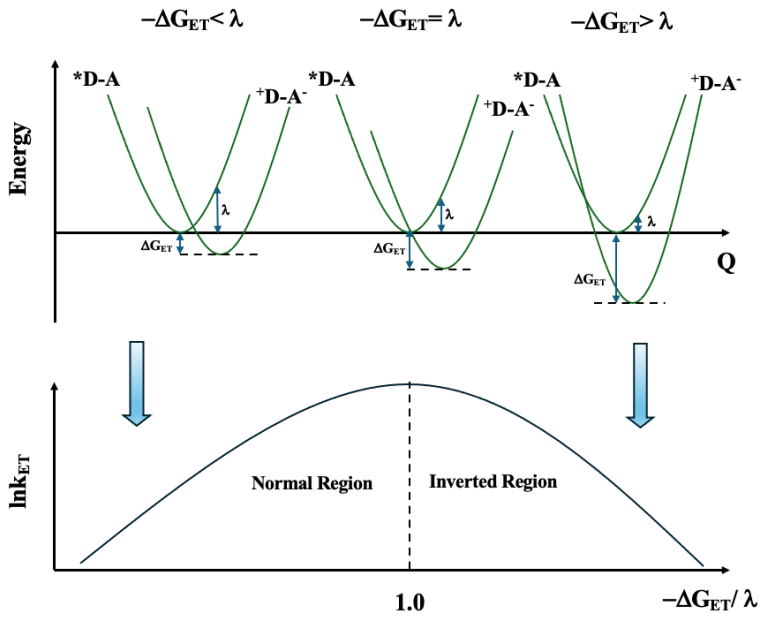

Figure 3. Graphical representation of Marcus Theory (adapted from ref 17)

Charge transfer (CT) complexes exhibit diverse structural and electronic behaviors depending on how the donor and acceptor units interact. Based on the nature and proximity of these interacting species, CT complexes can be broadly categorized into three main subgroups: intermolecular charge transfer complexes, where separate donor and acceptor molecules interact non-covalently; intramolecular through-bond charge transfer (TBCT) complexes, that electron transfer occurs via a covalent bridge connecting the donor and acceptor units; and intramolecular through-space charge transfer (TSCT) complexes, in which charge transfer takes place across spatially close but non-bonded moieties within the same molecule. This classification provides a useful framework for understanding how molecular architecture influences charge transfer efficiency, photophysical behavior, and potential applications.

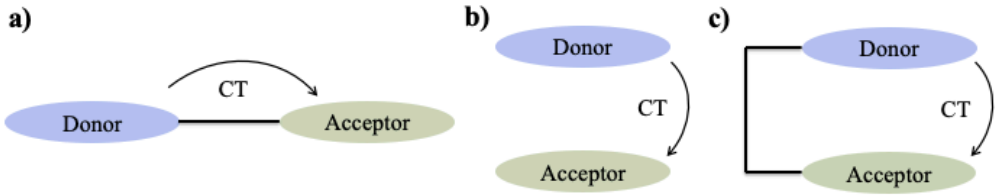

Figure 4. Schematic representation of a) Intramolecular Through-Bond CT, b) Intermolecular CT, and c) Intramolecular Through-Space CT

1.4.Intermolecular Charge Transfer

Intermolecular charge transfer is a process of electron transfer from a donor molecule to an acceptor molecule via noncovalent interactions, such as π–π stacking, Van der Waals forces, or hydrogen bonding. These interactions are possible due to the spatial proximity of the interacting molecules. These complexes were first described by Mulliken, where the donor and the acceptor keep their molecular identity but exhibit new optical absorption bands due to electron delocalization.[18]

Tetracyanoquinodimethane (TCNQ) and tetrathiafulvalene (TTF) complex is one of the well-studied examples that forms a highly conducting CT material used in molecular electronics.[19] It is known that TCNQ and TTF form crystals that are stacked parallelly and via pi-pi stacking. The color of TCNQ is yellow-green, and TTF is white-green, forming a complex that has a brown color.[20]

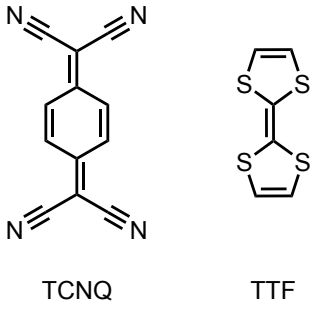

Figure 5. Structures of Tetracyanoquinodimethane (TCNQ) and tetrathiafulvalene (TTF)

A cocrystal of styrylpridine-tetracyanobenzene (TCN) that has a two-photon absorption property gained from its intermolecular charge transfer.[21] The driving force for the formation of cocrystals is the self-assembly via intermolecular CT between the donor and the acceptor molecules. Here, the interaction is not limited to a simple π–π stacking arrangement; rather, it involves a genuine intermolecular charge transfer between styrylpridine as the donor and TCN as the acceptor. This electron density redistribution distinguishes the system from the stacking interactions, leading to the formation of a new CT absorption band in the visible region. As a result, the cocrystal displays a distinct charge-transfer color, in contrast to the lighter shades of the individual components and exhibits unique optical properties such as enhanced two-photon absorption.

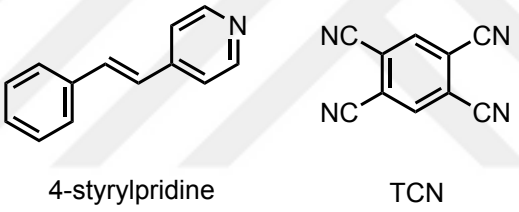

Figure 6. Structures of 4-styrylpridine and tetracyanobenzene

Another innovative study that benefits from intermolecular CT is a molecular necklace designed by Kim and coworkers in 2007.[22] In this design, a naphthalene moiety was connected to a dipyridyliumylethylene moiety by a methylene bridge to prevent intramolecular CT and facilitate intermolecular interactions. By using this Donor-Acceptor molecule and cucurbit[8]uril, the aggregation by host-stabilized CT interaction, the desired molecular necklace was obtained.

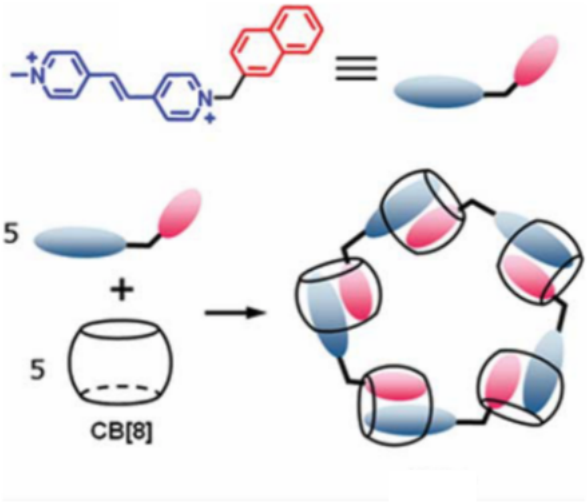

Figure 7. Molecular necklace synthesized from D-A complex and CB[8]. (reused from ref 22)

The adjustment of donor and acceptor groups is easy because they are synthesized separately and then mixed to form the complex. Thus, investigating and adjusting the CT property is very easy and quick. Since these complexes are interacting via non-covalent bonds and have orbital overlap, they can form well-defined crystalline structures. Also, the sensitivity of CT property against external stimuli such as pH, solvent polarity, and temperature makes them good candidates for use as stimuli-responsive materials.

However, they have some drawbacks regarding their effectiveness and stability because of the same reasons. Since these complexes have weak interactions and the interaction occurs between two different molecules, the effect of external factors such as solvent, temperature, or light becomes important in terms of CT property, in that, depending on the environment, the CT property may be diminished. In order to form efficient complex formation in solution, the donor and acceptor molecules need to interact even at low concentrations. This requires high binding constants to ensure the formation of the complexes. Also, most of the intermolecular charge transfer complexes release

energy via non-radiative relaxation, resulting in a low quantum yield for the materials. Determination of their optical properties is also harder.

1.5.Intramolecular Through-Bond Charge Transfer (TBCT)

Through-bond charge transfer occurs in systems where donor and acceptor moieties are connected via a π-conjugated system that facilitates the transfer of an electron through the system. A classic example of this class of molecules is push-pull polyenes, where electron donor and acceptor groups are attached at opposite ends of a polyene chain. These molecules are known for their nonlinear optical properties, like two-photon absorption, second harmonic generation, and sum frequency generation. Numerous works have been done to investigate the properties of this class of compounds.

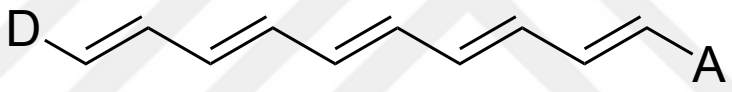

Figure 8. Structure of a push-pull polyene

Another type of these compounds is binding donor and acceptor groups to different positions of a benzene or other aromatic rings. One of the most studied examples is DMABN(p-*N*,*N*-dimethylaminobenzonitrile), which is known for its dual fluorescence, which was explained by twisted intramolecular charge transfer (TICT). [23] TICT was first proposed by Grabowski and coworkers to describe the presence of the new band in the fluorescence spectrum. According to the TICT model, DMABN has two different local minima in the S_1 state. Upon photoexcitation, it first goes to the local excited state with a planar configuration, then the dimethyl amino group rotates to a perpendicular position, and ICT takes place.

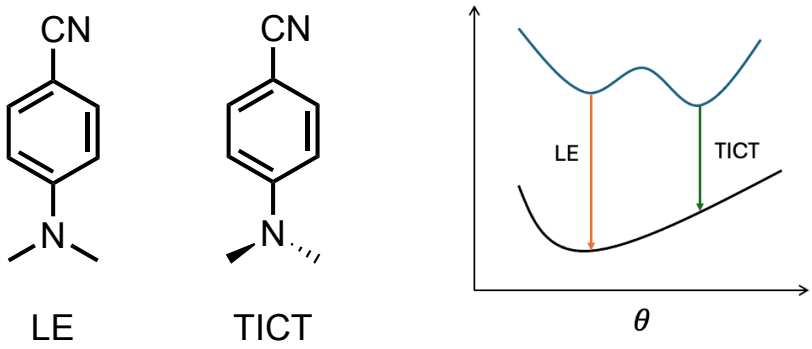

Figure 9. a) Locally excited and TICT state structures of DMABN. b) Potential energy graph for the TICT process. (Graph is adapted from ref 20)

TICT property is observed in a variety of dyes as well, and the TICT property can be diminished or increased through some modifications. Increasing TICT affects the lifetime and intensity of a dye, making it suitable for sensing applications. Inhibiting the TICT property, on the other hand, enhances the stability and brightness of the material, making it very suitable for use as fluorescent probes.[24]

To detect cysteine and homocysteine in living cells, Meng and coworkers developed sensors with ICT-based systems.[25] The sensors work based on two-photon fluorescence. They have *N,N*-dimethylaminobenzene and methoxybenzene as the donor moieties that are attached from their para position, and quinoline 2-carbaldehyde as the acceptor moiety linked via alkyne linkage.

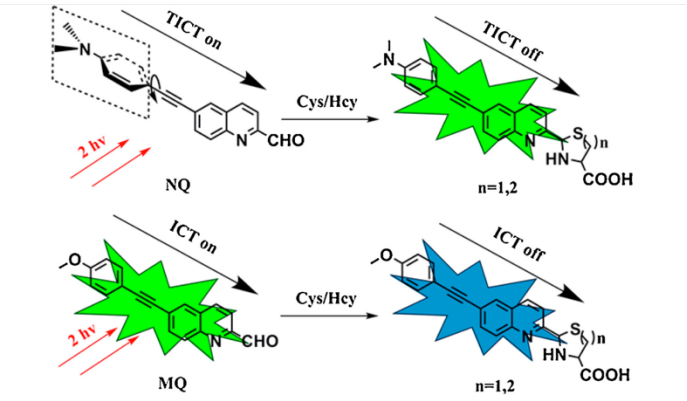

Figure 10. 2-photon absorption systems NQ and MQ (Reused from ref 25)

Another important application is designing colorimetric ion-sensing probes based on the ICT process. [26] The probe can detect F^- and CN^- ions by changing color in the presence of these ions; it changes its color from yellow to red in the presence of CN^- and to blue in the presence of F^- ions.

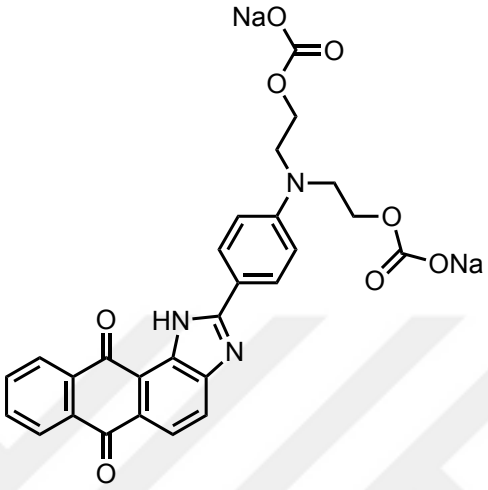

Figure 11. Ion-sensing probe that detects CN^- and F^- ions

1.6.Intramolecular Through-Space Charge Transfer Complexes

Intramolecular through-space charge transfer complexes offer significant advantages in the design without using conjugation. In these systems, CT takes place via non-covalent interactions, which happen due to the proximity and orbital overlap between donor and acceptor, like π–π stacking. The advantage of intramolecular through-space CT over intermolecular CT is that it is more structured, and the interaction distances are easy to control and kept stable. Thus, fine-tuning of photophysical properties such as quantum yield, emission wavelength, and charge separation efficiency is obtained. Systems such as bridged biphenyl derivatives, where π–π stacking or folded geometries bring donor and acceptor moieties into orbital alignment, are early examples of such systems.

Various spacers used in the design of TSCT complexes include aliphatic chains, non-conjugated tethers, and cyclic frameworks, all affecting donor-acceptor distances and their geometrical alignment.

There are various spacers used in the design of TSCT complexes, all of which have different effects on the CT property and have different applications. One of the most studied examples is phenyl linkers. Ortho-substituted benzenes are used for this purpose.[27] In these systems, charge transfer efficiency depends on the selection of donor and acceptor groups, in that the nature of the moieties affects the spatial positioning and the presence of charge transfer. BCZ-1 and BCZ-2 molecules are photosensitizers that were developed by Ji and coworkers, showing intramolecular TSCT. [28] These molecules were designed as carbazole-BODIPY dyads.

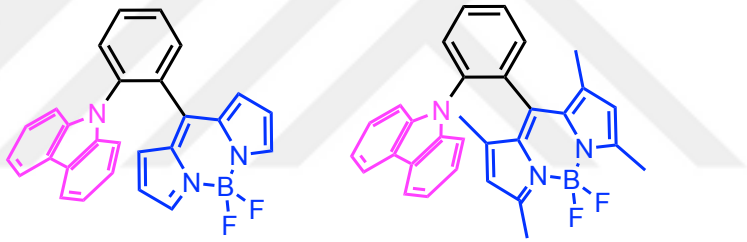

Figure 12. BCZ-1 (left) and BCZ-2 (right) molecules

Fluorene also serves as a spacer used for TSCT, providing a rigid structure and multiple functionalization sites, making it a great framework for thermally-activated delayed fluorescence (TADF) applications. DM-B, for example, which has spiro-triphenylamine (TPA) as the donor and triphenyltriazine (TRZ) as the acceptor on the fluorene linker, is a TADF material that has a photoluminescence quantum yield (PLQY) higher than 90% developed by Liao and coworkers.[29]

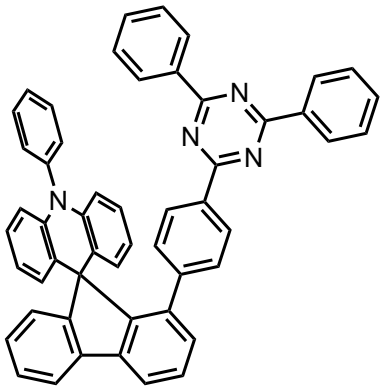

Figure 13. Structure of DM-B

A design using acenaphthene as a spacer with TPA and TRZ as donor and acceptor groups was shown to exhibit efficient TSCT property, making it usable for high-efficiency OLEDs.[30] The donor and acceptor are arranged in a pseudocofacial position in the design. The dominant contribution to the CT process is proven to be through-space in this system, which makes the complex an example for TSCT TADF materials.

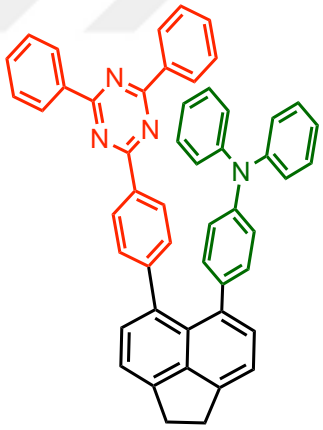

Figure 14. TPA-ace-TRZ complex

1,8-naphthalene is another spacer that is studied because it provides geometrical advantages in terms of interacting donor and acceptor groups. A 1,8-di(heteroaryl) naphthalene-based system was designed as a transparent frequency doubler.[31]

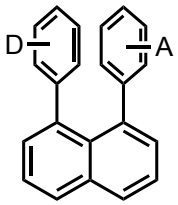

Figure 15. 1,8-di(heteroaryl)naphthalene system

Another important approach is to form a complex that shows dual or multiple emissions in its spectra. These systems, having dual or multiple emissions, increase the luminescence properties by increasing the possible charge transfer pathways. However, having a spacer that can be easily modulated is a challenge for these structures. Donor/Acceptor/Donor systems connected to a linker are designed for this purpose. Binding an additional donor to the system increases the TADF efficiency by enhancing the rigidity of the material. An example of this kind of system is given in Figure 16.[32]

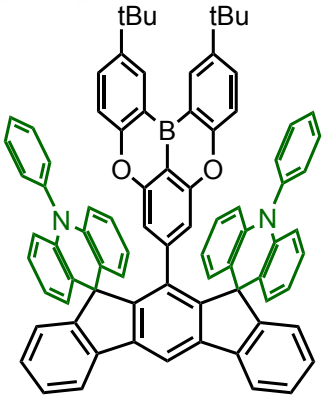

Figure 16. D/A/D system that shows a dual emission

1.7.Solvatochromism

Solvatochromism is a very important phenomenon that explains the behavior of charge transfer complexes in different solvents. Solvatochromism explains the behavior of a molecule with its surroundings in response to an external stimulus, e.g., excitation. There are different situations for the molecule of interest and for the solvent. If the molecule's structure remains still, the fluorescence spectra will give a signal with respect to that position; however, if the molecule moves within the molecule, the obtained data will be the average of the affected area that the molecule moves through. The solvent, on the other hand, may also retain its distribution, or it may rearrange to reach a new, lower energy distribution with respect to the new equilibrium of the excited molecule. All these changes will affect the emission spectra that are obtained in terms of the shape and the position of the peak. Charge transfer complexes show a significant change in their dipole moments during the excitation process, which affects the interactions of the molecule with the environment, e.g., solute-solvent interactions, hydrogen-bonding, and causes differences in the emission. [2,15,33]

The direction of the spectral shift (blue or red) observed in charge transfer molecules depends on which electronic state, ground or excited, is more stabilized by the solvent. As solvent polarity increases or as its hydrogen-bonding ability changes, differential stabilization of these states can lead to either a bathochromic (red) or hypsochromic (blue) shift in the emission or absorption spectrum. Bathochromic shift going to a more polar solvent is called positive solvatochromism, and it is mostly due to the stabilization of the excited state geometry of the molecule by a more polar solvent. [34,35]

1.8.Photoluminescence Quantum Yield (PLQY)

Photoluminescence quantum yield (PLQY) is the efficiency of a luminescent material. It determines the ratio of the amount of emitted energy to the absorbed energy. It gives information about how well the luminescent material emits the energy it absorbed radiatively. High quantum yield means that the relaxation of the excited molecule happens mostly via radiative pathways, while low QY indicates the dominance of non-radiative processes like intersystem crossing, internal conversion, and vibrational relaxation. PLQY value is a crucial factor for the efficiency of the emitting materials, such as OLEDs, TADF materials, and sensors.[36,37]

The structure of the molecule is one of the most important factors that affect the PLQY. In a TADF system, for example, the energy difference between the singlet and triplet states is small, which facilitates the reverse intersystem crossing, in that the electron can turn back to the singlet state and go to the ground state via radiative relaxation. As a result, the yield of radiative emission increases.[38]

There are also some external factors that affect PLQY other than the nature of the molecule. The solvent is a primary factor that affects the quantum yield. Its polarity and hydrogen bonding capacity may influence the stability of the geometry of the excited molecule and the relaxation path. In CT systems, polar solvents may cause a shift in the emission spectra and change the yield. High temperature may increase the rate of non-radiative processes and decrease the yield. Intermolecular interactions, on the other hand, may tune the aggregation and lower the yield. The presence of oxygen may quench the radiative processes and decrease the yield.[39]

1.9.Aim of the Project

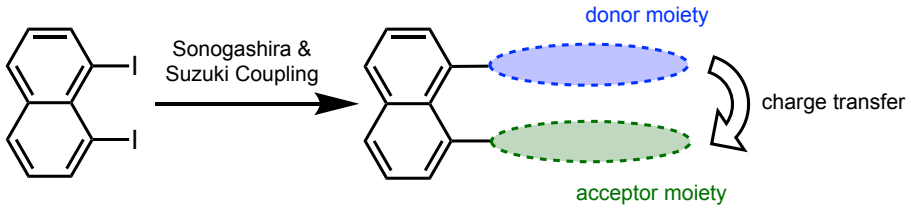

Scheme 1. TSCT complex design

Our group has previously designed a novel scaffold that exhibits intramolecular through-space charge transfer property.[40] In this design, naphthalene was used as the spacer, benzofuran as the donor moiety, and ynone as the acceptor moiety. The target complexes were synthesized by Suzuki and Sonogashira coupling reactions and were found to exhibit distinct CT absorption bands in the visible region along with dual emission features. These results highlighted the ability of the scaffold to promote efficient intramolecular TSCT and established it as a promising platform for further design of functional charge-transfer systems.

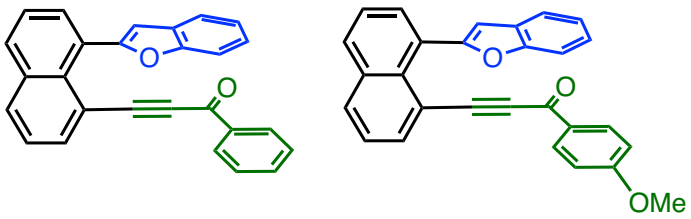

Figure 17. Compounds designed and analyzed in the previous study.

In this project, our main aim is to investigate the effect of different donor and acceptor groups on the TSCT property of a group of molecules with the same design by using different ynones and electron-donating rings. To observe the trend, compounds **5a, 5b, 5c, 5d, 5e, 5f,** and **5g** were synthesized, and their CT properties were investigated using UV-Vis and fluorescence spectra. The data obtained from the synthesized products

and the compounds that were previously reported by our group were collected and compared.

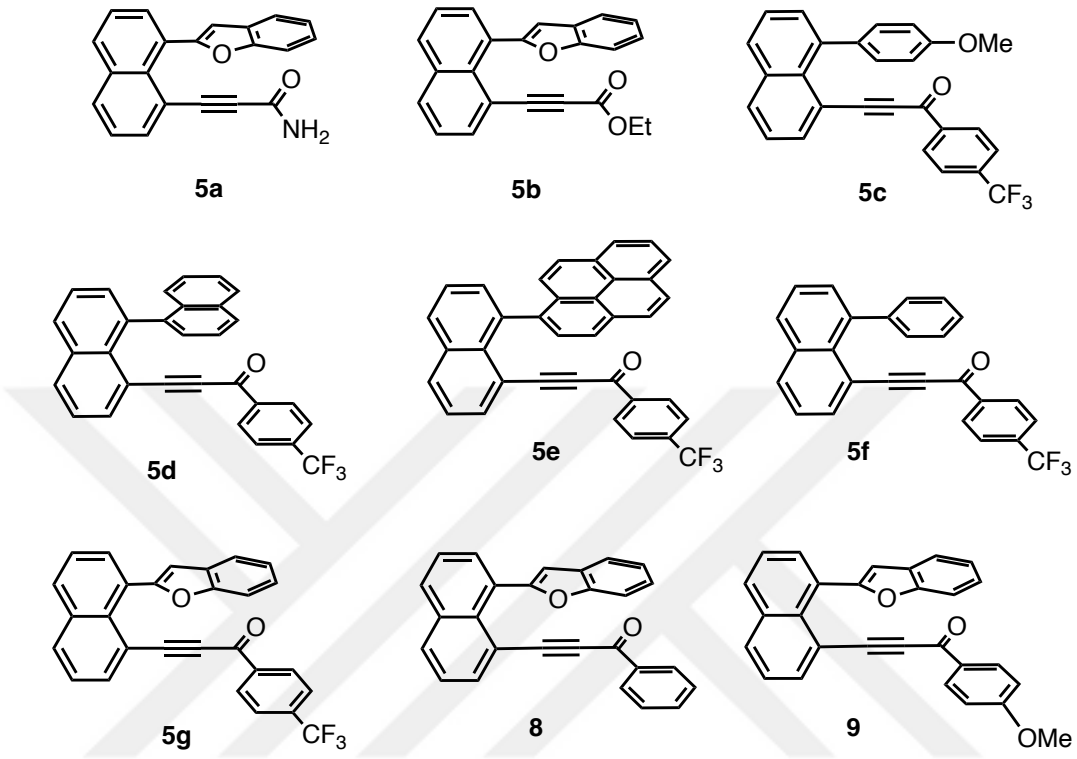

Figure 18. The compounds that are investigated

The scope of the research has also been expanded by a solvatochromism study. The investigation has been performed on **5b** to see the solvatochromic behavior and compared with the previously reported findings. During the studies, the photoluminescence quantum yields of the compounds in DCM was determined. To understand the effect of solvent on the quantum yield of the compounds, the QY values of compound **5b** in different solvents, from nonpolar to polar, were also experimentally determined. Since it is known that CT complexes are solvent-sensitive, the possible effect of H-donating solvents, Lewis acids, and Brønsted acids on the stability and properties of the compounds was also examined.

To support the experimental results, some DFT calculations were performed to see the HOMO-LUMO distribution on the molecules. Lastly, a crystal structure analysis was made to confirm whether the molecules satisfy the distance requirement for orbital overlap for TSCT.

2. RESULTS & DISCUSSION

2.1.The Synthetic Studies

In this section, the synthetic approaches employed to obtain the target complexes, along with the underlying reaction mechanisms, are presented. Three distinct synthetic routes were followed for the preparation of the desired CT complexes. The main reactions used for the syntheses are Sonogashira and Suzuki-Miyaura cross-coupling reactions. Sonogashira coupling reaction is a very useful reaction in C-C bond formation, which is used for the cross-coupling of a terminal alkyne with an aryl or vinyl halide, or triflate, via a palladium catalyst, a copper cocatalyst, and an amine base. The reaction proceeds generally in an inert atmosphere and under ambient conditions.[41] The presence of a cocatalyst eases the reaction and makes it feasible under mild conditions, allowing the usage of mild bases and room temperature. Its mechanism is thought to be a combination of Pd catalysis and Cu catalysis cycles. In the Pd-catalyzed cycle, a catalytically active species $Pd(0)L_2$ may be generated from Pd(II) via a reduction. This compound facilitates the oxidative addition of R_1-X. Then, Cu-acetylide undergoes transmetalation in the Cu-catalyzed cycle to produce $R_1Pd(C \equiv CR_2)L_2$. The reductive elimination from this intermediate gives the desired coupled product and Pd(0) catalyst.

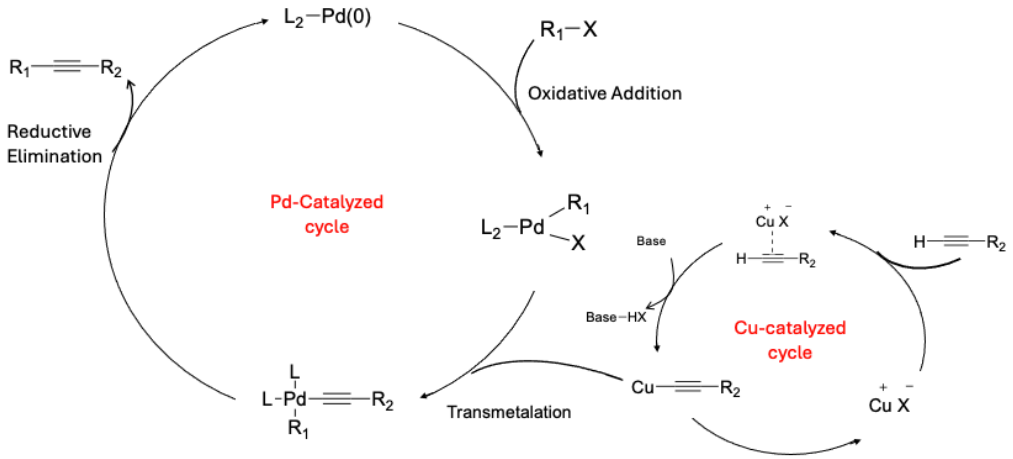

Figure 19. Catalytic cycle of Sonogashira reaction

For the Suzuki reaction, the C-C bond formation is made using organoboron compounds and organic halides or halide equivalents. It occurs in the presence of a palladium catalyst and a base.[42] The reaction conditions vary in the literature depending on the substrates. One important advantage of this reaction is that organoboron compounds are stable against various conditions and they are environmentally friendly. Also, the reaction is tolerant towards various functional groups and steric hindrance. The reaction cycle starts with the oxidative addition of the alkyl or aryl halide to the active Pd(0) catalyst and formation of an organopalladium intermediate, which then forms another intermediate via transmetalation, which is triggered by the addition of a base. The reductive elimination of the intermediate affords the desired product and the regenerated Pd(0) catalyst.

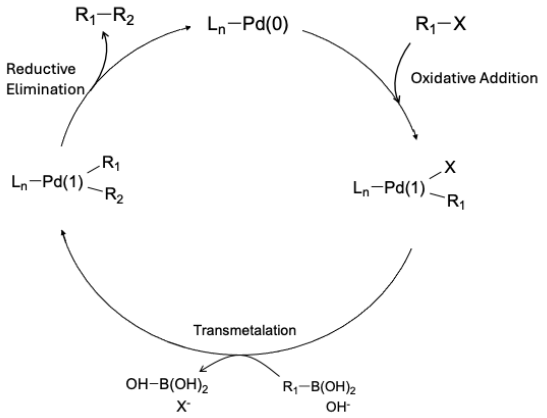

Figure 20. Catalytic cycle of the Pd-catalyzed Suzuki-Miyaura coupling reaction

Compounds **5c**, **5e**, **5f**, and **5g** were synthesized with the purpose of seeing the effect of the donor group while keeping the same acceptor moiety. For the synthesis of the compound **3c**, which is the acceptor group for complexes **5c**, **5e**, **5f**, and **5g**, compound **2** was synthesized through nucleophilic alkynylation of 4-(trifluoromethyl) benzaldehyde. In this reaction, the deprotonation of the terminal hydrogen of TMS-acetylene was by *n*-BuLi, followed by the nucleophilic attack of this alkynyl anion to

benzaldehyde, leading to the formation of propargylic alcohol. By using a base and a proton source, the TMS group leaves, and the desired product **2** was obtained with 58% yield. This propargylic alcohol is then attached to naphthalene via Sonogashira coupling reaction to afford compound **3c** with 82% yield. In the Sonogashira coupling reaction, 4 equivalents of 1,8-diiodonaphthalene, 0.07 equivalents of Pd catalyst, 0.14 equivalents of CuI cocatalyst, and triethyl amine as both the solvent and the base were used. An excess of 1,8-diiodonaphthalene (4 equiv.) was required, since otherwise bis-alkynylation occurred. THF was used to ensure the complete dissolution of the reactants. Before the attachment of the donor group, the alcohol is oxidized to a ketone by an oxidation reaction using excess MnO_2 as the oxidizing agent. This oxidation reaction is performed before the Suzuki-Miyaura coupling reaction to eliminate any effect coming from the alcohol that reduces the yield. Oxidation reaction afforded compound **4c** with 92% yield. In the final step, the Suzuki coupling reaction was carried out to attach 4-OMe-phenyl, pyrene, phenyl, and 2-benzofuranyl donor groups. For compounds **5e** and **5f**, the reaction was performed using $Pd(PPh_3)_4$, K_3PO_4 as the base, and dioxane/H_2O as the solvent at 100 °C, giving yields of 63% and 36%, respectively. For compounds **5c** and **5g**, however, these conditions resulted in decomposition and side products as observed by TLC. Therefore, the conditions were modified to milder ones ($Pd(PPh_3)_4$, K_2CO_3 as base, DMF as solvent, 80 °C), under which the desired products **5c** and **5g** were obtained in 43% and 56% yields, respectively.

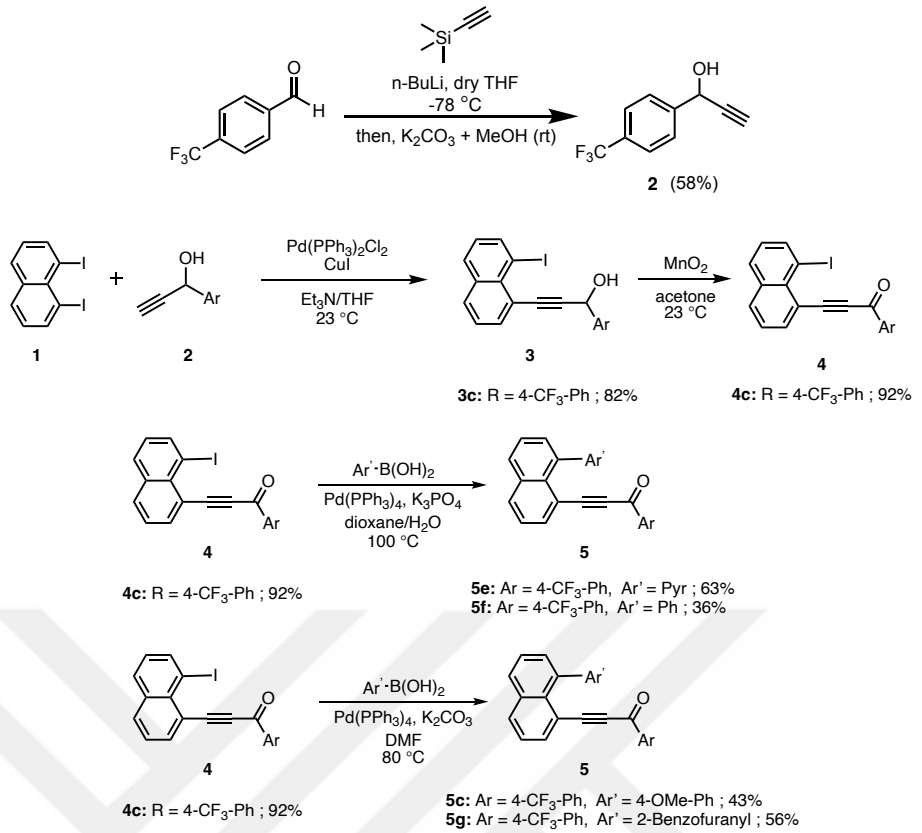

Scheme 2. Synthesis of compounds **5c**, **5e**, **5f**, and **5g**

To investigate the effect of substituents other than ketones on the electronic properties of the alkyne and on the charge-transfer properties, an amide and an ester were selected for study. For the synthesis of compounds **5a** and **5b**, the corresponding acceptor groups were attached to 1,8-diiodonaphthalene via Sonogashira coupling reaction (Scheme 2). In this step, 4 equivalents of 1,8-diiodonaphthalene, 0.07 equivalents of Pd catalyst, 0.14 equivalents of CuI, and triethyl amine as both the solvent and the base were used. This reaction afforded compounds **4a** and **4b** in 82% and 33% yield, respectively. Subsequently, a Suzuki coupling reaction was performed using 2 equivalents of benzofuran boronic acid, 0.05 equivalents of Pd catalyst, and 3 equivalents of base. This step successfully introduced the benzofuran group to compounds **4a** and **4b,** and the desired products **5a** and **5b** were obtained in 65% and 73% yields, respectively.

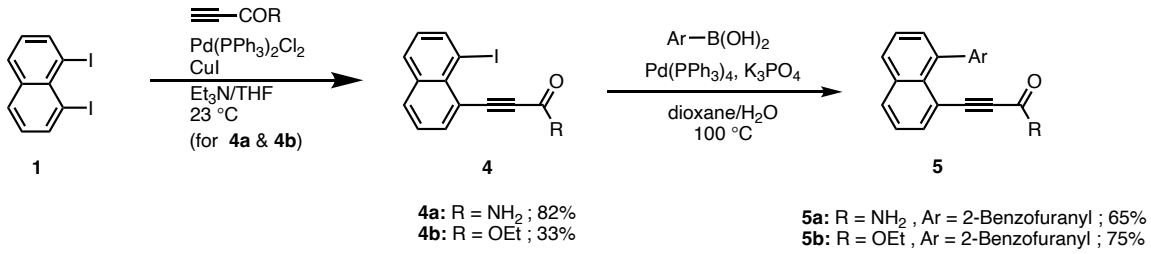

Scheme 3. Synthesis of compounds **5a** and **5b**

Compound 5d was also synthesized for the comparison of the effect of the donor group on the charge transfer. For the synthesis of compound **5d**, the sequence of the reactions was exchanged to minimize yield loss arising from steric hindrance and electronic factors. Firstly, the naphthalene group was attached via a Suzuki coupling reaction between compound **1** and naphthaleneboronic acid (1.1 eq) in the presence of Pd catalyst (0.05 eq) and K_2CO_3 (4 eq) in DMF at 80 °C, affording compound **6** in 72% yield. Subsequently, compound **2** was coupled to compound **6** via Sonogashira coupling reaction to give compound **7** with 25% yield. Finally, the benzylic alcohol group of **7** was oxidized with excess MnO_2 in acetone to obtain the desired product **5d** in 61% yield.

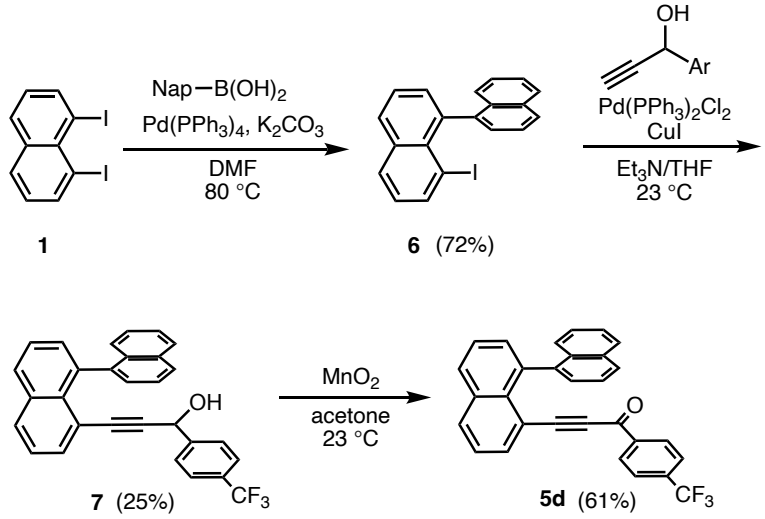

Scheme 4. Synthesis of compound **5d**

For the identification of the synthesized compounds, several characteristic signals were used as indicators other than ^{1}H NMR. The presence of the alkyne moiety was confirmed by the strong stretching band observed in the IR spectrum in the range of 2180-2195 cm^{-1}, since these carbons cannot be directly distinguished in the ^{1}H NMR spectrum. For the compounds containing fluorine atoms, ^{19}F NMR spectroscopy was employed to verify their incorporation. In addition, the coupling of fluorine with the directly bonded carbon resulted in characteristic splitting patterns in the ^{13}C NMR spectrum. The carbonyl functional group was also detected in the ^{13}C NMR spectrum, appearing in the typical ranges depending on the functional group between 160 ppm and 190 ppm.

2.2.Analysis of Compounds

2.2.1. Color of the Compounds

The charge transfer properties of all synthesized compounds were examined using UV-Vis absorption and fluorescence spectroscopy. The first indication of the CT behavior was their distinct colors under both visible light and UV light (figure 20). Compounds **8** and **9,** which were synthesized in our previous study, exhibit intense orange and yellow colors while the majority of compounds **5a, 5b, 5c, 5d, 5e, 5f,** and **5g** display a lighter shade of yellow, **5f** and **5g** standing out due to a deeper orange color. These visual observations are linked to the differences in CT properties, since compounds that appear orange–yellow must absorb in the near-UV region and slightly above it. [43] The more intense orange colors suggest a stronger absorption in this spectral range, while the compounds with lighter colors indicate a weaker absorption. These observations only indicate a qualitative proof of the presence of CT interactions; in the next section, these CT properties will be investigated in more detail with the help of spectral data.

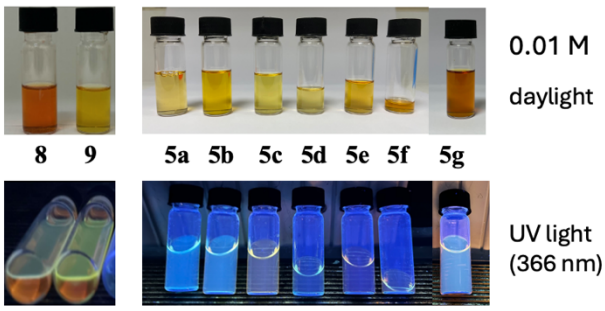

Figure 20. Colors of the compounds in DCM (10^{-2} M) under visible light (top), and under 366 nm UV light (bottom).

2.2.2. UV-Vis Absorption Spectra

Fo the absorption spectrum measurements, the compounds were dissolved in DCM (10^{-4} M). Each compound exhibited different absorption profiles in its UV-Vis absorption spectrum, arising from the different nature of the donor and acceptor groups. To better illustrate the influence of the substituents on CT behavior, two comparative graphs were plotted, highlighting the changes in CT band properties depending on different donor and acceptor groups.

The first graph illustrates the effect of the acceptor group on the CT behavior. Compounds **8** and **9** were synthesized previously, so **5a** and **5b** were synthesized to see when the acceptor group is placed with functional groups other than ketones and electron-rich, whether we see the CT band or not. **5g** was synthesized to see the effect of a more electron-poor acceptor on the CT behavior since CF_3 withdraws electrons from the aromatic ring and makes the alkyne more electron-deficient.

Theoretically, the presence of an electron-withdrawing group on the alkyl group attached to the acceptor increases its electron deficiency. As a result, the energy difference between the HOMO and the LUMO decreases, and a bathochromic shift is expected to be observed in the UV-Vis absorption of the compound. Based on this rationale,

compound **5g** would be expected to display the longest-wavelength absorption, followed by compound **8**, while compound **9** should absorb at shorter wavelengths due to the electron-donating effect of the methoxy group and the electron-withdrawing nature of CF_3. For compounds **5a** and **5b**, the presence of electron-donating -NH_2 and -OEt groups, -NH_2 being more electron-donating, makes them more electron-rich acceptors. So, it is expected that they will show little or no CT property. The graph depicts that in **5a** and **5b**, the CT band vanishes as expected. However, the comparison of **8**, **9**, and **5g** is the opposite of the expected results. The CT band of **9** has the longest wavelength, then **8**, and **5g** has the shortest wavelength. This shows us that the HOMO-LUMO energy gap is not the only factor that affects the CT property. Additional factors, such as the orbital overlap and vibrational motions of the molecules, might affect the CT property as well.

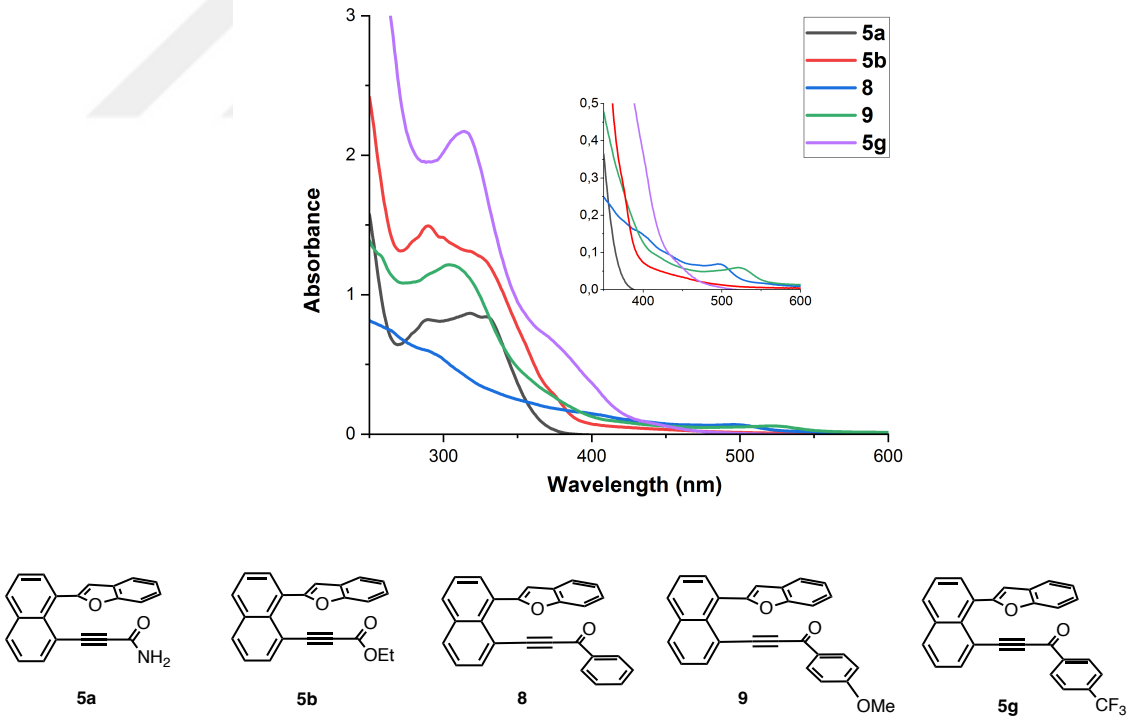

Figure 21. UV-Vis absorbance spectra, and structures of compounds **5a**, **5b**, **8**, **9**, and **5g** (10^{-4} M in DCM)

To clarify whether compounds **5a** and **5b** truly exhibit charge-transfer bands, curve fitting was applied using Origin software. For **5a**, there appears to be a very weak band, while in **5b** the feature is more visible but still not definitive. The fitted spectra are presented in Figure 22. The fitting data for **5a** reveal the presence of an additional absorption band, with a λ_{max} around 355 nm, whose intensity is significantly lower than the main absorption bands at 268, 315, and 336 nm. Similarly, **5b** is suggested to possess a CT band with its λ_{max} at 375 nm, again with a very low intensity compared to the absorption at 320 nm.

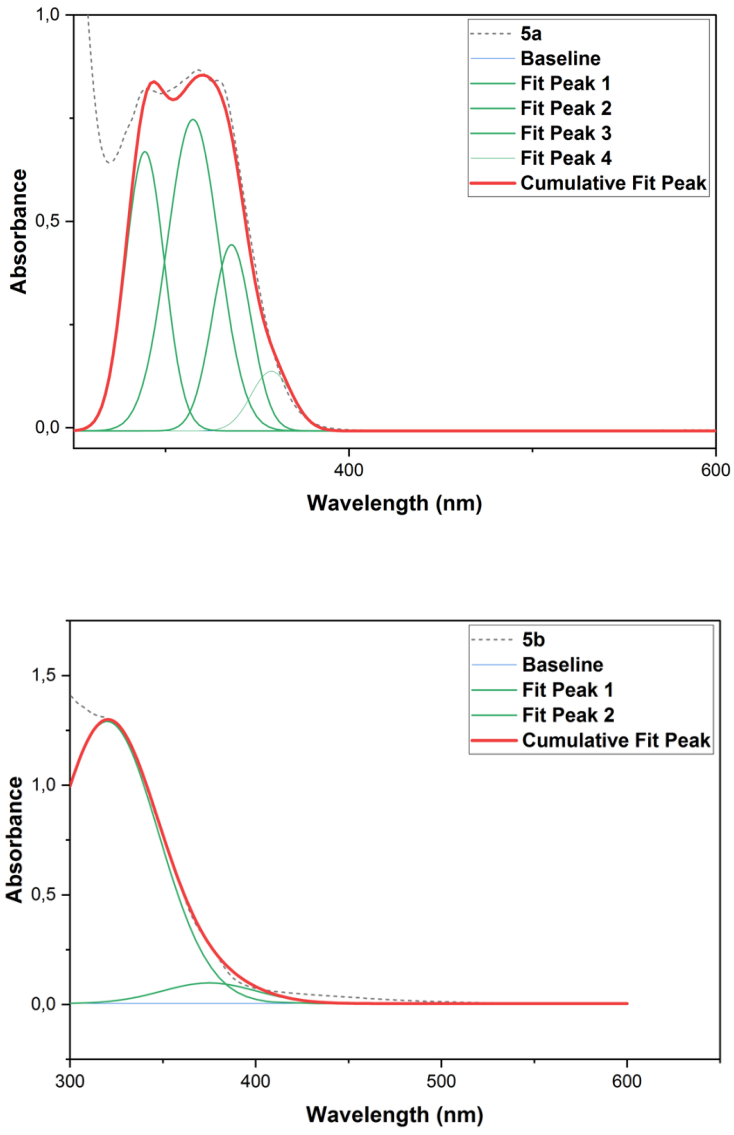

Figure 22. Curve fitting for compounds **5a** (top) and **5b** (bottom)

A similar, tail-like absorption pattern is also observed in compounds **5d** and **5e**. To uncover their CT band, curve fitting was applied to their spectra as well. The fitting data indicate that a CT band is observed around 358 nm for **5d** and around 380 nm for **5e**.

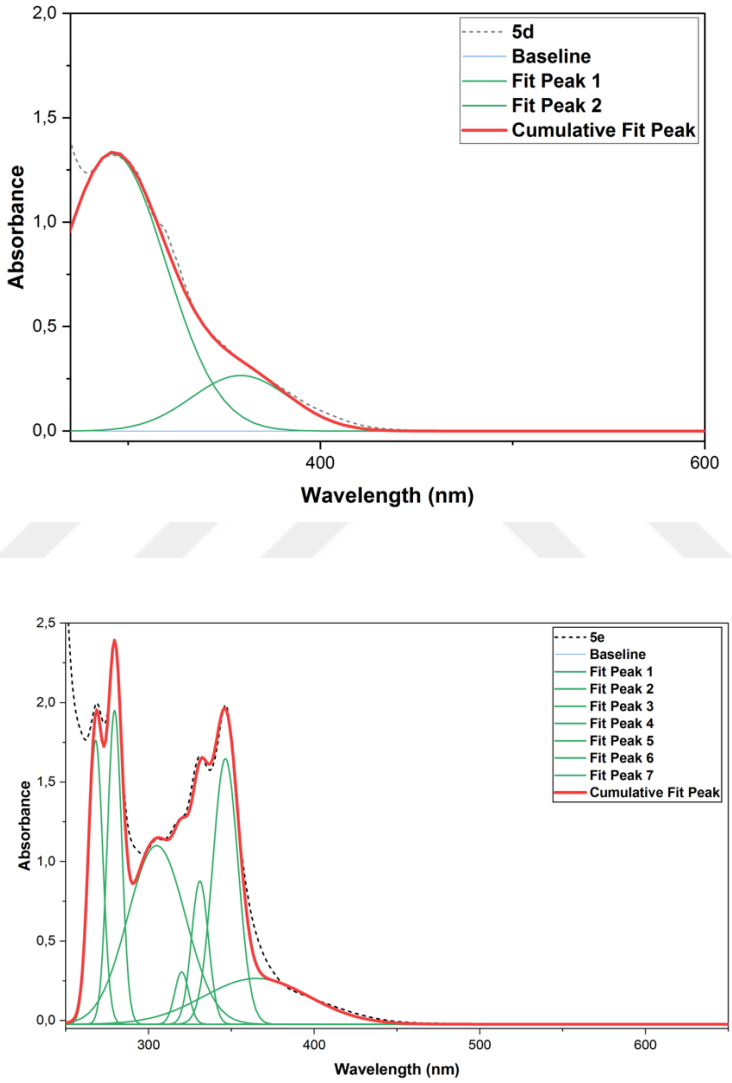

Figure 23. Curve fitting for compounds **5d** (top) and **5e** (bottom)

The graph in Figure 24 shows the effect of the donor groups on the charge transfer property. Benzofuran, naphthalene, 4-methoxybenzene, benzene, and pyrene rings were

examined for this purpose. In general, having a more electron-rich ring causes bathochromic shifts in the CT band by lowering the energy difference between the HOMO and the LUMO. From the data, it can be concluded that benzofuran is the most electron-rich donor among those investigated, providing the strongest orbital overlap. A comparison between benzene and 4-methoxybenzene further supports this trend: the electron-donating methoxy substituent increases the electron density of the aromatic ring, shifting the CT band to longer wavelengths relative to unsubstituted benzene. Consistent with this expectation, compound **5g**, which bears a benzofuran unit, exhibits the CT band at the longest wavelength. Similarly, compound **5e** shows a slightly longer-wavelength CT band than **5d**, most likely due to the greater electron-donating ability and spatial positioning of its donor ring.

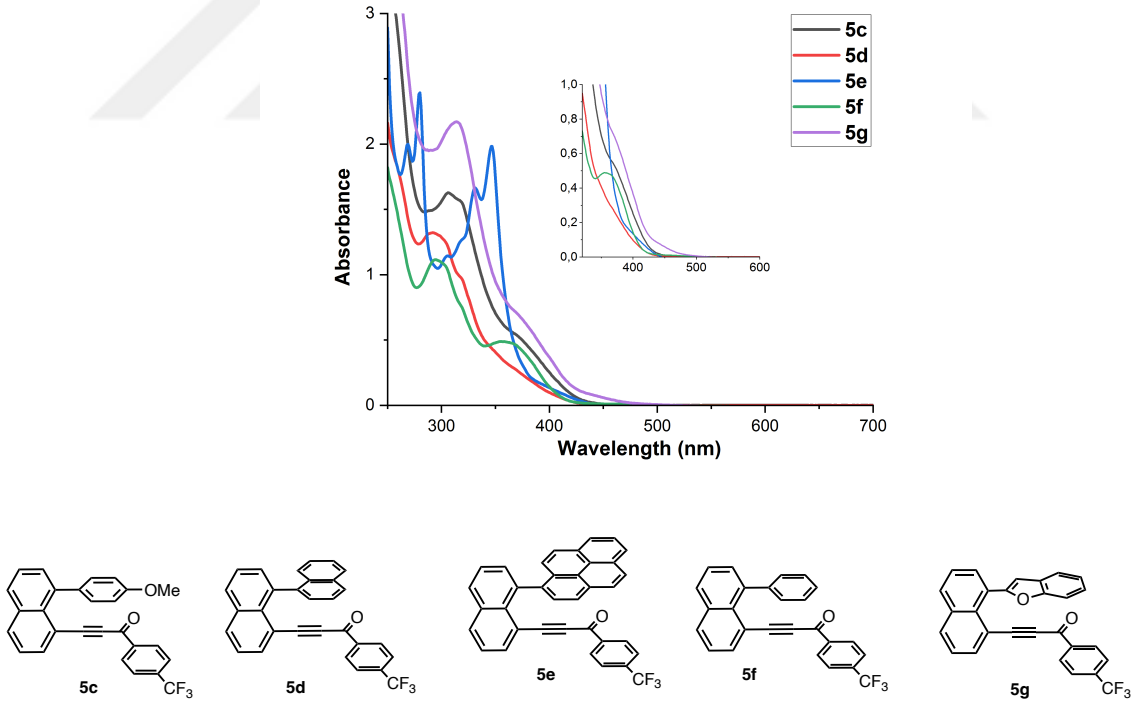

Figure 24. UV-Vis absorbance Spectra and structures of compounds **5c**, **5d**, **5e**, **5f**, **5g** (10^{-4} M dissolved in DCM)

The λ_{max} and molar absorptivity values of the compounds are given in Table 1. It was not feasible to measure the molar absorptivity values for compounds **5a**, **5b**, and **5d** because of the tail-like nature of their absorption bands. Nevertheless, it is evident that the molar absorptivity of the charge-transfer band is approximately an order of magnitude lower than that of the main absorption bands. This observation is consistent with the low oscillator strength of the charge transfer band compared to the local excitation. Oscillator strength is about both the probability and intensity of an electronic transition and it is proportional to the square of the transition dipole moment. In the case of charge-transfer bands, the electron density shifts from a donor fragment to a spatially separated acceptor fragment, in which the orbital overlap is reduced, and consequently reduces the transition dipole moment. As a result, the oscillator strength is lower in a charge transfer transition compared to a local excitation

Table 1: Molar absorptivity and λ_{max} values of compounds in DCM (10^{-4} M)

Compound	**Absorbance (LE)**		**Absorbance (CT)**	
	λ_{max} (nm)	**ε ($M^{-1}cm^{-1}$)**	**λ_{max} (nm)**	**ε ($M^{-1}cm^{-1}$)**
5a	292	8.29×10^3	Tailing up to 400	-
5b	293	1.45×10^4	Tailing up to 525	-
5c	306	1.61×10^4	380	4.51×10^3
5d	292	1.29×10^4	Tailing up to 450	-
5e	270	2.13×10^4	Tailing up to 430	4.51×10^3
5f	295	1.08×10^4	358	4.76×10^3
5g	319	2.17×10^4	370 with tailing up to 500	6.19×10^3
8	289	2.39×10^4	500	2.69×10^3
9	306	4.84×10^4	526	2.40×10^3

2.2.3. Fluorescence Spectra

To further examine the CT property, fluorescence measurements of the compounds were taken in DCM (10^{-5} M). Fluorescence spectroscopy provides valuable insight into the nature of the excited states of the molecules. As discussed in the introduction, certain charge-transfer systems may display dual emission bands, which arise from an additional low-energy emissive state stabilized in the excited state. Compounds **8**, **9**, and **5d** exhibit this property in their emission spectra, which supports that there are two radiative pathways that the molecule relaxes, one corresponding to the local excited state and the other to the charge transfer state.

The Stokes shift values of the compounds are given in Table 2. Large Stokes shifts are a well-known characteristic of charge-transfer complexes, as they reflect the reorganization of both molecular geometry and electronic charge distribution upon excitation. In particular, molecules that undergo significant changes in dipole moment between the ground and excited states experience a greater degree of solvent stabilization in the excited state, which results in larger Stokes shifts.[2] The data show that some of the complexes undergo more significant structural and electronic reorganization than others, highlighting differences in the extent of charge-transfer character within the series.

Depending on the donor-acceptor pairs, the emission wavelength and Stokes shift values exhibit clear differences. Compounds **5a** and **5b** show moderate Stokes shift and they emit at relatively shorter wavelengths, which may be correlated with their low CT characters. Compound **5c** exhibits a larger Stokes shift and a bathochromic shift in its emission, indicating higher stabilization in the excited state. Compound **5g** also shows emission at a long wavelength with a large Stokes shift, attributed to the strong electron-donating ability of the benzofuran ring and the CT stabilization. In contrast, compounds **8** and **9** display relatively small Stokes shifts, suggesting that the excited-state

reorganization in these molecules is less significant compared to compounds such as **5c** or **5g**.

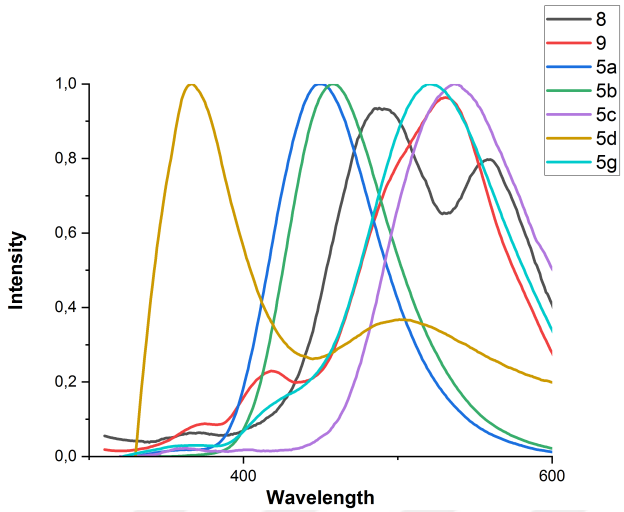

Figure 25. Fluorescence spectra of compounds **5a** (10^{-5}M)**, 5b** (10^{-5}M)**, 5c** (10^{-4}M)**, 5d** (10^{-4}M)**, 5g** (10^{-5}M)**, 8** (2.5×10^{-5}M)**,** and **9** (2.5×10^{-5}M) in DCM.

Table 2. Emission maxima and Stokes Shift values of the compounds.

Compound	**5a**	**5b**	**5c**	**5d**	**5e**	**5f**	**5g**	**8**	**9**
Emission (nm)	450	460	540	369,505	-	-	520	410,532	493,560
Stokes Shift (nm)	50	80	160	55	-	-	150	32	34

2.2.4. Crystal Structure Analysis

For the CT process to occur, an orbital overlap is required. This requirement is supposed to be satisfied by arranging the spatial positioning of the donor and acceptor groups. Compound **5a** was crystallized and analyzed by single-crystal XRD. For crystallization, the compound was dissolved in DCM, and crystals were obtained by vapor diffusion of pentane into the solution. The analysis revealed that the distance

between the benzofuran ring and the ynone is 3.2 Å, which is in the range of the typical π–π stacking distance.[44,45] The crystal structure confirms that the requirement for orbital overlap for the CT process is satisfied. In addition, the angle between the naphthalene carbons to which the substituents are attached is 125°, reflecting a spatial orientation that may facilitate orbital overlap between the donor and acceptor units. Another noteworthy intramolecular feature is observed between the benzofuran moiety and the amide NH hydrogen. The distance measured is 2.7 Å, which is consistent with the characteristic distance of an NH–π interaction.[46] As a result of his interaction, the two hydrogens of amide are not equivalent and they appear as two different signals, at 3.71 ppm and 4.77 ppm, in the NMR spectra. Hydrogen that makes NH- π interaction is more shielded due to the increased electron density provided by the aromatic ring.

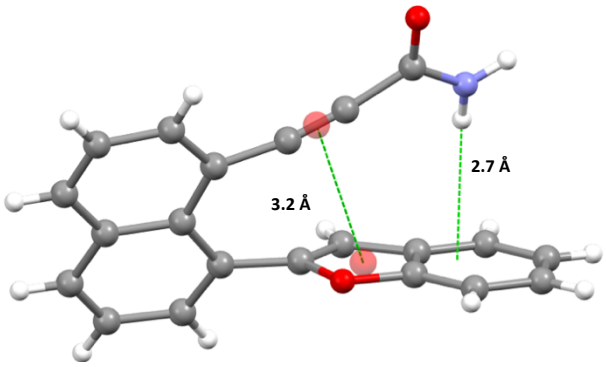

Figure 26. Crystal structure of compound **5a**

2.3.Computational Studies

Computational studies were performed using ORCA 6.0 software,[47] the B3LYP functional,[48,49] and the DEF2-SVP[50] basis set for the ground state optimization and DEF2-TZVP[50] basis set for the excited state calculations. All calculations were performed using the conductor-like polarizable continuum model (CPCM)[51] to incorporate solvent effects using dichloromethane as the solvent.

Illustration of HOMO and LUMO of the compounds and the HOMO-LUMO energy difference are given in Table 3. In all molecules, the HOMO is predominantly located on the donor group, while the LUMO is placed on the acceptor group. In some molecules, both HOMO and LUMO orbitals are also observed on the naphthalene spacer. These orbitals may originate from the local excitation of naphthalene itself, but they could also contribute to system by through-bond charge transfer process.

Table 3. Energy difference between HOMO and LUMO of the compounds.

Compound	HOMO	LUMO	HOMO-LUMO Energy Gap (eV)
5a	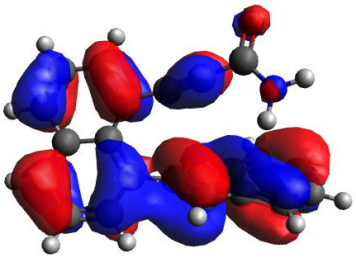	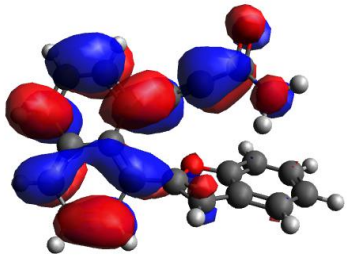	3.80
5b	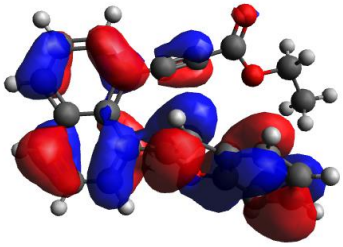	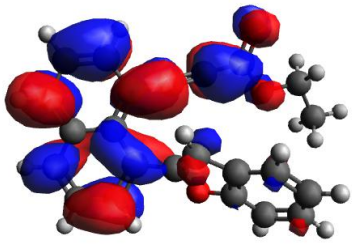	3.53
5c	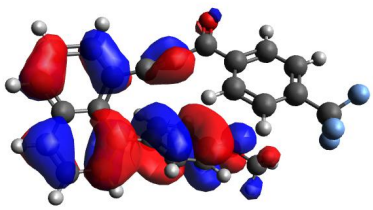	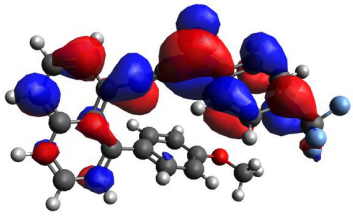	3.16

5d	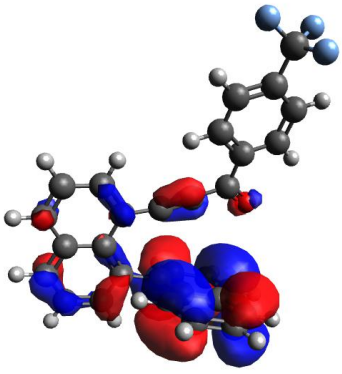	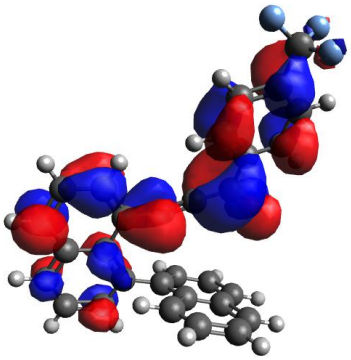	3.27
5e	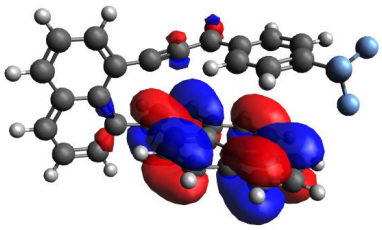	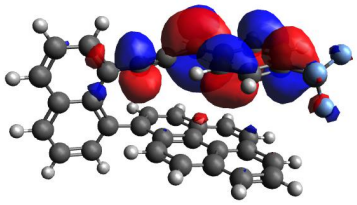	3.10
5f	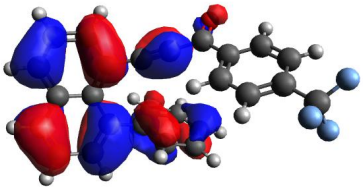	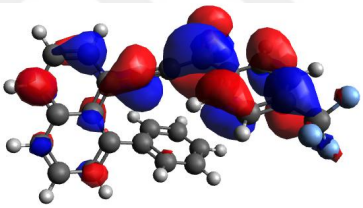	3.45
5g	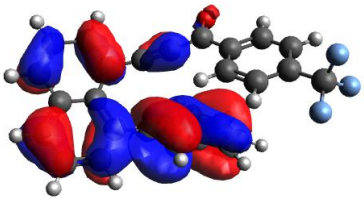	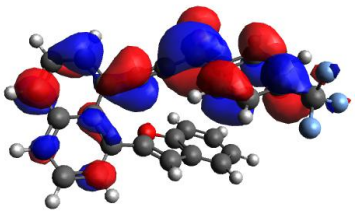	3.24
8	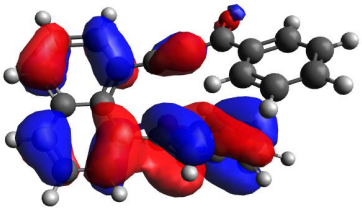	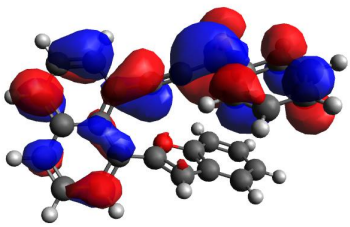	3.39

9	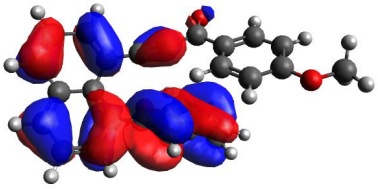	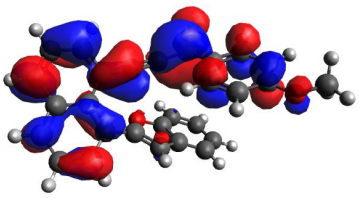	3.50

To further illustrate the spatial arrangement of the frontier orbitals, both the HOMO and LUMO of compound **5g** were plotted on the same molecular framework (Figure 27). The visualization reveals that the donor and acceptor units exhibit direct spatial contact at their interacting sites, leading to an effective overlap of frontier orbitals. Such overlap strongly supports the structural feasibility of through-space charge transfer in this compound.

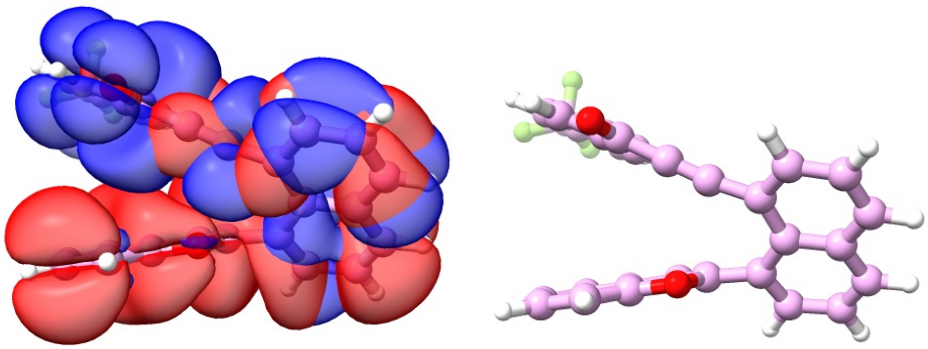

Figure 27. HOMO and LUMO orbitals of compound **5g** on the same molecular framework (left) and structure of compound **5g** (right)

To see whether the trends that are observed in experimental results are relevant in computational predictions as well, two graphs were plotted using the computational data. The predicted UV-Vis absorbance spectra for the compounds are given in Figure 27 and Figure 28. Figure 27 illustrates the effect of the acceptor group on the CT property. The result of the computed spectra predicts the CT bands at a longer wavelength as the electron deficiency of the acceptor group increases due to a lower HOMO-LUMO energy

gap. Calculated orbital energy difference for **5a** and **5b** is the biggest, so they are expected to have the smallest wavelength in their CT absorption and the graph supports this expectation. In the predicted absorption graph, **5g** has the longest absorption wavelength, followed by **8** and **9**, which is in correlation with the energy differences between HOMO and LUMO of these compounds. However, the experimental results for the comparison of compounds **5g**, **8**, and **9** were the opposite of this trend. This shows that there are other factors in the solution that affect this process, which are not considered by the computations. Figure 28 shows the effect of the donor group on the CT behavior. The HOMO-LUMO energy gap calculation seems to be in line with the absorption spectroscopy prediction. However, the experimental data do not fully match the computational trend. This might be coming from the error margins of the basis set and functional used in the calculations. Repeating the calculations with different basis sets and functionals may result in a better interpretation with more consistent data.

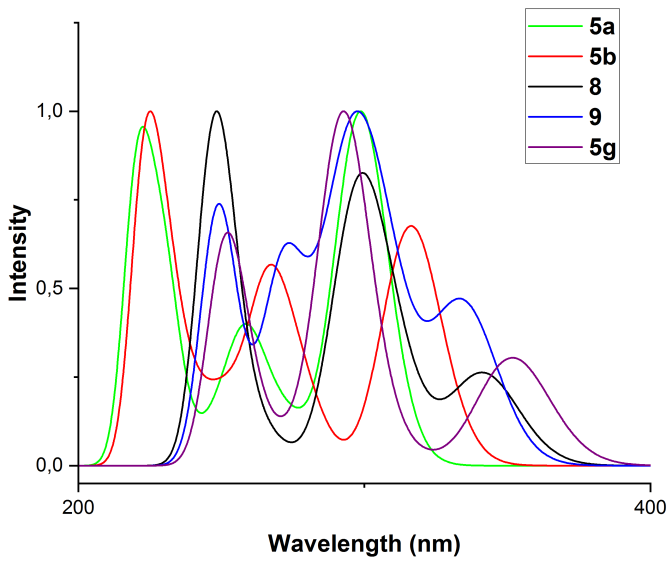

Figure 28. Predicted UV-Vis absorption spectra of compounds **5a**, **5b**, **8**, **9**, and **5g**

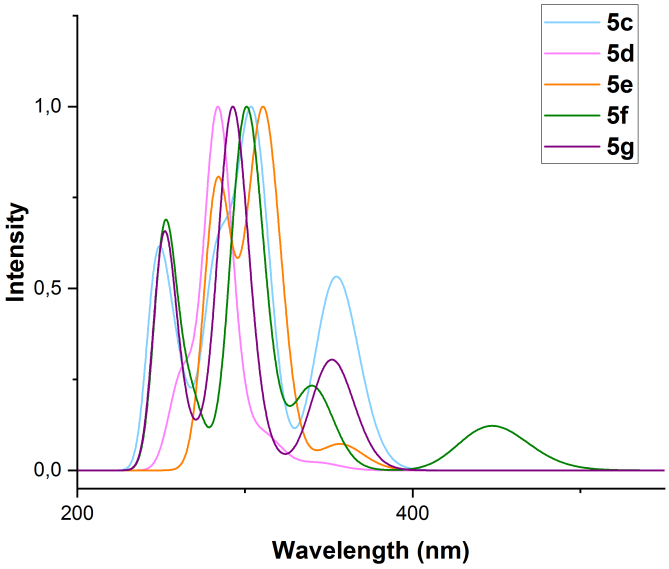

Figure 29. Predicted UV-Vis absorption spectra of compounds **5c**, **5d**, **5e**, **5f**, and **5g**

2.4.Effect of Solvents

2.4.1. Solvatochromism Behavior

In the next phase of our studies, the solvatochromism behaviour of compound **5b** was investigated. The amount of these shifts is low, which indicates that the structural changes during the CT process is not very significant. A blue shift is observed in the absorbance going from non-polar to polar solvents. In the emission spectra, however, a red shift is observed. Most generally, the solvatochromic trend follows as bathochromic or hypsochromic for both emission and absorption spectra. This symmetrical solvatochromism is a typical feature observed in hemicyanine dyes.[34] The reason for this property is that the ground state is stabilized by more polar solvents, thus excitation requires more energy. After the reorganization of solvent and the molecule, the molecule is stabilized more by the polar solvent, causing a red shift in the emission spectrum.

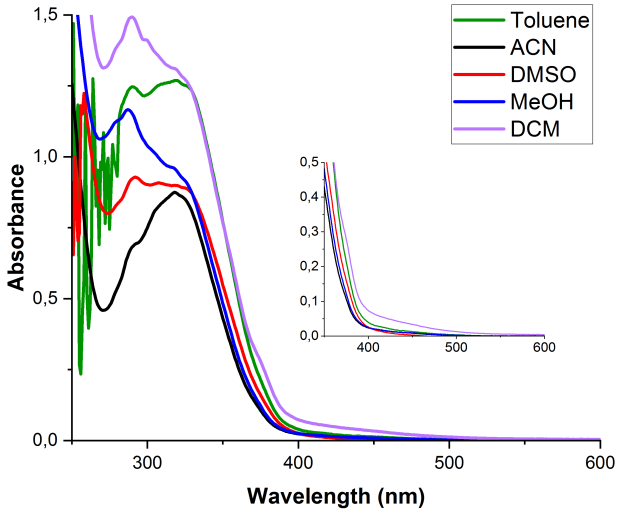

Figure 30. Absorption spectra of compound **5b** in different solvents (2.5×10^{5} M).

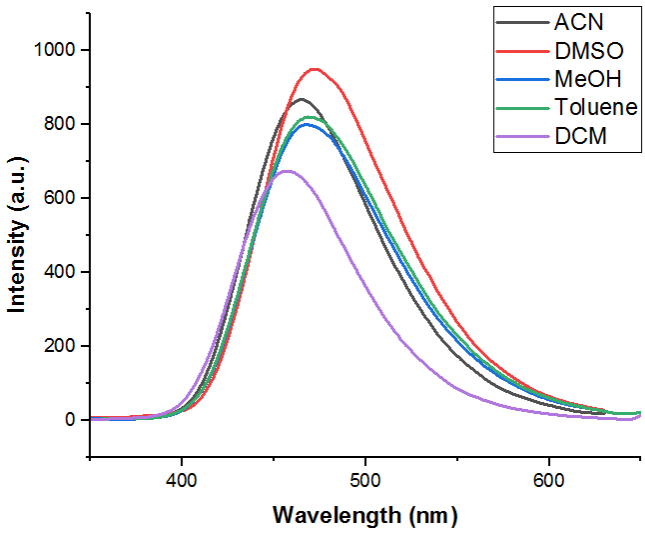

Figure 31. Emission spectra of compound **5b** in different solvents (2.5×10^{-5} M).

Absorption maxima, emission maxima, and Stokes shifts of the compound **5b** in different solvents are given in Table 4. The values show that there is an increase in the shift value in polar solvents. This increase indicates that there are structural changes and some energy is spent during the reorganization of the molecule and the solvent. After the reorganization process, the molecule is more stabilized by a polar solvent than a nonpolar one, so the energy released during the radiative relaxation is less in polar solvents.

Table 4. Absorption, emission, and Stokes shift values for compound **5b** in different solvents.

Solvent	Absorption (nm)	Emission (nm)	Stokes Shift (nm)	Dielectric Comstant (ε)
Toluene	378	450	72	2.4
DCM	380	460	80	9
MeOH	370	468	98	33
ACN	367	460	93	37
DMSO	368	475	89	47

2.4.2. Effect of Solvents on the Stability

Further experiments were performed on compound **9**, to investigate the effect of solvent on the stability of the molecule, where hydrogen bond donating solvents, and Lewis acids were used. When dissolved in 2,2,2-trifluoroethanol (TFE, pKa=12.4) , the compound was stable, and its λ_{max} value exhibited a hypsochromic shift, consistent with the solvatochromic behavior observed previously while going to a polar solvent. Then, a stronger hydrogen-donating solvent, 1,1,1,3,3,3-hexafluoroisopropanol (HFIP, pKa= 9.4), was used to probe the effect further. In this case, the color of the solution turned into dark brown, indicating that a reaction had occured. To confirm whether the compound gave a reaction or not, the NMR of the compound was analyzed. The NMR data revealed that the compound decomposed; however, it the decomposition product could not be identified.

To see the effect of a Lewis acid on the molecule, 1 equivalent of $Zn(OTf)_2$ was added to a solution of compound 9 in deuterated ACN, and changes were monitored by TLC and ^1H NMR spectroscopy. There was no change right after the addition of $Zn(OTf)_2$.

Over time, there were new spots on the TLC, and the NMR spectrum also showed new peaks while the peaks of compound **9** gradually decreased. After 4 days, the new spot on the TLC was isolated, and its NMR data were recorded to identify the compound. However, the structure of the newly formed compound could not be solved.

Boron trifluoride diethyl ether complex ($BF_3{\cdot}OEt_2$) was also used for the same study, where 1 equivalent of BF_3 was added to the compound **9**. A rapid color change from yellow to dark red was observed, and its ^{1}H-NMR spectrum also confirmed the change in the compound. Since the compound's NMR data after the addition of Lewis acids could not be assigned, the product or the reaction of the compound with the acid is unknown for now. Nevertheless, these results clearly show that the complexes are prone to decomposition under acidic conditions.

2.5.Photoluminescence Quantum Yields

Quantum yields of the compounds in DCM were determined using quinine sulfate as the reference material. The formula used for the calculations is as follows:

$$\Phi_X = \Phi_{ST}\left(\frac{Gradient_x}{Gradient_{ST}}\right)\left(\frac{\eta_x^2}{\eta_{ST}^2}\right)$$

Oxygen quenches the triplet excited state of the molecules and reduces the photoluminescence quantum yield.[52] Since it is uncertain for us whether the compounds' excited states include the triplet state, we needed to eliminate any possible quenching. Because of this possibility, the solvents were deoxygenated by purging N_2 gas to eliminate any quenching effect coming from the oxygen.

PLQY values are given in Table 5; they are all lower than 10%. Compounds **5e** and **5f** have very low fluorescence, so their quantum yields could not be determined. These low quantum yield values show that non-radiative relaxation routes dominate the relaxation process for these compounds.

Table 5. Photoluminescence Quantum Yield values of compounds in DCM

Compound	Excitation wavelength (nm)	Quantum Yield (%)
5a	320	8.9
5b	330	5.6
5c	320	0.7
5d	320	5.2
5e	-	-
5f	-	-
5g	320	2.2
8	310	4
9	310	2

The effect of solvent on the PLQY is investigated by measuring it in 5 different solvents with varying polarity. There is not a dramatic change in the quantum yield as the solvent changes. In MeOH and ACN, the yield is lower, probably due to a slight increase in the non-radiative relaxations in polar solvents. There is not a drastic increase in the DMSO, which means the viscosity is not an important factor that affects the system. In conclusion, the molecule's photoluminescence quantum yield is mostly affected by internal motions of the molecule rather than interactions with the solvent.

Table 6. Photoluminescence Quantum Yield values of compound **5b** in different solvents.

Solvent	Quantum Yield (%)
DCM	5.6
Toluene	7.1
ACN	5.2
MeOH	4.9
DMSO	5.9

2.6.Conclusion

In this study, the effect of different substituents on the previously designed through-space charge transfer model developed by our group was investigated. The main objective of the study was to understand how structural and electronic changes on the donor and the acceptor groups affect the charge transfer property. Seven new compounds were synthesized to achieve this by changing the donor and acceptor groups systematically, either by keeping the donor constant and modifying the acceptor group or by fixing the acceptor group and changing the donor.

The synthesis was carried out mainly by Suzuki and Sonogashira coupling reactions, along with the oxidation reaction. The compounds were obtained with good yields, and their characterization confirmed the formation of the desired products. Crystal structural and computational analyses supported the presence of required structural and electronic features for charge transfer.

Investigation of photophysical properties by UV-Vis absorption and fluorescence spectra confirmed the presence of charge transfer in the molecules with varying absorption and emission features depending on the nature of the donor and the acceptor. Computational analyses were also performed to rationalize the CT behavior of the complexes. The studies revealed that having an amide or ester group instead of ketone in the acceptor moiety reduces the CT property due to increased electron density on the acceptor alkyne moiety. However, it was seen that electron density is not the only factor that affect the CT property since the theoretical predictions do not fully align with the experimental data.

The solvatochromism behavior of compound **5b** was investigated; a hypsochromic shift in the emission and bathochromic shift in the absorption spectra were observed

going from a nonpolar solvent to a polar solvent. The compound is not stable in hydrogen bond donating solvents and Lewis acidic media. Lastly, the photoluminescence quantum yield of the compounds was around 7% and the quantum yield values are not significantly affected by the solvent properties.

Overall, a system that exhibits charge transfer property is developed with relatively easy synthesis, and its properties can be tuned by modifying the donor and acceptor groups. These features make this system a promising candidate for application purposes.

3. EXPERIMENTAL SECTION

3.1.Materials and Methods

The reactions were performed under inert conditions and in oven-dried glassware if needed. The solvents were deoxygenated by purging N_2 gas for the cross-coupling reactions. To monitor the progress of the reactions, TLC from Silicycle ultrapure silica gel (F-254 indicator) was used, and the spots were visualized by 254 nm UV light. For the purification of the products, flash column chromatography was performed using silica gel with 40-63 μm (230-400 mesh) particle size. All commercially available compounds were used from Sigma-Aldrich, TCI, Acros, abcr, Alfa Aesar, and Thermo Scientific.

For the characterization process, NMR, ATR-FTIR, UV-Vis Absorption spectroscopy, fluorescence spectroscopy, and Q-TOF/LCMS were used. Bruker Avance III 400 (^{1}H NMR 400 MHz, ^{13}C NMR 100 MHz, ^{19}F NMR 376 MHz) spectrometer was used at the National Research Center and Institute of Materials Science and Nanotechnology (UNAM) for the NMR measurements. Calibration of the spectra was done by either with internal standard TMS 0.0 ppm or the residual solvent peaks (signal of $CHCl_3$ in $CDCl_3$ at 7.26 ppm in ^{1}H NMR and at 77.16 ppm in ^{13}C NMR) for ^{1}H and ^{13}C NMR measurements, and external standard (signal of TFA at -76.55 ppm) for ^{19}F NMR measurements. For reporting the NMR spectra, chemical shifts, integrals, coupling constants, and multiplicities were used (s = singlet, d = doublet, dd = doublet of doublets, t = triplet, dt = doublet of triplet, q quartet, m = multiplet). ATR-FTIR measurements were utilized using Bruker Alpha Platinum. For mass spectrometry measurements, the Agilent Technologies 6224 Q-TOF/LC-MS instrument, for UV-Vis measurements Carry-5000 UV-Vis-NIR Spectrophotometer, and for the fluorescence measurements Carry, Eclipse Fluorescence Spectrophotometry at UNAM is used. Prof. Dr. Onur Şahin performed the crystallographic analysis at Sinop University.

3.2.Experimental Procedures

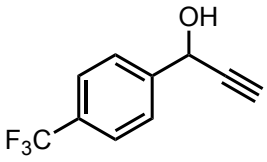

2

To an oven-dried 50 mL 2-neck round-bottomed flask, evacuation of the air and refilling with nitrogen was applied three times. Trimethylsilylacetylene (442 μL, 3.19 mmol) was transferred into the flask and dissolved in dry THF (13 mL). The resulting solution was cooled down to -78 °C and stirred for 10 min. *n*-BuLi (2M in hexane, 1.32 mL, 3.3 mmol) was added dropwise at -78 °C, and the reaction mixture was stirred for 10 min. The solution was warmed to 0 °C and stirred for 20 min. Then, the solution was cooled down to -78 °C and stirred for 30 min. 4-(trifluoromethyl)benzaldehyde (384 μL, 2.87 mmol) was dissolved in dry THF (3 mL) and transferred into the flask at -78 °C. The mixture was stirred at -78 °C for 10 min and then warmed up to 0 °C and stirred for 4.5 h. After 4.5 h, K_2CO_3 (130 mg) and MeOH (10 mL) were added to the mixture and stirred at room temperature for 2 h. After this time, the reaction was quenched with 5 mL of saturated aquesous solution of NH_4Cl and the resulting mixture was diluted with H_2O (10 mL). The crude product was extracted using EtOAc (3×20 mL). After filtration and concentration under reduced pressure, the crude product was purified by flash column chromatography (EtOAc:hexanes = 1:19 → 1:9) to afford compound **2** as a colorless oil (331 mg, 58%).

R_f: 0.22 (EtOAc:hexanes = 1:9)

TLC Visualization: UV-active under 254 nm light

^{1}H-NMR (400 MHz; $CDCl_3$) δ: 7.74 – 7.56 (m, 4H), 5.52 (d, *J* = 3.7 Hz, 1H), 2.70 (d, *J* = 2.3 Hz, 1H)

^{19}F NMR (376 MHz; $CDCl_3$) δ: -61.50

The ^{1}H NMR spectral data correlate with the spectral data given in the literature.[53]

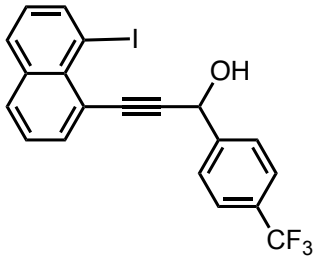

3c

To an oven-dried 50 mL 2-neck round-bottomed flask, evacuation of the air and refilling with nitrogen was applied three times. 1,8-Diiodonaphthalene (800 mg, 2.10 mmol) was put into the flask and dissolved in Et_3N (7 mL). $Pd(PPh_3)_2Cl_2$ (25.8 mg, 0.0368 mmol) and CuI (14.0 mg, 0.0735 mmol) were added to the mixture. Compound **2** (105 mg, 0.53 mmol) was dissolved in Et_3N (2 mL) and transferred into the flask dropwise. The walls of the flask were washed with additional Et_3N (2 mL), and THF (2mL) was added to dissolve the precipitates in the mixture. The reaction mixture was stirred at 23 °C for 2 h. After the full consumption of compound **2** was observed on TLC, the solvent was removed under reduced pressure. The crude product was extracted using EtOAc (3×12 mL). Then the combined organic phase was washed with H_2O (10 mL), and brine (4 mL). After filtration and concentration under reduced pressure, the crude product was purified by flash column chromatography (EtOAc:hexanes = 1:4) to afford compound **3c** as an orange solid (158 mg, 66%).

R_f: 0.29 (EtOAc:hexanes = 1:4)

TLC Visualization: UV active under 254 nm light

^{1}H-NMR (400 MHz; $CDCl_3$) δ: 8.27 (dd, *J* = 7.3, 1.1 Hz, 1H), 7.88 – 7.77 (m, 5H), 7.68 (d, *J* = 8.3 Hz, 2H), 7.42 (t, *J* = 8.0 Hz, 1H), 7.11 (t, *J* = 7.8 Hz, 1H), 5.86 (d, *J* = 5.0 Hz, 1H).

The ^{1}H NMR spectral data correlate with the spectral data given in the literature.[53]

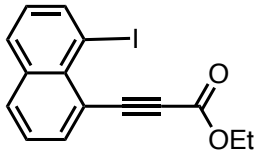

4b

To an oven-dried 50 mL 2-neck round-bottomed flask, evacuation of the air and refilling with nitrogen was applied three times. 1,8-Diiodonaphthalene (620 mg, 1.63 mmol) was put into the flask and dissolved in Et_3N (7 mL). $Pd(PPh_3)_2Cl_2$ (20.0 mg, 0.029 mmol) and CuI (10.9 mg, 0.057 mmol) were added to the mixture. Ethyl propiolate (40.0 mg, 0.41 mmol) was into the flask dropwise. The inner walls of the flask were washed with additional Et_3N (3 mL), and THF (2mL) was added to dissolve the precipitates in the mixture. The reaction was stirred at 23 °C for 4 h. After the full consumption of compound **2** was observed on TLC, the solvent was removed under reduced pressure. The crude product was extracted using EtOAc (3×13 mL). Then the combined organic phase was washed with H_2O (7 mL), and brine (2 mL). After filtration and concentration under reduced pressure, the crude product was purified by flash column chromatography (EtOAc:hexanes = 1:19) to afford compound **4b** as a brown oil (157.6 mg, 66.4%).

R_f: 0.41 (EtOAc:hexanes = 1:19)

TLC Visualization: UV active under 254 nm light

^{1}H-NMR (400 MHz; $CDCl_3$ δ: 8.31 (d, *J* = 7.3 Hz, 1H), 7.99 (d, *J* = 7.2 Hz, 1H), 7.91 (d, *J* = 8.1 Hz, 1H), 7.85 (d, *J* = 8.1 Hz, 1H), 7.45 (t, *J* = 7.7 Hz, 1H), 7.14 (t, *J* = 7.8 Hz, 1H), 4.33 (q, *J* = 7.0 Hz, 2H), 1.37 (t, *J* = 7.1 Hz, 3H).

The ^{1}H NMR spectral data correlate with the spectral data given in the literature.[54]

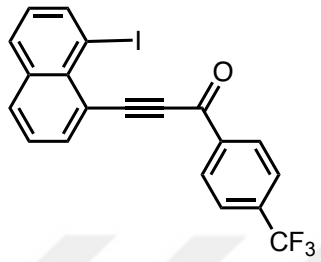

4c

Alkynol **2** (100 mg, 0.22 mmol) was put into a 50 mL round-bottomed flask and dissolved in acetone (9 mL). MnO_2 (382.5 mg, 4.40 mmol) was added, and the reaction was stirred at 23 °C for 2 h. After this time, full consumption of alkynol **2** was observed on TLC, the reaction was diluted with CH_2Cl_2 and filtered. Silica was added, and the solvent was removed under reduced pressure. The purification by flash column chromatography (EtOAc: hexanes= 1:7→1:5) yielded a yellow solid (91.0 mg, 92%).

R_f: 0.58 (EtOAc:hexanes = 1:5)

TLC Visualization: UV active under 254 nm light

^{1}H-NMR (400 MHz; $CDCl_3$): 8.42 (d, *J* = 8.1 Hz, 2H), 8.33 (dd, *J* = 7.4,1.1 Hz, 1H), 8.10 (dd, *J* = 7.3,1.3 Hz, 1H) 7.97 (dd, *J* = 8.2, 1.1 Hz, 1H), 7.90 (dd, *J* = 8.1, 0.8 Hz, 1H), 7.80 (d, *J* = 8.3 Hz, 2H), 7.52 (t, *J* = 8.0 Hz, 1H), 7.19 (t, *J* = 7.8 Hz, 1H).

The ^{1}H NMR spectral data correlate with the spectral data given in the literature.[53]

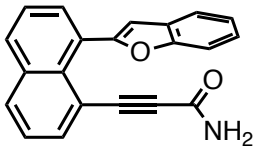

5a

In an oven-dried 25 mL Schlenk tube, air was evacuated and replaced with nitrogen gas via three vacuum–nitrogen cycles. Compound **4a** (25 mg, 0.078 mmol) was put into the flask and dissolved in 1,4-dioxane (1 mL). 2-Benzofuranboronic acid (25.2 mg, 0.156 mmol) and $Pd(PPh_3)_4$ (4.5 mg, 3.9×10^{-3} mmol) were added sequentially. The inner walls of the tube were washed with 1,4-dioxane (0.5 mL). K_3PO_4 (49.7 mg, 0.234 mmol) and H_2O (0.5 mL) were added. The reaction was stirred at 100 °C for 2 h 15 min. After the full consumption of compound **4a** was observed on TLC, the reaction was cooled down to room temperature and quenched with 5 mL H_2O. The crude mixture was extracted using CH_2Cl_2 (3×12 mL). Then the combined organic phase was washed with H_2O (5 mL), and the combined organic layers were dried over anhydrous Na_2SO_4. After filtration and concentration under reduced pressure, the crude product was purified by flash column chromatography (EtOAc:hexanes = 1:3 → 1:1) to afford compound **5a** as a yellow solid (15.8 mg, 65%).

R_f: 0.14 (EtOAc:hexanes = 1:2)

TLC Visualization: UV active under 254 nm light

^{1}H-NMR (400 MHz; $CDCl_3$) δ: 8.01 (dd, *J* = 8.2, 1.3 Hz, 2H), 7.97 (d, *J* = 7.2 Hz, 1H), 7.70 (t, *J* = 6.7 Hz, 2H), 7.65 – 7.58 (m, 2H), 7.54 (dd, *J* = 15.2, 7.8 Hz, 1H), 7.41 – 7.28 (m, 2H), 6.96 (s, 1H), 4.77 (s, 1H), 3.71 (s, 1H).

^{13}C NMR (100 MHz; $CDCl_3$) δ: 157.1, 154.7, 154.6, 137.9, 134.2, 131.9, 131.9, 131.6, 131.4, 129.6, 128.10 125.9, 125.8, 124.9, 123.5, 121.3, 117.4, 112.4, 106.1, 87.0, 85.0.

FTIR ν_{max} (ATR, solid)/cm^{-1}: 3450, 3310, 3177, 3059, 2195, 1655, 1589

HRMS (+APCI) Calculated for $C_{21}H_{13}NO_2$ $[M+H]^+$ 311.0946, found: 311.0939.

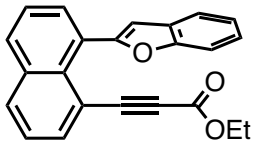

5b

In an oven-dried 25 mL Schlenk tube, air was evacuated and replaced with nitrogen gas via three vacuum–nitrogen cycles. Compound **4b** (48.0 mg, 0.14 mmol) was put into the flask and dissolved in 1,4-dioxane (1.5 mL). 2-Benzofuranboronic acid (44.4 mg, 0.27 mmol) and $Pd(PPh_3)_4$ (7.9 mg, 6.85×10^{-3} mmol) were added sequentially. The inner walls of the flask were washed with additional 1,4-dioxane (1 mL). K_3PO_4 (87.2 mg, 0.411 mmol), and H_2O (1.5 mL) were then added. The reaction was stirred at 100 °C for 2 h. After the full consumption of compound **4b** was observed on TLC, the reaction mixture was cooled down to room temperature and quenched with 5 mL H_2O. The crude mixture was extracted using CH_2Cl_2 (3× 12 mL). Then the combined organic phase was washed with H_2O (5 mL), the combined organic layers were dried over anhydrous Na_2SO_4. After filtration and concentration under reduced pressure, the crude product was purified by flash column chromatography (EtOAc:hexanes = 1:3 → 1:1) to afford compound **5b** as a yellow solid (33.7 mg, 75%).

R_f: 0.24 (EtOAc:hexanes = 1:19)

TLC Visualization: UV active under 254 nm light

^{1}H-NMR (400 MHz; $CDCl_3$) δ: 7.99 (d, *J* = 8.3 Hz, 2H), 7.87 (dd, *J* = 7.2, 1.2 Hz, 1H), 7.72 (dd, *J* = 7.0, 1.3 Hz, 1H), 7.68 – 7.63 (m, 1H), 7.54 (ddd, *J* = 19.7, 15.4, 7.8 Hz, 3H), 7.29 (dddd, *J* = 8.4, 7.3, 5.7, 1.2 Hz, 2H), 6.94 (d, *J* = 0.7 Hz, 1H), 3.74 (q, *J* = 7.1 Hz, 2H), 1.06 (t, *J* = 7.1 Hz, 3H).

^{13}C NMR (100 MHz; $CDCl_3$) δ: 156.0, 154.8, 153.53 136.3, 134.2, 132.4, 131.9, 131.5, 131.1, 129.7, 128.6, 125.9, 125.6, 124.3, 122.9, 121.3, 117.2, 112.1, 106.8, 84.8, 61.5, 14.0.

FTIR ν_{max} (ATR, solid)/cm^{-1}: 3056, 2980, 2213, 1703

HRMS (+APCI) Calculated for $C_{23}H_{16}O_3$ $[M+H]^+$ 340.1099, found: 340.1102.

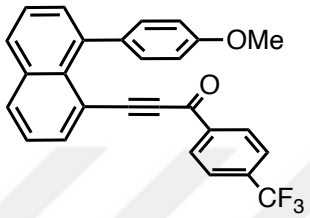

5c

Anhydrous DMF (4 mL) was transferred into a round-bottomed flask and degassed by bubbling nitrogen gas through the solvent for 15 min. In a separate oven-dried 25 mL Schlenk tube, air was evacuated and replaced with nitrogen gas via three vacuum–nitrogen cycles. Compound **4c** (26.4 mg, 0.059 mmol) was put into the flask and dissolved in DMF (2 mL). 4-Methoxyphenylboronic acid (9.9 mg, 0.064 mmol) and $Pd(PPh_3)_4$ (3.4 mg, 2.95×10^{-3} mmol) were added sequentially. The inner walls of the tube were washed with additional DMF (1 mL). K_2CO_3 (32.6 mg, 0.236 mmol) was then added. The reaction mixture was stirred at 80 °C for 20 h. After the full consumption of compound **4c** was observed on TLC, the reaction was cooled down to room temperature and quenched with distilled H_2O (5 mL). The aqueous mixture was extracted with dichloromethane (3 × 12 mL). The combined organic phase was washed with brine (3 mL) and water (3 mL), and was dried over anhydrous Na_2SO_4. After filtration and concentration under reduced pressure, the crude product was purified by flash column chromatography (EtOAc:hexanes = 1:19) to afford compound **5c** as a yellow solid (10.8 mg, 42%).

R_f: 0.65 (EtOAc:hexanes = 1:19 (×3 runs))

TLC Visualization: UV active under 254 nm light

^{1}H-NMR (400 MHz; $CDCl_3$) δ: 8.03 (dd, *J* = 8.2, 1.2 Hz, 1H), 8.00 (d, *J* = 8.7 Hz, 2H), 7.91 (dd, *J* = 8.2, 1.2 Hz, 1H), 7.86 (dd, *J* = 7.2, 1.3 Hz, 1H), 7.69 (d, *J* = 8.2 Hz, 2H), 7.61 – 7.43 (m, 3H), 7.33 – 7.27 (m, 2H), 6.67 – 6.61 (m, 2H), 3.52 (s, 3H).

^{13}C NMR (100 MHz; $CDCl_3$). δ: 176.6, 159.4, 140.0, 139.4, 135.7, 134.4, 134.4, 131.9, 130.3, 129.9, 128.6, 126.2, 125.4 (q, $J_{C\text{-}F}$ = 3.7 Hz), 125.1, 117.4, 113.6, 95.0, 94.3, 55.0, 29.9. (Because of the crowded nature of the aromatic region, it was not possible to reliably identify the two quartets associated with ^{13}C–^{19}F couplings.)

^{19}F NMR (376 MHz; $CDCl_3$) δ: -61.97

FTIR ν_{max} (ATR, solid)/cm^{-1}: 2961, 2922, 2852, 2181, 1643.

HRMS (+APCI) Calculated for $C_{27}H_{17}F_3O_2$ $[M+H]^+$ 430.1181, found: 430.1175.

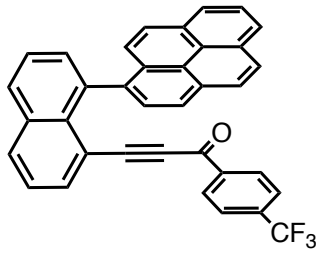

5e

H_2O (2 mL) and 1,4-dioxane (4 mL) were put into a round-bottomed flask, degassed by bubbling nitrogen gas through the solvent for 15 min. In a separate oven-dried 25 mL Schlenk tube, air was evacuated and replaced with nitrogen gas via three vacuum–nitrogen cycles. Compound **4c** (25.0 mg, 0.056 mmol) was put into the flask and dissolved in 1,4-dioxane (1 mL). 1-Pyreneboronic acid (15.0 mg, 0.061 mmol), $Pd(PPh_3)_4$ (4.5 mg, 3.89×10^{-3} mmol), and K_3PO_4 (35.3 mg, 0.166 mmol) were added sequentially. The inner walls of the tube were washed with additional solvent (2 mL). The reaction

was stirred at 100 °C for 20 h. After the full consumption of compound **4c** was observed on TLC, the reaction was cooled down to room temperature and quenched with 5 mL H_2O. The crude mixture was extracted using EtOAc (3 × 13 mL). Then the combined organic phase was washed with H_2O (5 mL). After filtration and concentration under reduced pressure, the crude product was purified by flash column chromatography (EtOAc:hexanes = 1:19) to afford compound **5e** as a yellow solid (18.3 mg, 63%).

R_f: 0.45 (EtOAc:Hexanes = 1:19 (×2 runs))

TLC Visualization: UV active under 254 nm light

^{1}H-NMR (400 MHz; $CDCl_3$) δ: 8.12 (dd, *J* = 8.3, 1.2 Hz, 1H), 8.10 (dd, *J* = 8.0, 1.5 Hz, 1H), 8.03 (dt, *J* = 10.8,7.8 Hz, 3H), 7.89-7.86 (m, 3H), 7.80 (d, *J* = 8.9 Hz, 1H), 7.76 – 7.66 (m, 4H), 7.60 (d, *J* = 9.2 Hz, 1H), 7.53 (dd, *J* = 8.1, 7.3 Hz, 1H), 6.73 (dd, *J* = 39.9,8.2 Hz, 4H).

^{13}C NMR (100 MHz; $CDCl_3$) δ: 175.4, 134.7, 131.6, 131.5, 130.9, 129.4, 129.3, 128.1, 127.8, 127.6, 127.1, 126.3, 126.2, 125.4, 125.2, 125.2, 125.0, 124.5, 123.9 (q, $J_{C\text{-}F}$ = 3.7 Hz), 117.6, 93.6, 91.9. (Because of the crowded nature of the aromatic region, it was not possible to reliably identify the two quartets associated with ^{13}C–^{19}F couplings.)

^{19}F NMR (376 MHz; $CDCl_3$) δ: -62.20

FTIR νmax (ATR, solid)/cm^{-1}: 3047, 2927, 2852, 2185, 1643.

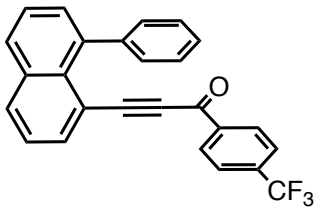

5f

H_2O (2 mL) and 1,4-dioxane (4 mL) were was transferred into a round-bottomed flask and degassed by bubbling nitrogen gas through the solvent for 15 min. In a separate oven-

dried 25 mL Schlenk tube, air was evacuated and replaced with nitrogen gas via three vacuum–nitrogen cycles. Compound **4c** (25.0 mg, 0.056 mmol) was put into the flask and dissolved in the solvent (1 mL). Phenylboronic acid (7.4 mg, 0.061 mmol), $Pd(PPh_3)_4$ (4.5 mg, 3.89×10^{-3} mmol), and K_3PO_4 (35.3 mg, 0.166 mmol) were added sequentially. The inner walls of the tube were washed with additional solvent (1.5 mL). The reaction was stirred at 100 °C for 42 h. After this time, the reaction was cooled down to room temperature and quenched with 5 mL H_2O. The crude mixture was extracted using EtOAc (3 ×13 mL). Then the combined organic phase was washed with H_2O (3 mL), and brine (2 mL). After filtration and concentration under reduced pressure, the crude product was purified by flash column chromatography (DCM: hexanes = 1:2 → 1:1) to afford compound **5f** as a yellow solid (7.9 mg, 36%).

R_f: 0.59 (DCM:hexanes = 2:1)

TLC Visualization: UV active under 254 nm light

^{1}H-NMR (400 MHz; $CDCl_3$): 8.0 (dd, *J* = 8.2, 1.1 Hz, 1H), 7.96-7.92 (m, 3H), 7.87 (dd, *J* = 7.2, 1.3 Hz, 1H), 7.68 (d, *J* = 8.2 Hz, 2H), 7.59 (dd, *J* = 8.1, 7.2 Hz, 1H), 7.52 (dd, *J* = 8.1, 7.3 Hz, 1H), 7.47 (dd, *J* = 7.1, 1.3 Hz, 1H), 7.41 (dd, *J* = 8.1, 1.2 Hz, 2H), 7.16 (t, *J* = 7.6 Hz, 2H), 7.08 – 6.97 (m, 1H).

^{13}C NMR (100 MHz; $CDCl_3$): 176.5, 142.0, 140.3, 139.3, 135.9, 134.4, 132.0, 130.5, 130.5, 130.0, 128.8, 128.1, 128.0, 126.2, 125.4 (q, $J_{C\text{-}F}$ = 3.7 Hz), 125.2, 117.3, 94.6, 94.2. (Because of the crowded nature of the aromatic region, it was not possible to reliably identify the two quartets associated with ^{13}C–^{19}F couplings.)

^{19}F NMR (376 MHz; $CDCl_3$) δ: -62.11

FTIR ν_{max} (ATR, solid)/cm^{-1} : 2956, 2922, 2852, 2187, 1644.

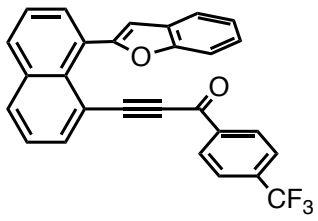

5g

Anhydrous DMF (5 mL) was transferred into a round-bottomed flask and degassed by bubbling nitrogen gas through the solvent for 15 min. In a separate oven-dried 25 mL Schlenk tube, air was evacuated and replaced with nitrogen gas via three vacuum–nitrogen cycles. Compound **4c** (20.0 mg, 0.044 mmol) was put into the flask and dissolved in the solvent (1 mL). Benzofuran-2-boronic acid (7.9 mg, 0.049 mmol), $Pd(PPh_3)_4$ (2.6 mg, 2.2×10^{-3} mmol), and K_2CO_3 (24.3 mg, 0.176 mmol) were added sequentially. The inner walls of the tube were washed with additional solvent (1.5 mL). The reaction was stirred at 80 °C for 20 h. After this time, the reaction mixture was cooled down to room temperature and quenched with 5 mL H_2O. The crude mixture was extracted using EtOAc (3 ×13 mL). Then the combined organic phase was washed with H_2O (3 mL) and brine (2 mL). After filtration and concentration under reduced pressure, the crude product was purified by flash column chromatography (EtOAc:hexanes = 1:19 → 1:9) to afford compound **5g** as an orange solid (10.9 mg, 56%).

R_f: 0.46 (EtOAc:hexanes = 1:19)

TLC Visualization: UV active under 254 nm light

^{1}H-NMR (400 MHz; $CDCl_3$) δ: 8.05 (t, *J* = 7.6 Hz, 2H), 7.96 (d, *J* = 7.2 Hz, 1H), 7.79 – 7.72 (m, 3H), 7.68 – 7.51 (m, 4H), 7.20 (d, *J* = 8.2 Hz, 1H), 7.13 (d, *J* = 7.7 Hz, 1H), 7.02 – 6.94 (m, 1H), 6.90 (t, *J* = 7.4 Hz, 1H), 6.86 (s, 1H)

^{13}C NMR (100 MHz; $CDCl_3$) δ: 175.7, 155.9, 154.14 138.8, 136.0, 134.3, 132.5, 131.9, 131.8, 131.2, 129.6, 129.3, 128.5, 126.1, 125.7, 125.1 (q, $J_{C\text{-}F}$ = 3.7 Hz), 124.4, 122.99, 121.0, 117.2, 111.9, 107.0, 93.4, 91.0. (Because of the crowded nature of the aromatic

region, it was not possible to reliably identify the two quartets associated with $^{13}C–^{19}F$ couplings.)

^{19}F NMR (376 MHz; $CDCl_3$) δ: -63.13

FTIR ν_{max} (ATR, solid)/cm^{-1}: 2923, 2852, 2186, 1643.

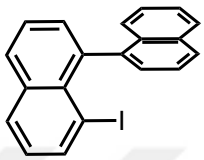

6

Anhydrous DMF (4 mL) was transferred into a round-bottomed flask and degassed by bubbling nitrogen gas through the solvent for 15 min. In a separate oven-dried 25 mL Schlenk tube, air was evacuated and replaced with nitrogen gas via three vacuum–nitrogen cycles. 1,8-Diiodonaphthalene (50 mg, 0.13 mmol) was put into the flask and dissolved in DMF (2 mL). 1-naphthylboronic acid (172 mg, 0.15 mmol), $Pd(PPh_3)_4$ (7.6 mg, 6.6×10^{-3} mmol), and K_2CO_3 (73.0 mg, 0.53 mmol) were added sequentially. The inner walls of the tube were washed with additional DMF (0.5 mL). The reaction was stirred at 80 °C for 24 h. After this time, the reaction was cooled down to room temperature and quenched with distilled H_2O (5 mL). The aqueous mixture was extracted with dichloromethane (3 × 12 mL). Then the combined organic phase was washed with brine (3 mL) and water (3 mL), and the combined organic layers were dried over anhydrous Na_2SO_4. After filtration and concentration under reduced pressure, the crude product was purified by flash column chromatography (only hexanes) to afford compound **6** as a yellow solid (39.2 mg, 78%).

R_f: 0.32 (only hexanes)

TLC Visualization: UV active under 254 nm light

^{1}H-NMR (400 MHz; $CDCl_3$) δ : 8.18 (dd, *J* = 7.3, 1.2 Hz, 1H), 8.02 – 7.96 (m, 3H), 7.94 (d, *J* = 8.2 Hz, 1H), 7.61 – 7.53 (m, 3H), 7.49 (ddd, *J* = 8.1, 6.6, 1.4 Hz, 1H), 7.43 (dd, *J* = 7.0, 1.2 Hz, 1H), 7.34 (ddd, *J* = 7.8, 6.6, 1.2 Hz, 1H), 7.31 – 7.24 (m, 1H), 7.12 (dd, *J* = 8.0, 7.4 Hz, 1H).

^{13}C NMR (100 MHz; $CDCl_3$) δ: 142.6, 139.3, 139.0, 135.4, 135.3, 133.5, 132.3, 131.9, 130.2, 130.0, 129.5, 128.2, 128.2, 126.8, 126.7, 126.1, 125.8, 125.4, 125.3, 91.8.

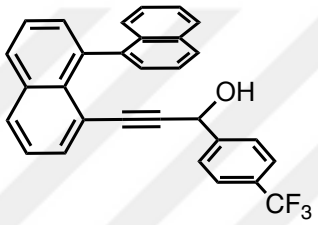

7

Et_3N (4 mL) was transferred into a 50 mL 2-neck round-bottomed flask and degassed by bubbling nitrogen gas through the solvent for 15 min. To an oven-dried 50 mL round-bottomed flask, air was evacuated and replaced with nitrogen gas via three vacuum–nitrogen cycles. Compound **6** (40.0 mg, 0.105 mmol) was put into the flask and dissolved in Et_3N (1.5 mL). $Pd(PPh_3)_2Cl_2$ (5.2 mg, 7.35×10^{-3} mmol) and CuI (2.8 mg, 0.015 mmol) were added to the mixture. Compound **2** (105 mg, 0.53 mmol) was dissolved in Et_3N (1 mL) and transferred into the flask dropwise. The inner walls of the flask were washed with additional Et_3N (1.5 mL). The reaction mixture was stireed at 70 °C for 48 h. After this time, the mixture was concentrated under reduced pressure. The crude product was extracted using EtOAc (3 × 13 mL). Then the combined organic phase was washed with H_2O (10 mL). After filtration and concentration under reduced pressure, the crude product was purified by flash column chromatography (EtOAc: hexanes = 1:9 →1:7) to afford product **7** as an orange solid (12.0 mg, 25%).

R_f: 0.11 (EtOAc:hexanes = 1:5)

TLC Visualization: UV active under 254 nm light

^{1}H-NMR (400 MHz; $CDCl_3$) δ: 8.03 – 7.94 (m, 2H), 7.87 (d, *J* = 8.0 Hz, 1H), 7.75 (d, *J* = 8.2 Hz, 1H), 7.63 – 7.58 (m, 2H), 7.58 – 7.38 (m, 8H), 7.38 – 7.29 (m, 2H), 7.02 (d, *J* = 8.4 Hz, 2H), 4.88 (d, *J* = 6.4 Hz, 1H).

^{13}C NMR (100 MHz; $CDCl_3$) δ: 144.2, 141.5, 138.0, 135.2, 134.5, 134.4, 132.8, 131.9, 131.0, 130.4, 129.3, 128.1, 127.9, 127.4, 126.8, 126.7, 126.5, 126.2, 125.8, 125.4 (d, *J*_C-F = 2.7 Hz), 125.3 (d, *J*_C-F = 3.8 Hz), 119.43 94.1, 87.3, 63.6. (Because of the crowded nature of the aromatic region, it was not possible to reliably identify the two quartets associated with ^{13}C–^{19}F couplings.)

^{19}F NMR (376 MHz; $CDCl_3$) δ: -61.85

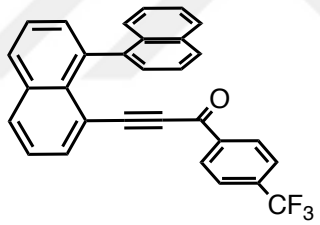

5d

Compound 7 (25.0 mg, 0.056 mmol) was put into a 50 mL round-bottomed flask and dissolved in acetone (3 mL). MnO_2 (46.1 mg, 53 mmol) was added, and the reaction was stirred at room temperature for 72 h. After this time, the reaction mixture was diluted with CH_2Cl_2 and filtered. Silica was added to the solution for dry loading, and the solvent was removed under reduced pressure. The purification by flash column chromatography (EtOAc: hexanes= 1:9 → 1:7→1:5) yielded a yellow solid (7.3 mg, 61%).

R_f: 0.55 (EtOAc:hexanes = 1:5)

TLC Visualization: UV active under 254 nm light

^{1}H-NMR (400 MHz; $CDCl_3$) δ: 8.09 (dd, *J* = 8.2, 1.1 Hz, 1H), 8.03 (dd, *J* = 8.3, 1.1 Hz, 1H), 7.73 (dd, *J* = 7.2, 1.3 Hz, 1H), 7.66 (dd, *J* = 8.1, 7.1 Hz, 1H), 7.54 (dd, *J* = 6.9, 1.3 Hz, 1H), 7.53 – 7.39 (m, 9H), 7.38 – 7.28 (m, 3H), 7.27 – 7.20 (m, 1H)

^{13}C NMR (100 MHz; $CDCl_3$) δ: 176.2, 139.3, 139.1, 137.9, 135.2, 134.4, 133.9, 133.4, 132.0, 131.8, 131.0, 129.4, 129.2, 129.2, 128.9, 128.3, 126.2, 126.2, 126.0, 125.9, 125.3 (dd, $J_{C\text{-}F}$ = 7.9, 3.9 Hz), 117.4, 100.2, 94.4, 92.4. (Because of the crowded nature of the aromatic region, it was not possible to reliably identify the two quartets associated with ^{13}C–^{19}F couplings.)

^{19}F NMR (376 MHz; $CDCl_3$) δ: -62.45

FTIR νmax (ATR, solid)/cm^{-1}: 2961, 2924, 2853, 2186, 1645

HRMS (+APCI) Calculated for $C_{23}H_{16}O_3$ $[M+H]^+$ 432.1326, found: 432.1322.

4. APPENDIX

4.1.NMR Data

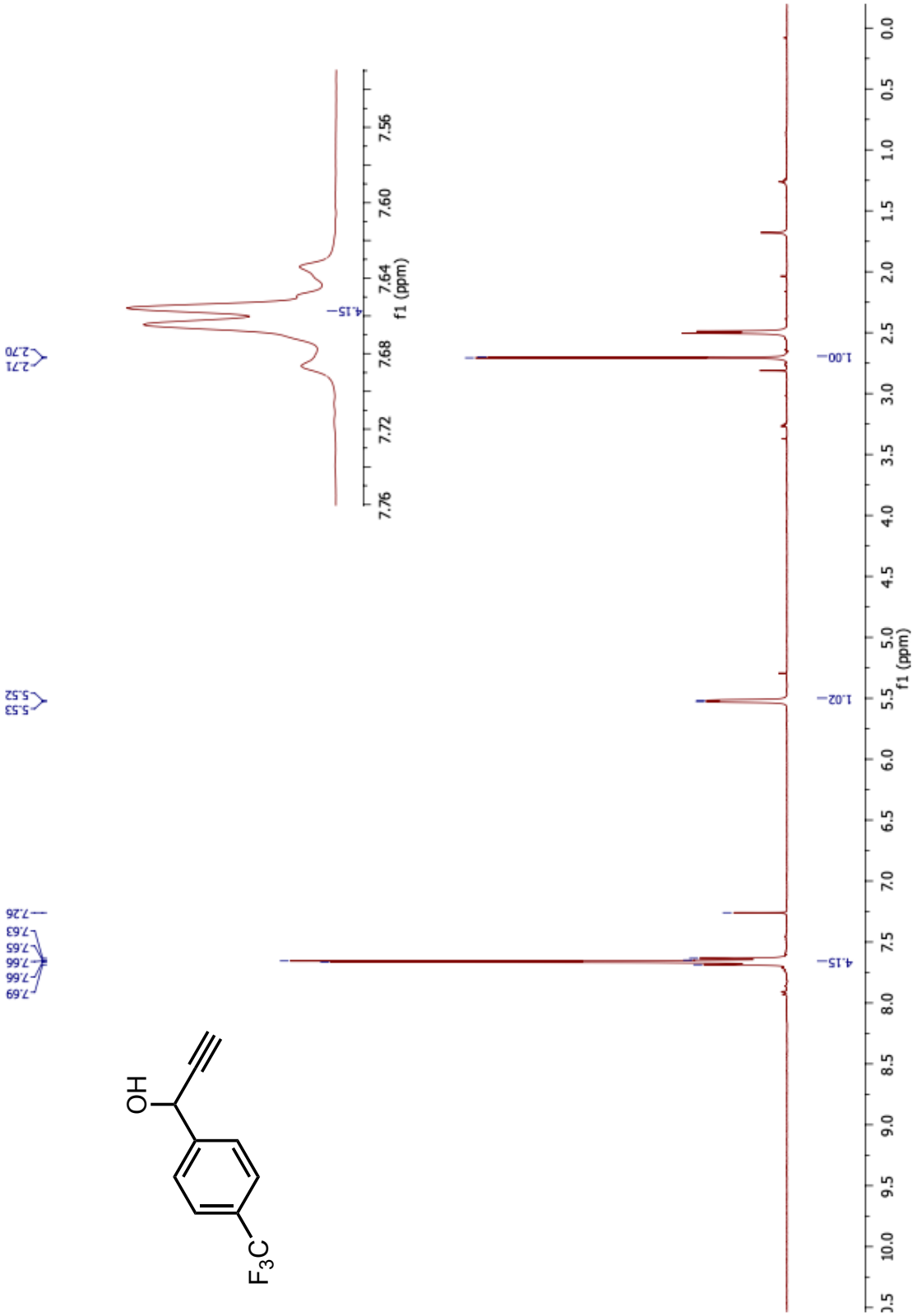

Figure 32. ^{1}H-NMR spectrum of compound **2** in $CDCl_3$

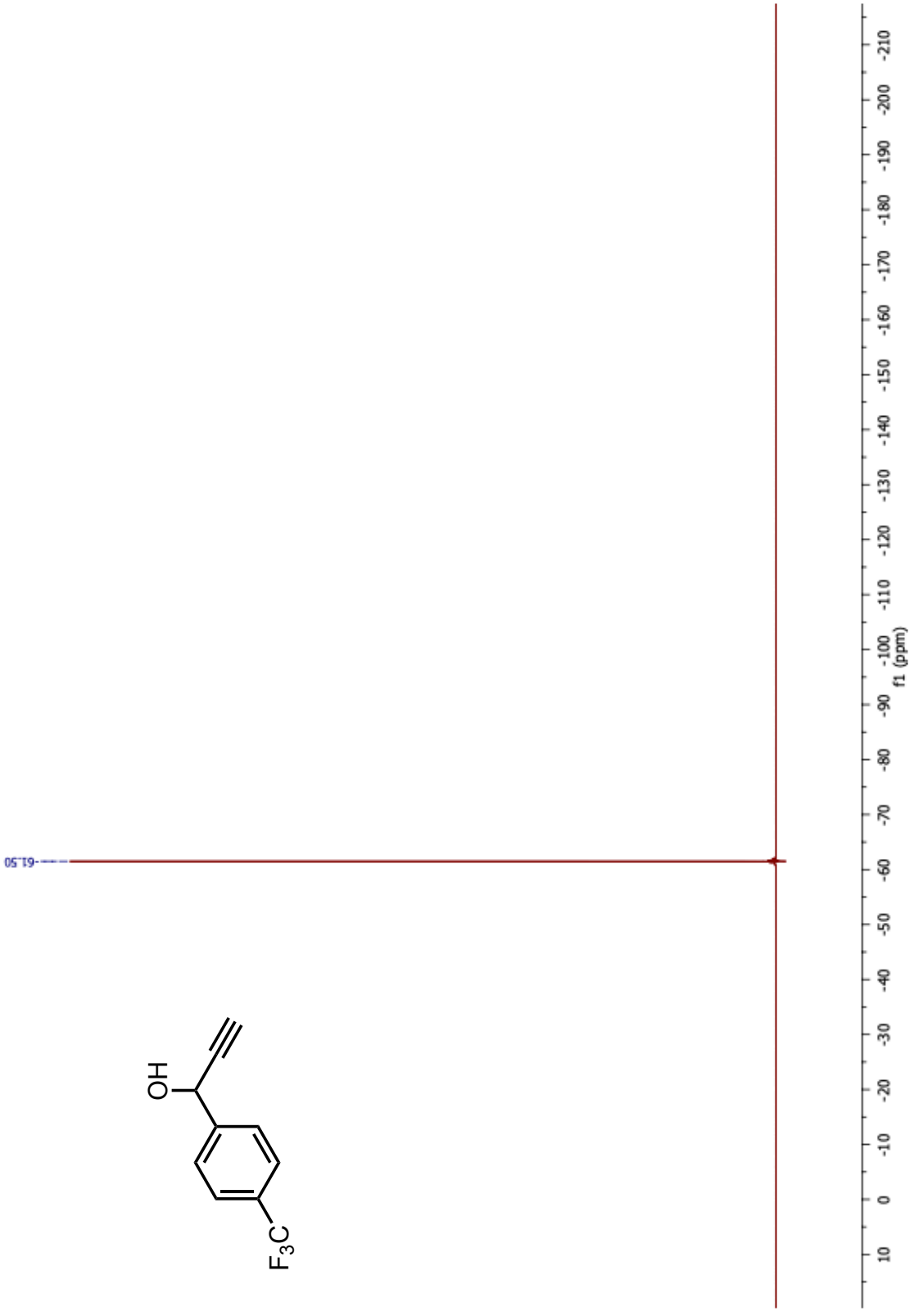

Figure 33. ^{19}F-NMR spectrum of compound **2** in $CDCl_3$

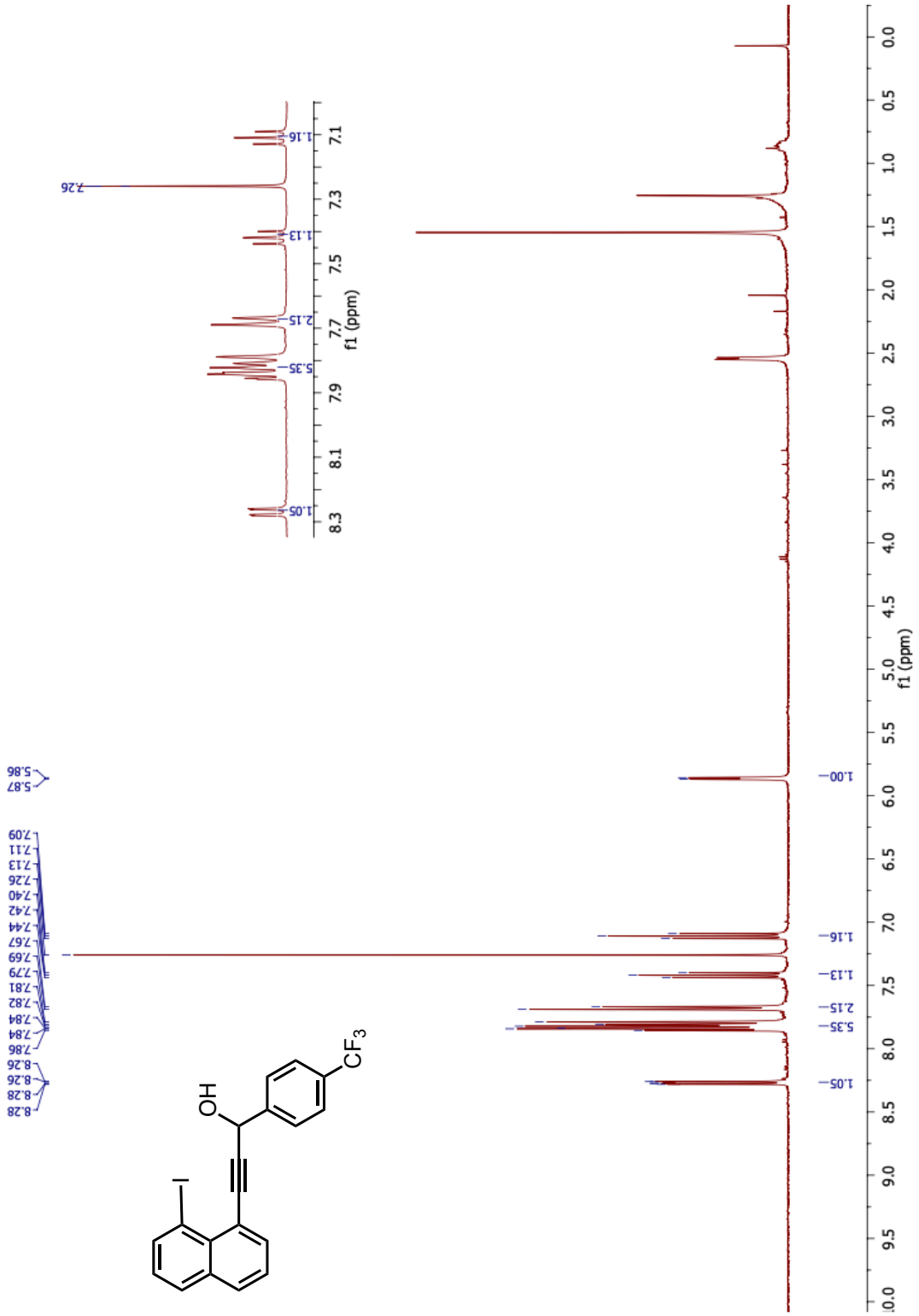

Figure 34. ^{1}H-NMR spectrum of compound **3c** in $CDCl_3$

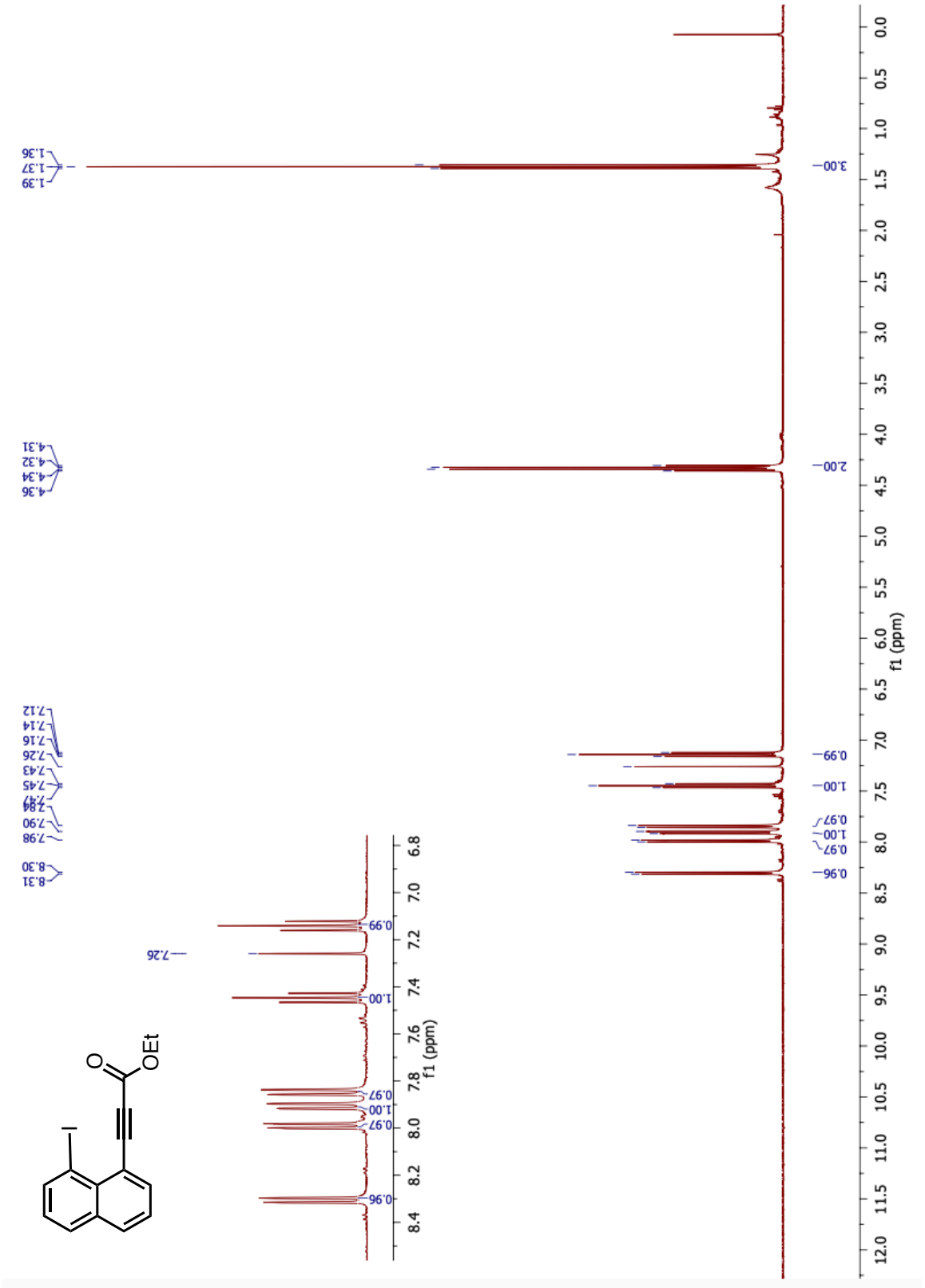

Figure 35. ^{1}H-NMR spectrum of compound **4b** in $CDCl_3$

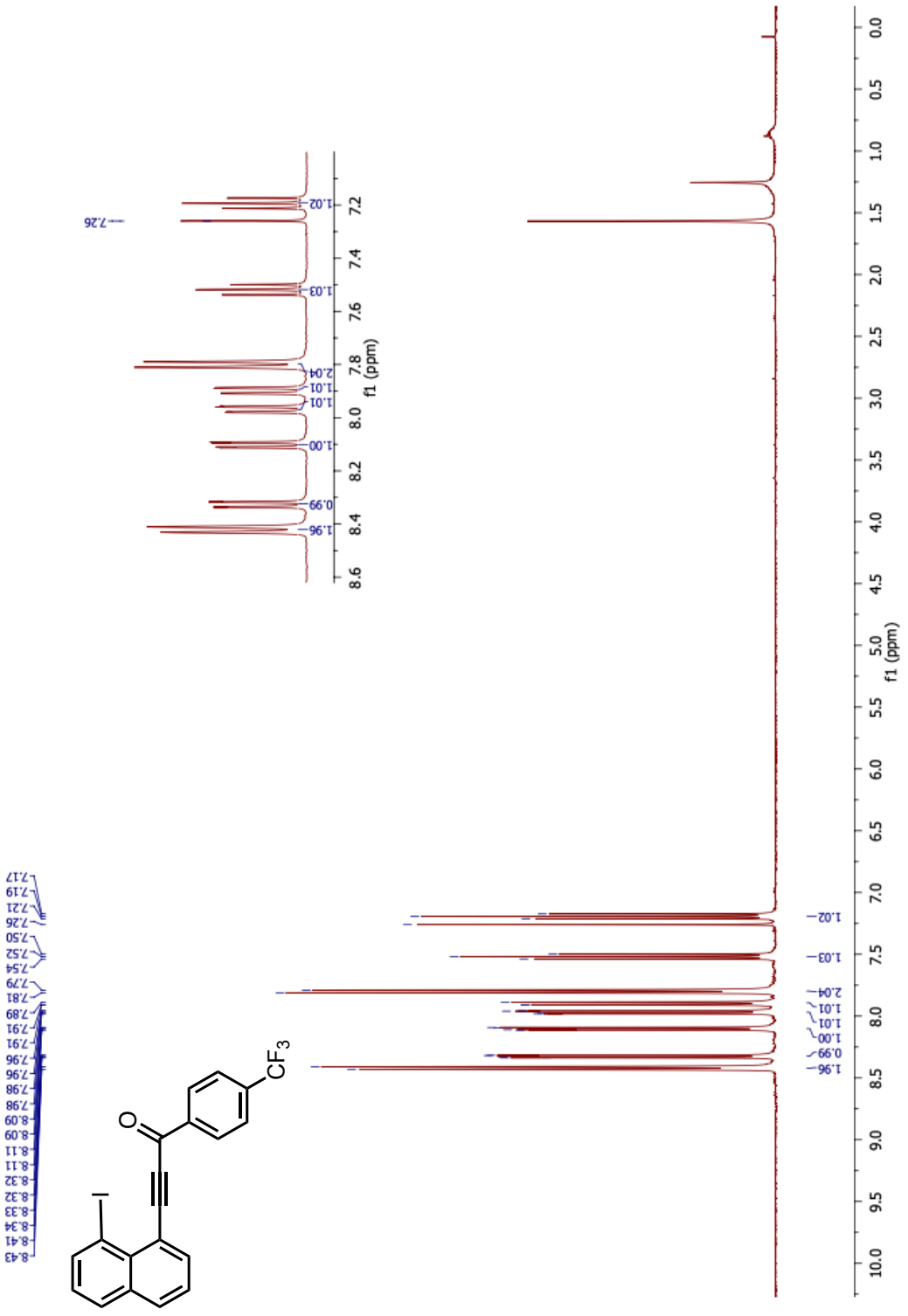

Figure 36. ^{1}H-NMR spectrum of compound **4c** in $CDCl_3$

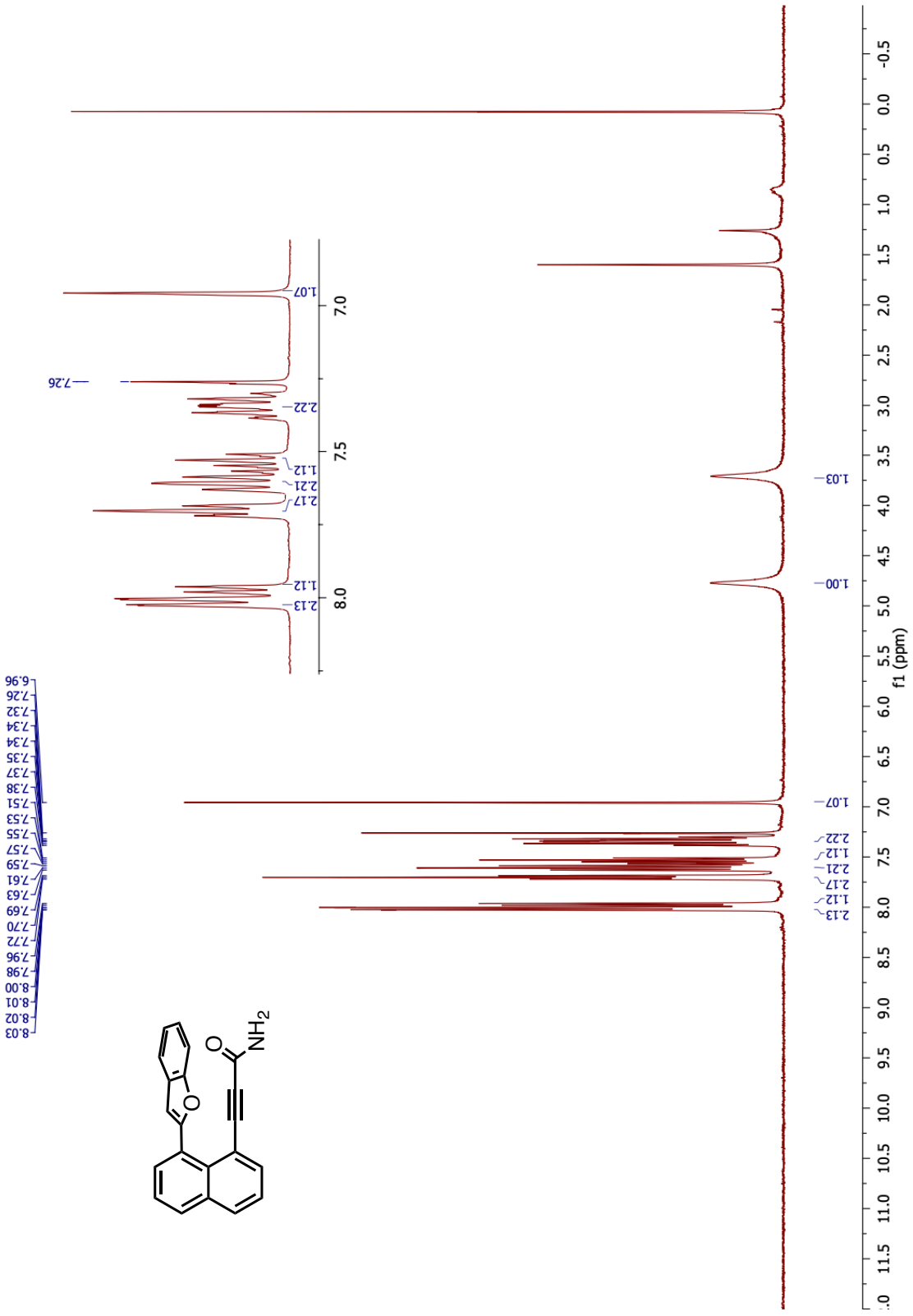

Figure 37. ^{1}H-NMR spectrum of compound **5a** in $CDCl_3$

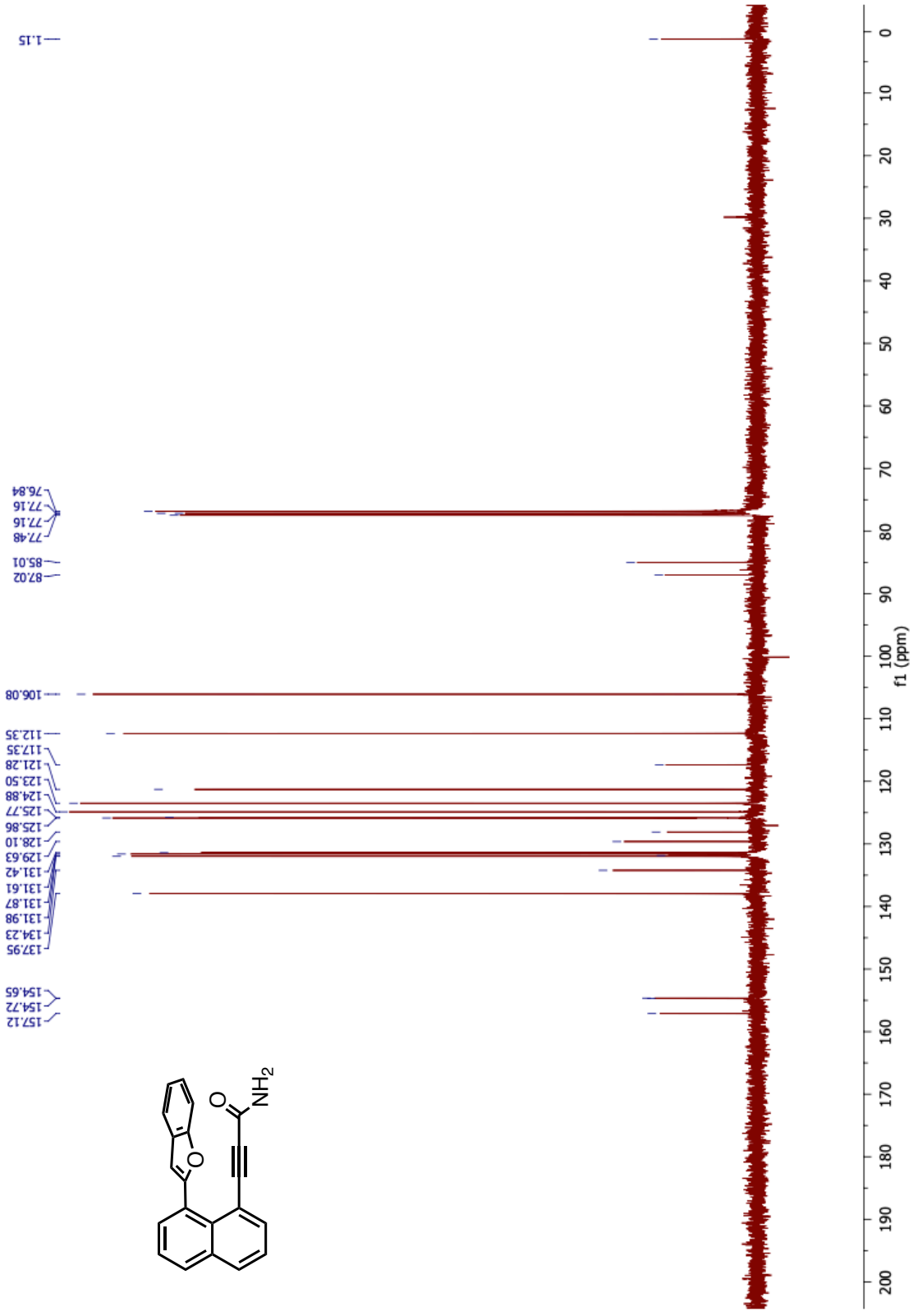

Figure 38. ^{13}C-NMR spectrum of compound **5a** in $CDCl_3$

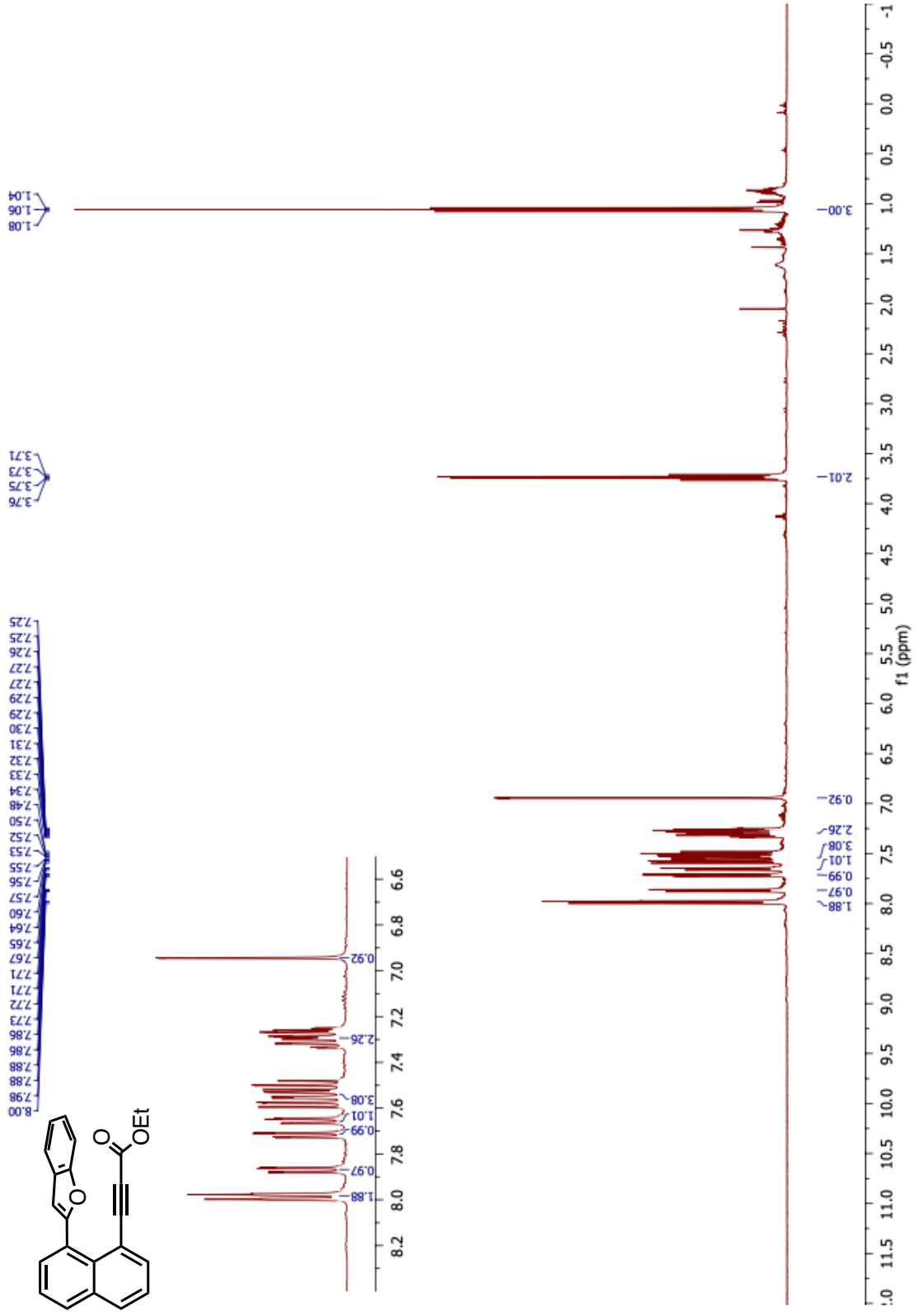

Figure 39. ^{1}H-NMR spectrum of compound **5b** in $CDCl_3$

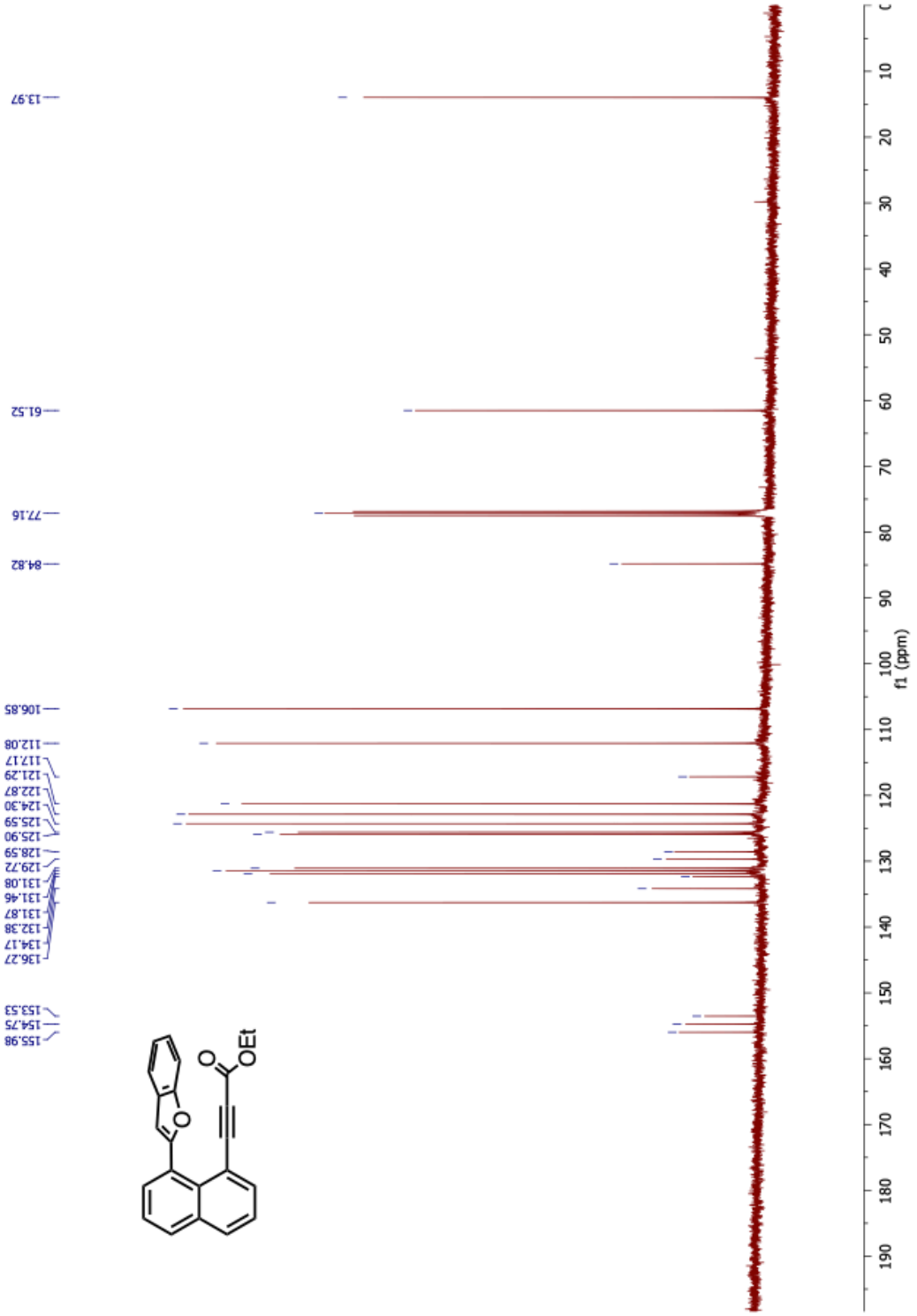

Figure 40. ^{13}C-NMR spectrum of compound **5b** in $CDCl_3$

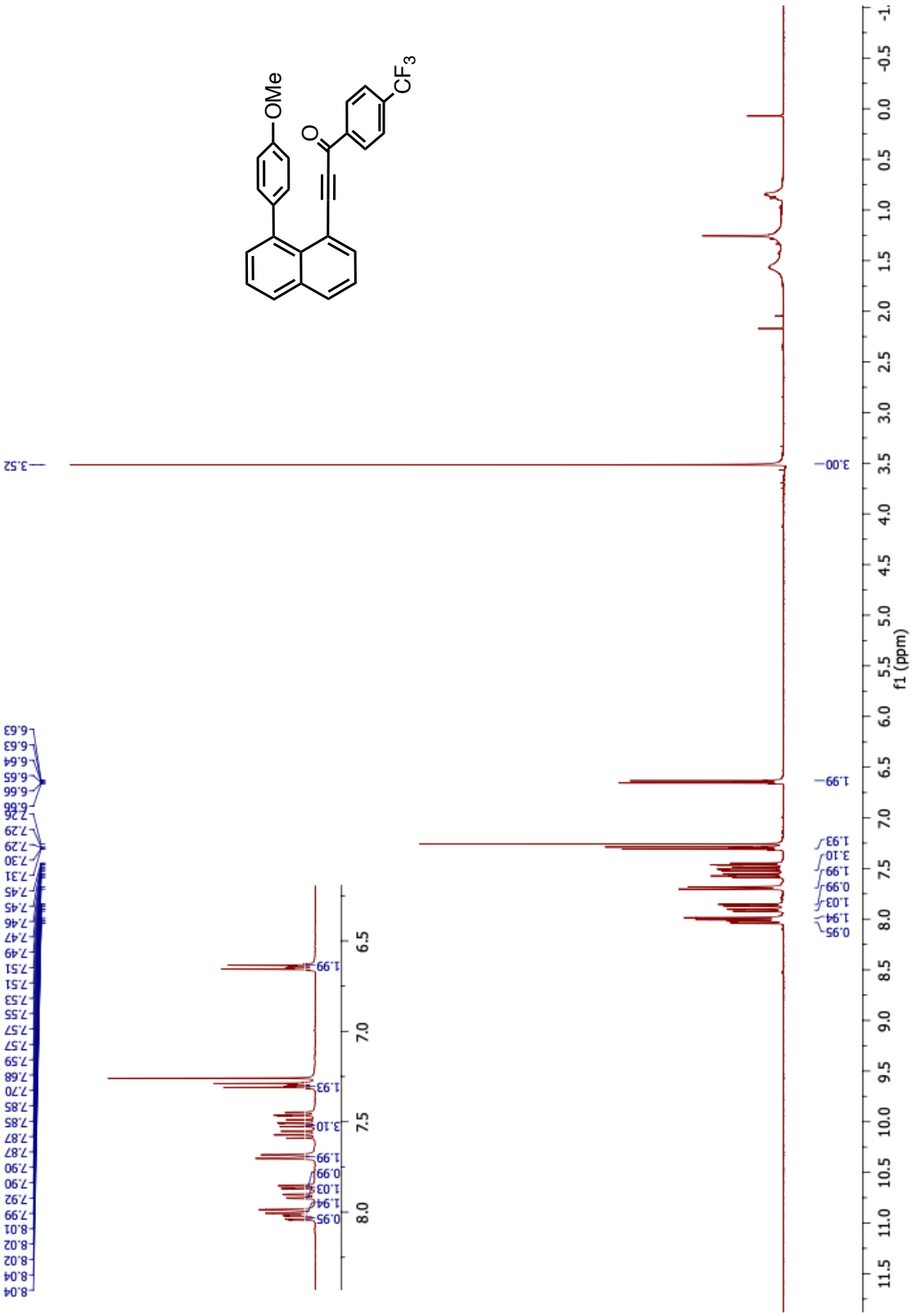

Figure 41. ^{1}H-NMR spectrum of compound **5c** in $CDCl_3$

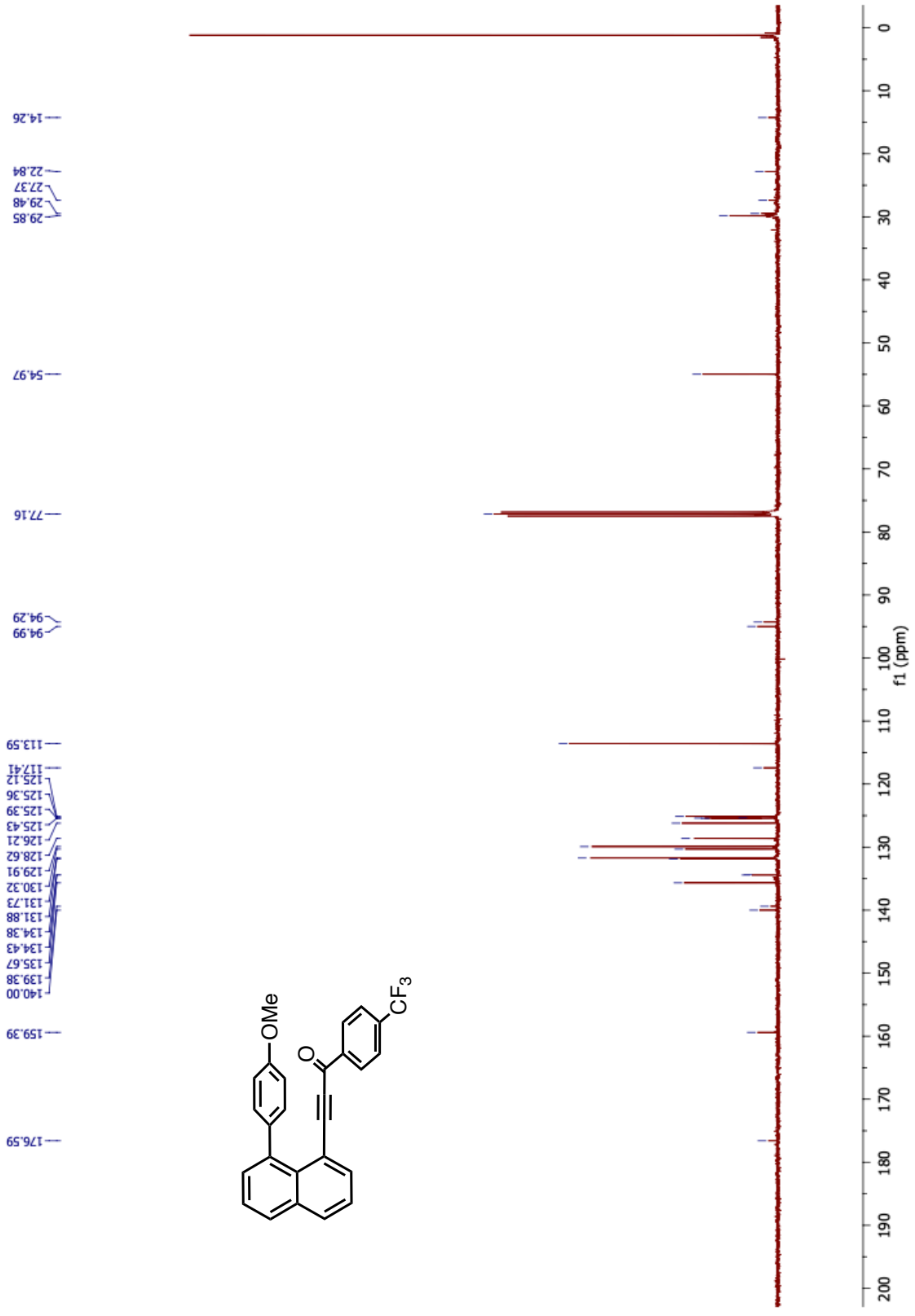

Figure 42. ^{13}C-NMR spectrum of compound **5c** in $CDCl_3$

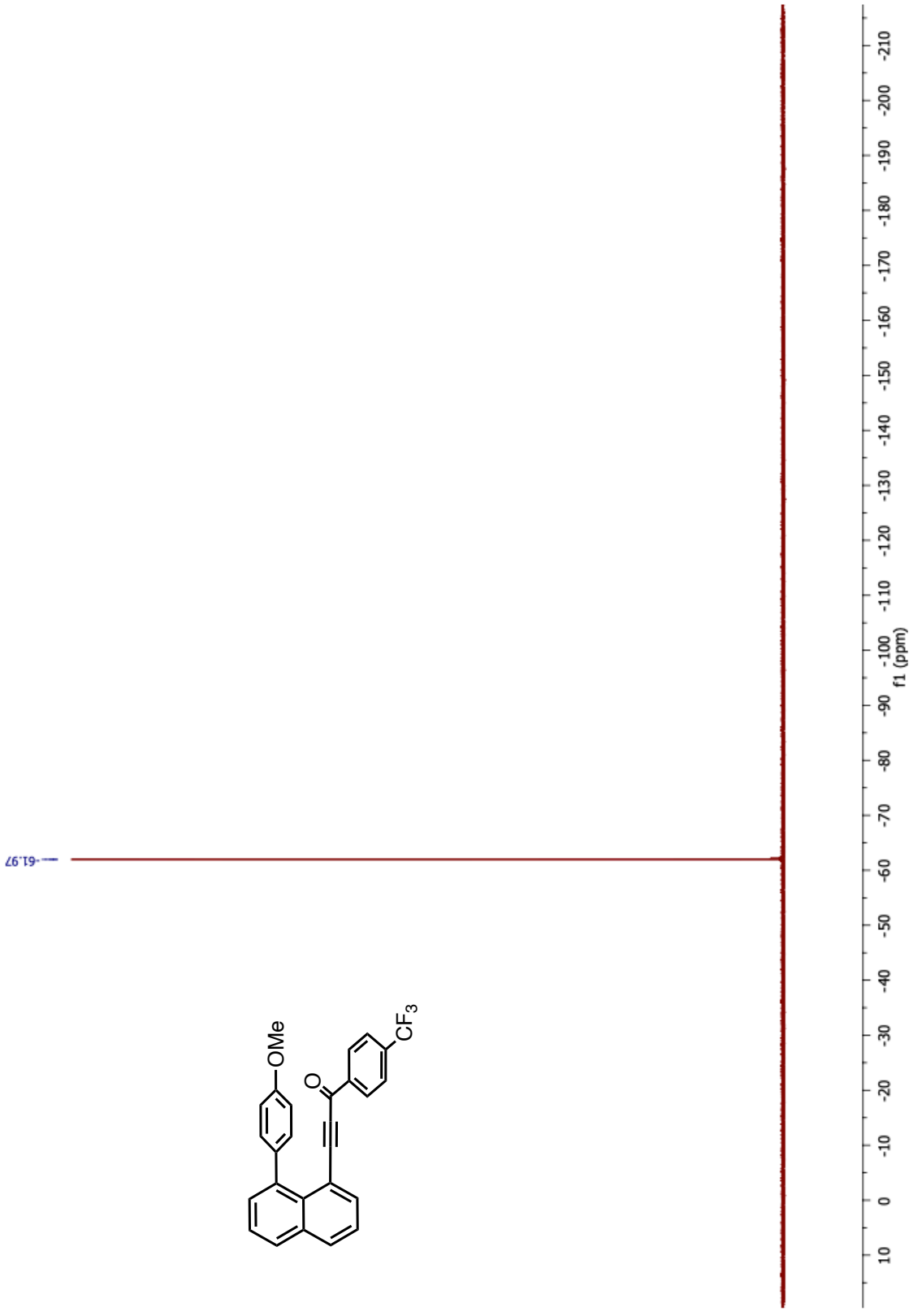

Figure 43. ^{19}F-NMR spectrum of compound **5c** in $CDCl_3$

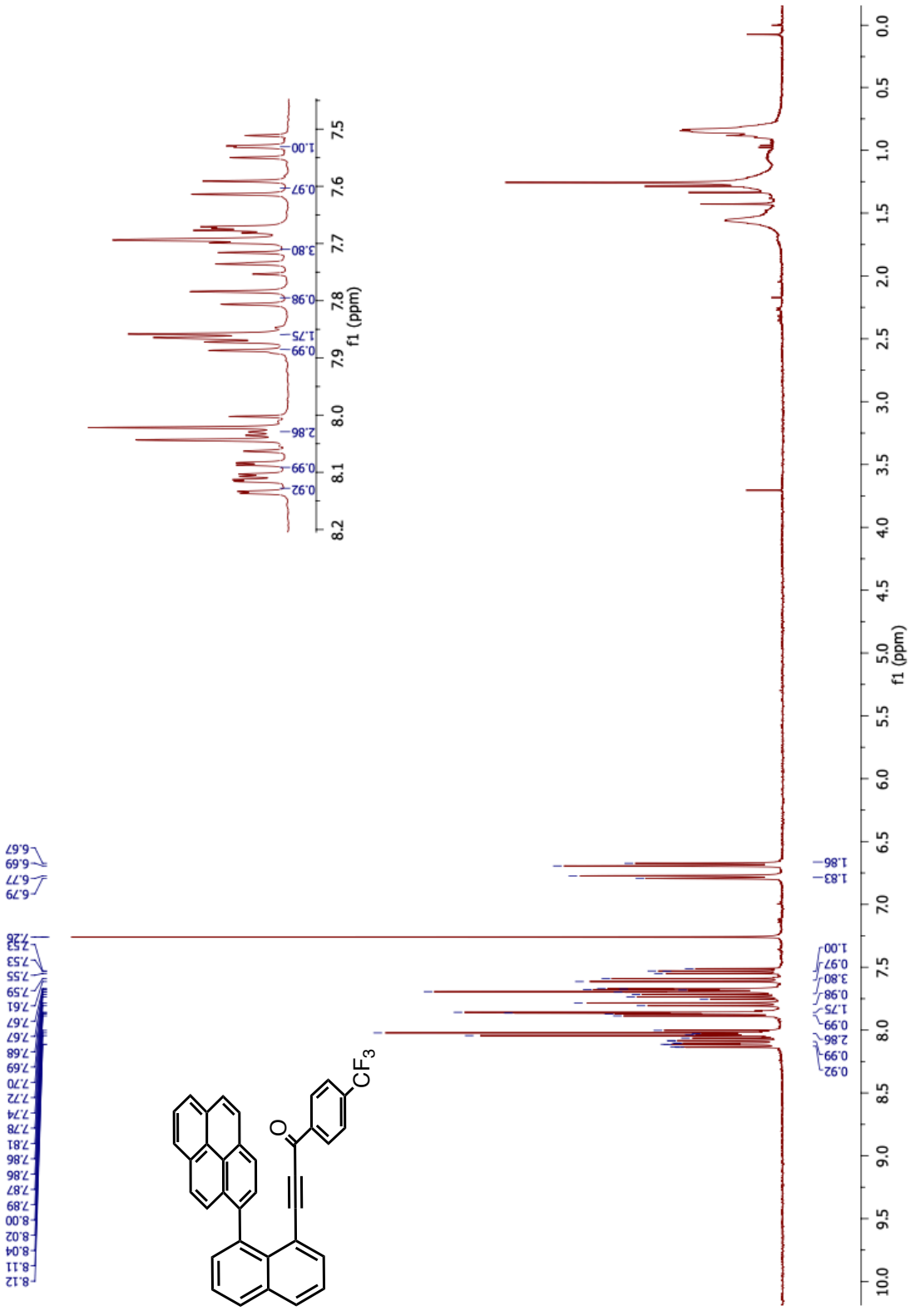

Figure 44. ^{1}H-NMR spectrum of compound **5e** in $CDCl_3$

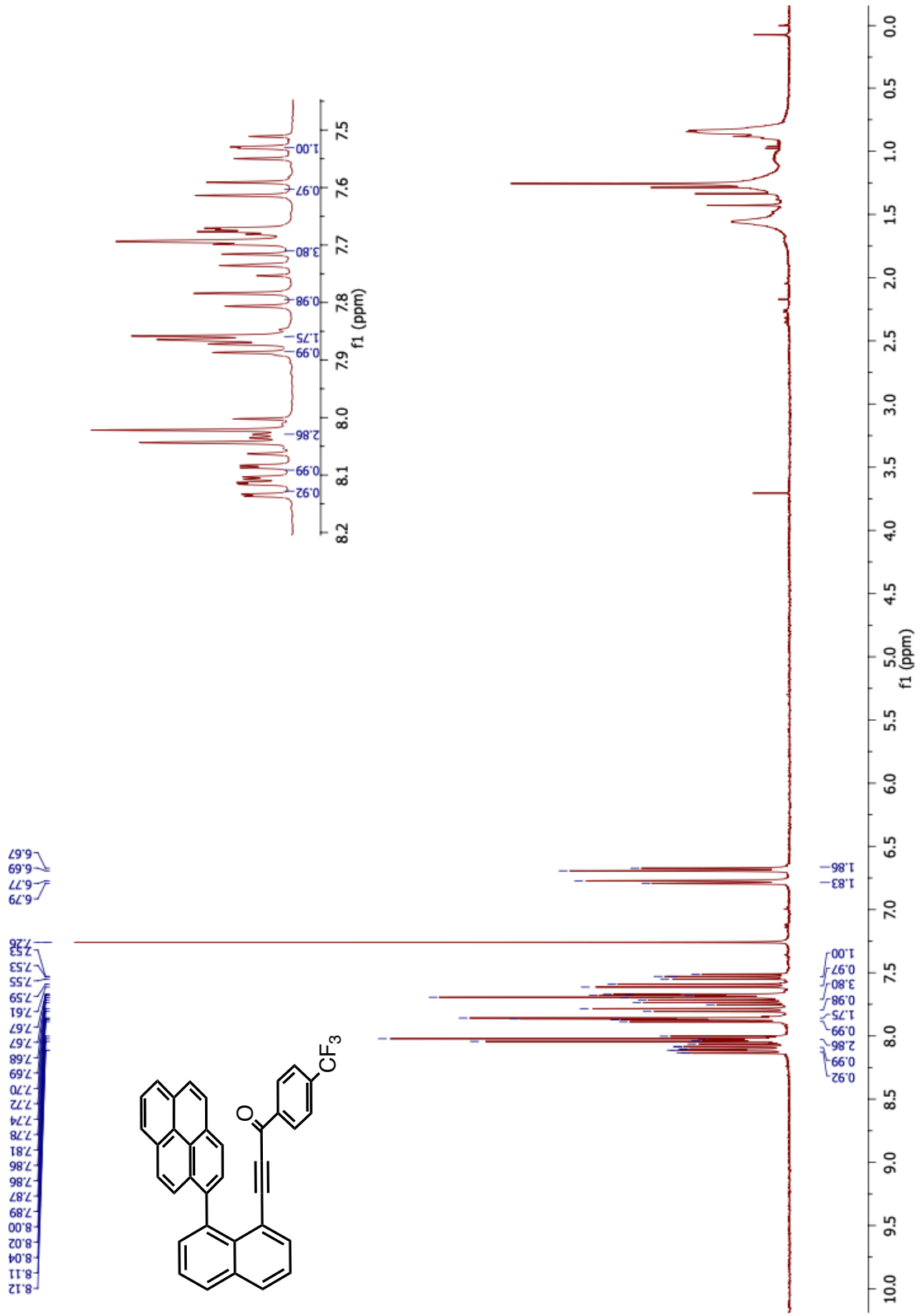

Figure 45. ^{13}C-NMR spectrum of compound **5e** in $CDCl_3$

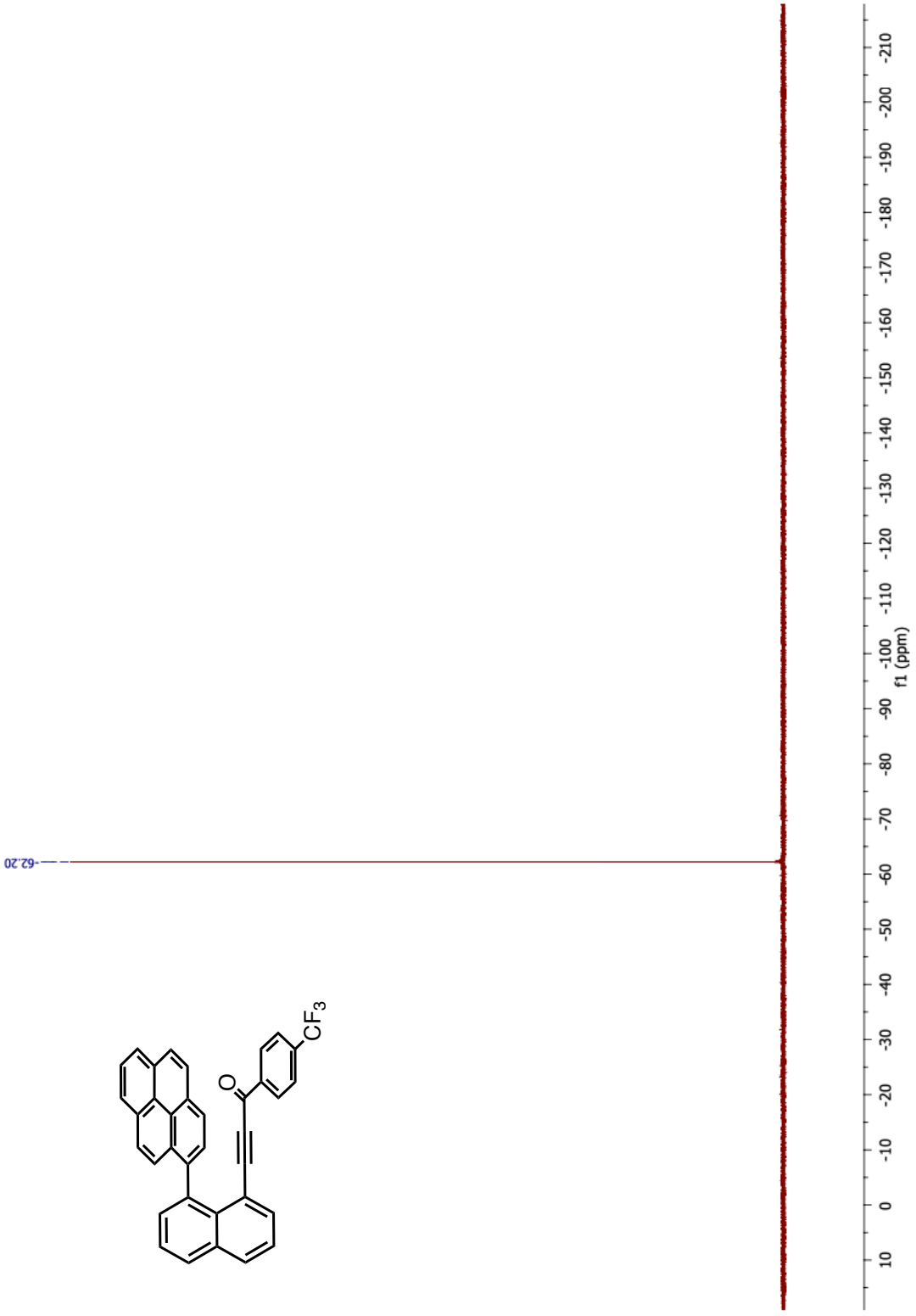

Figure 46. ^{19}F-NMR spectrum of compound **5e** in $CDCl_3$

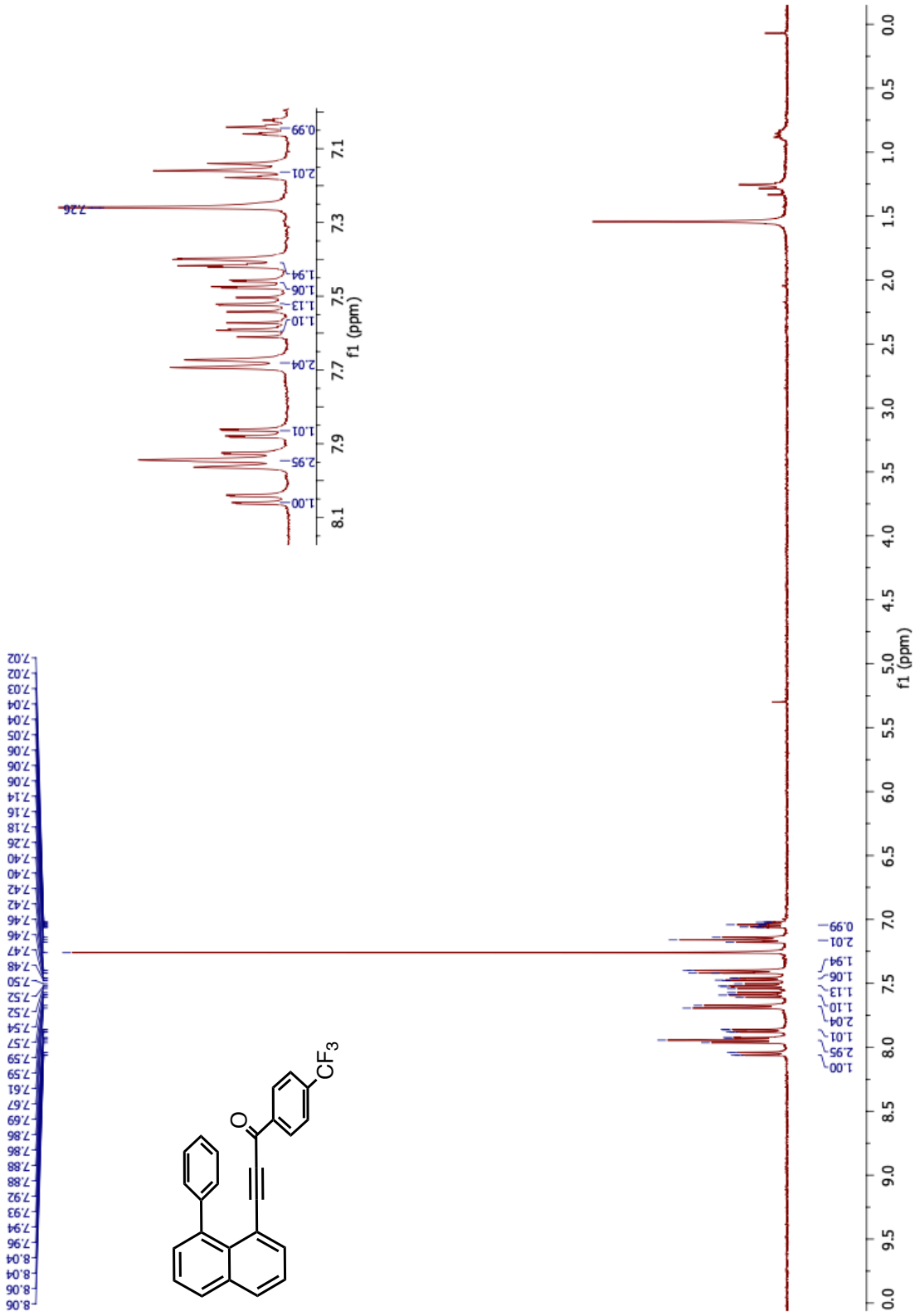

Figure 47. ^{1}H-NMR spectrum of compound **5f** in $CDCl_3$

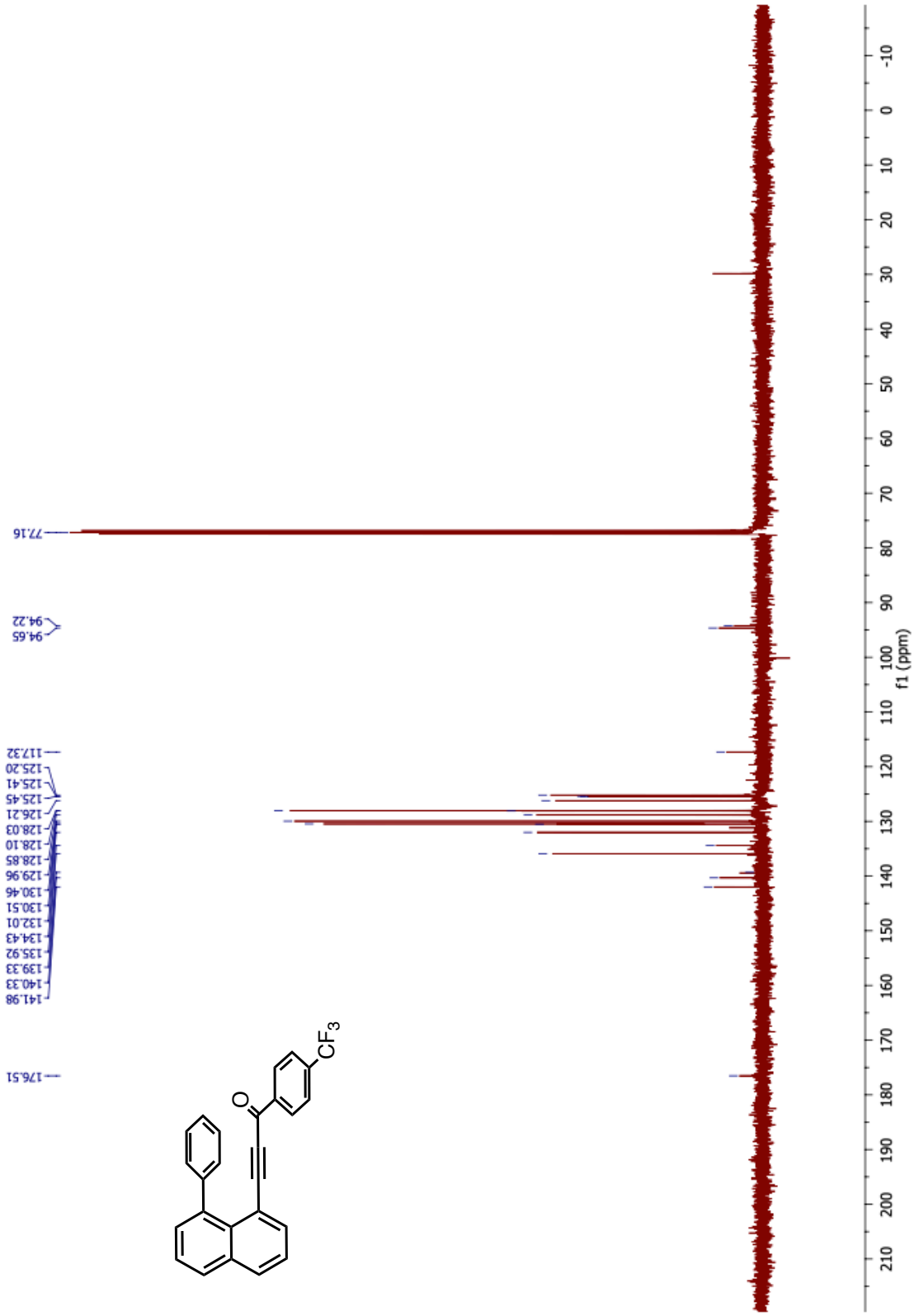

Figure 48. ^{13}C-NMR spectrum of compound **5f** in $CDCl_3$

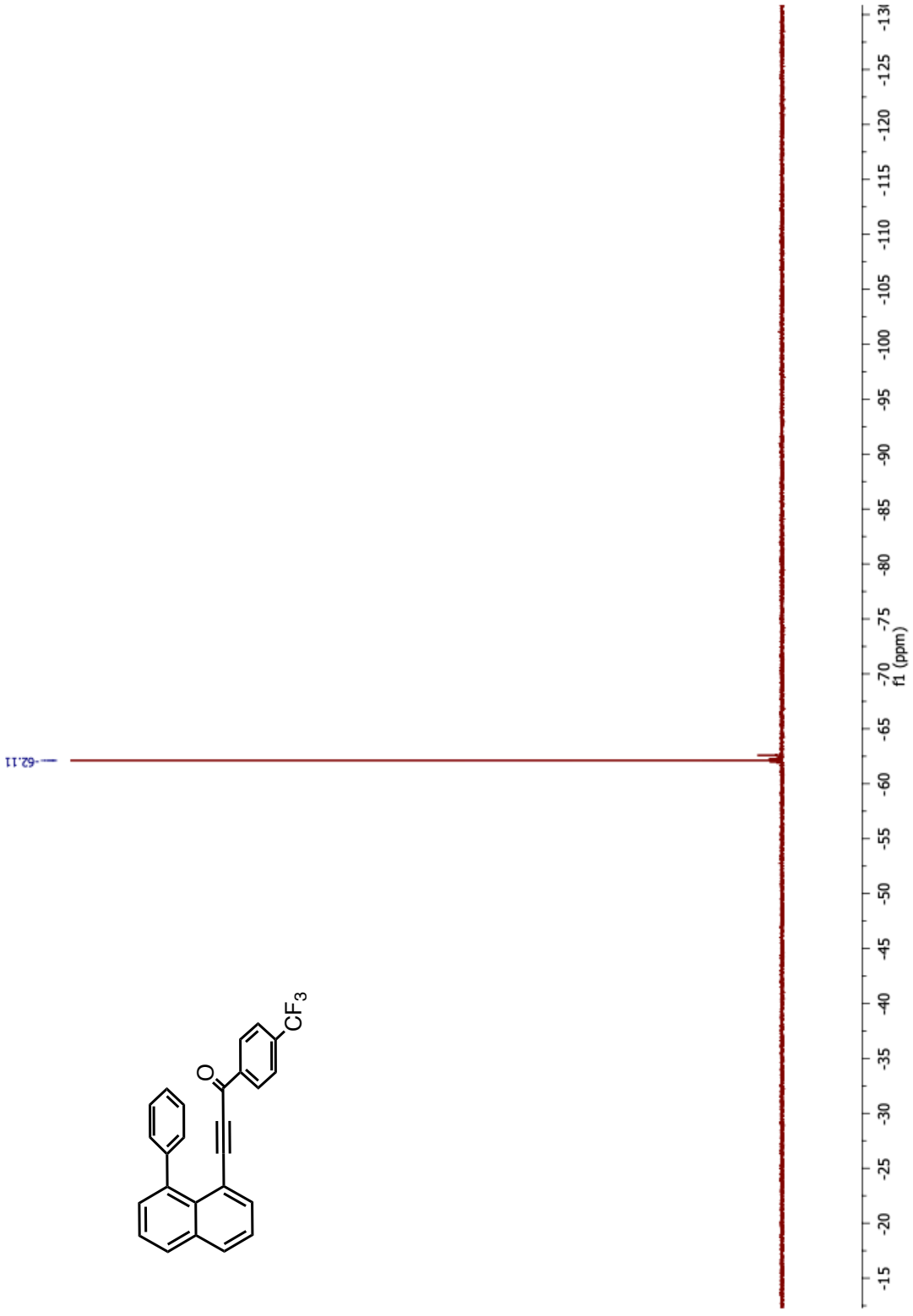

Figure 49. ^{19}F-NMR spectrum of compound **5f** in $CDCl_3$

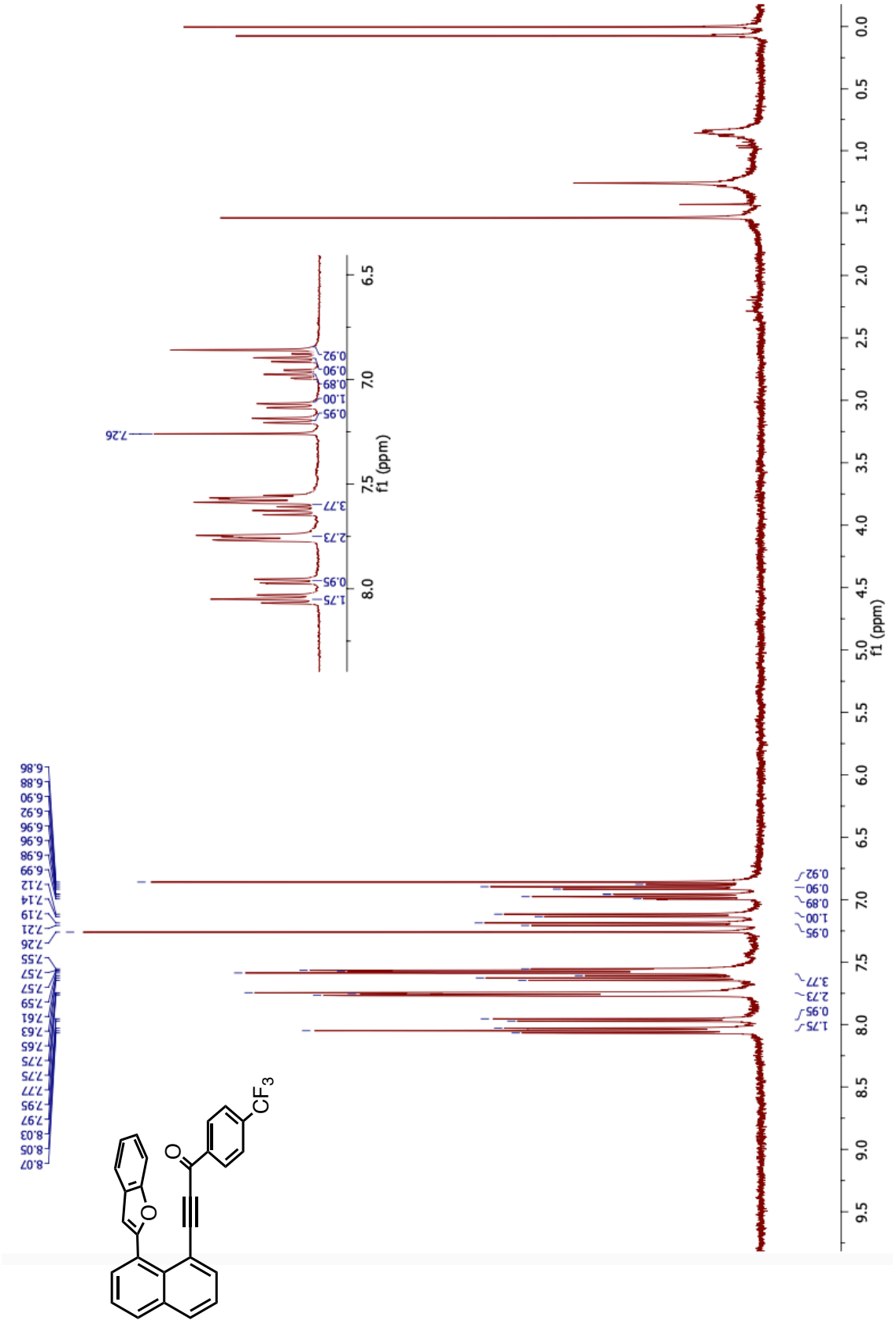

Figure 50. ^{1}H-NMR spectrum of compound **5g** in $CDCl_3$

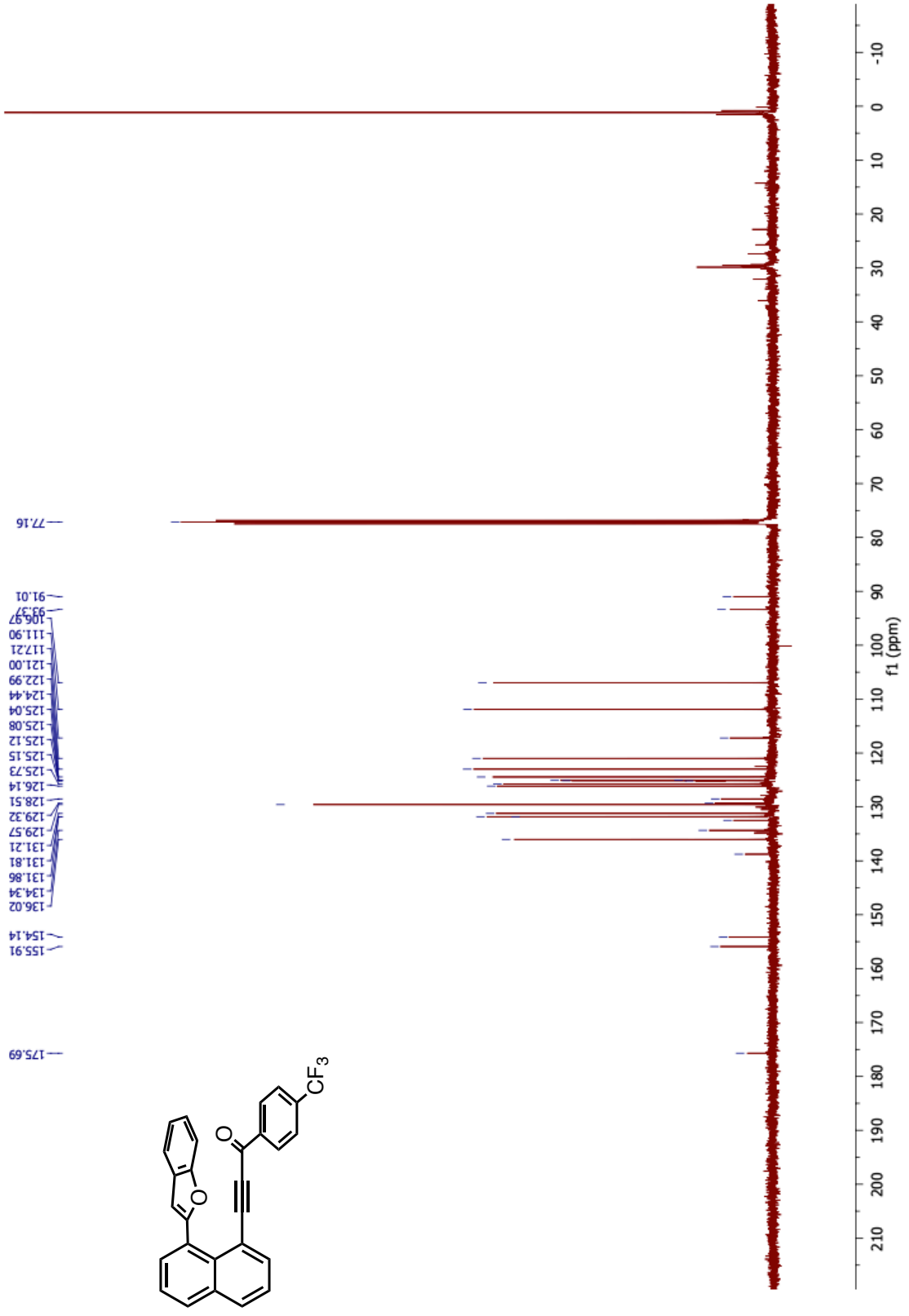

Figure 51. ^{13}C-NMR spectrum of compound **5g** in $CDCl_3$

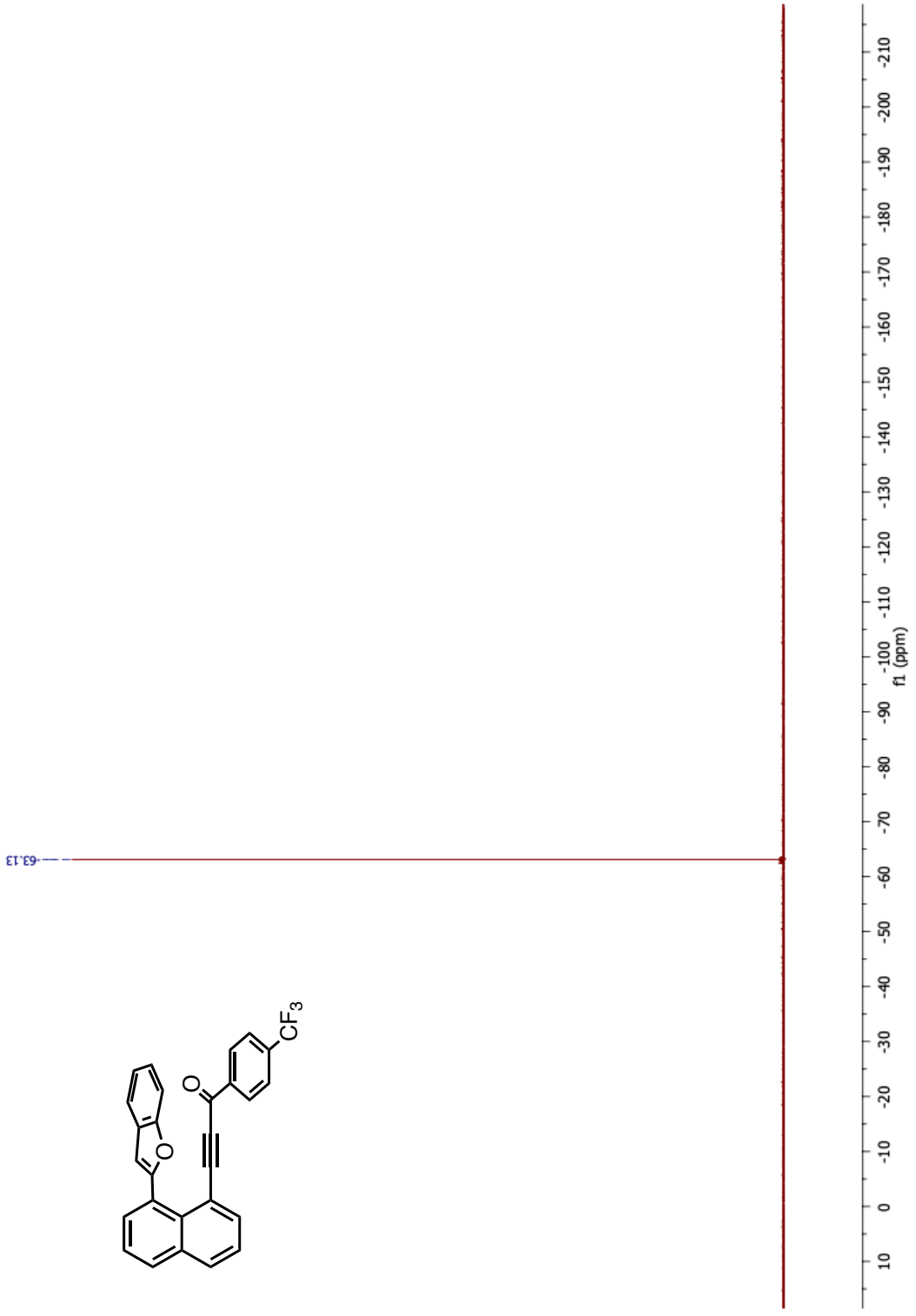

Figure 52. ^{19}F-NMR spectrum of compound **5g** in $CDCl_3$

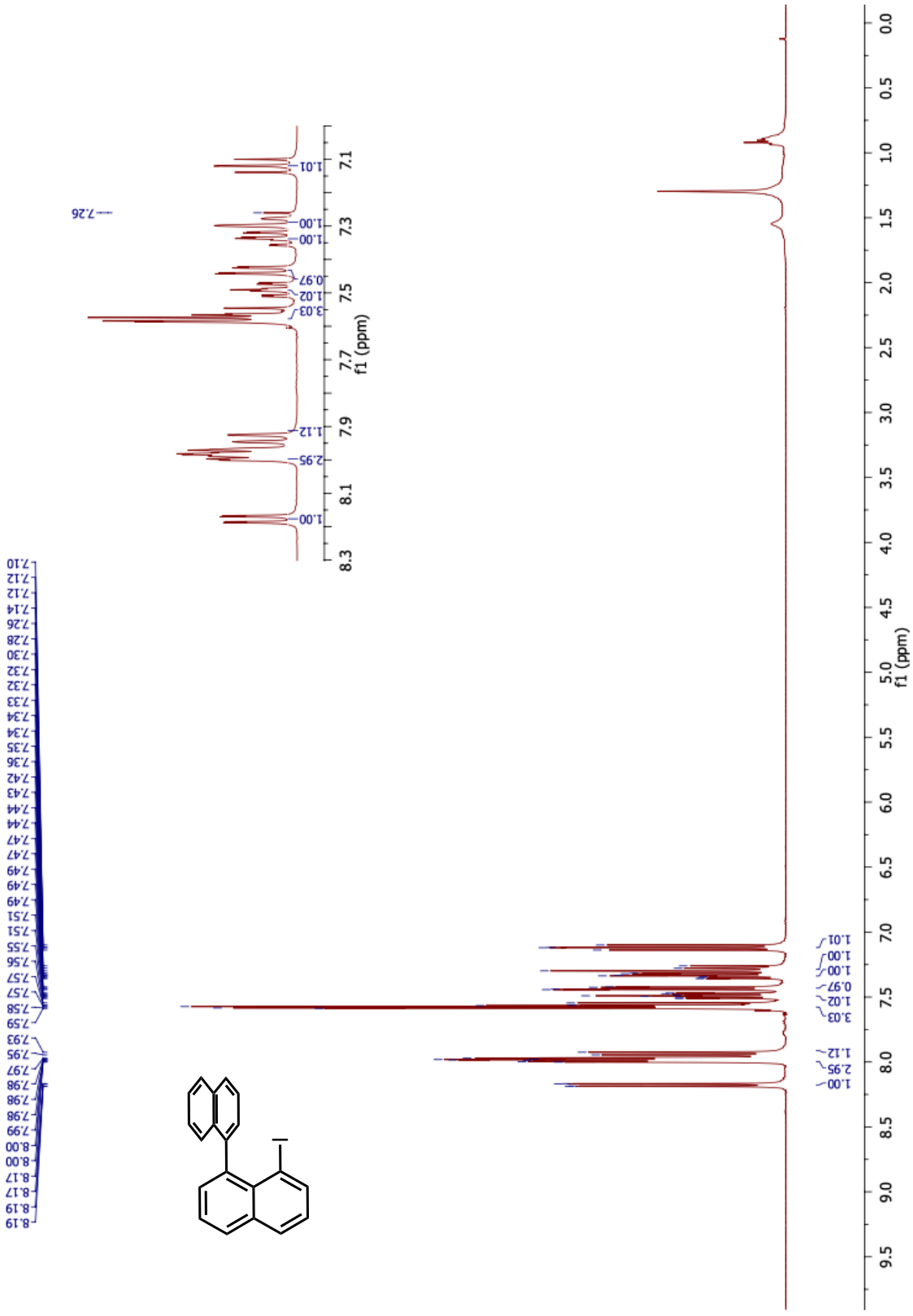

Figure 53. ^{1}H-NMR spectrum of compound **6** in $CDCl_3$

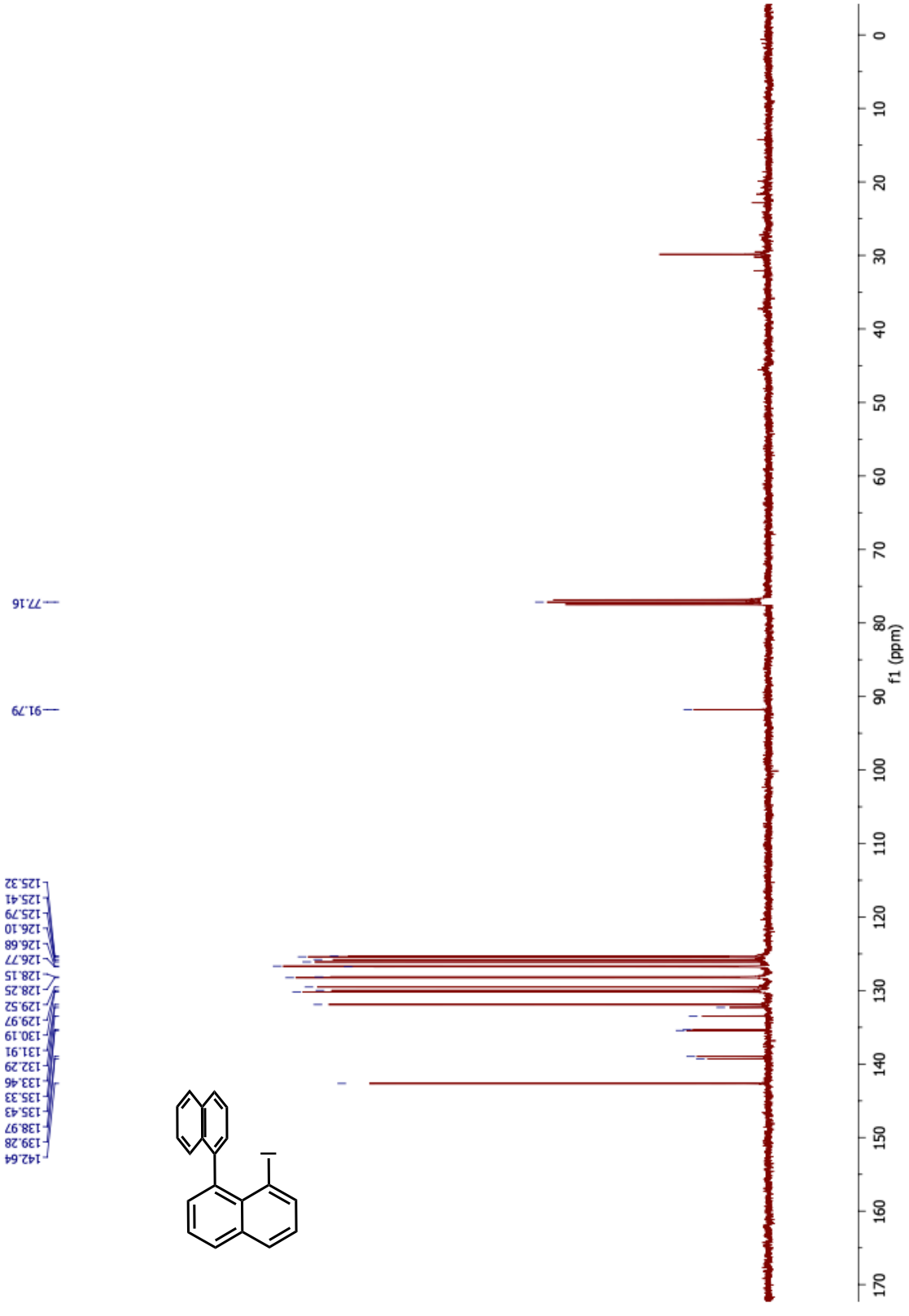

Figure 54. ^{13}C-NMR spectrum of compound **6** in $CDCl_3$

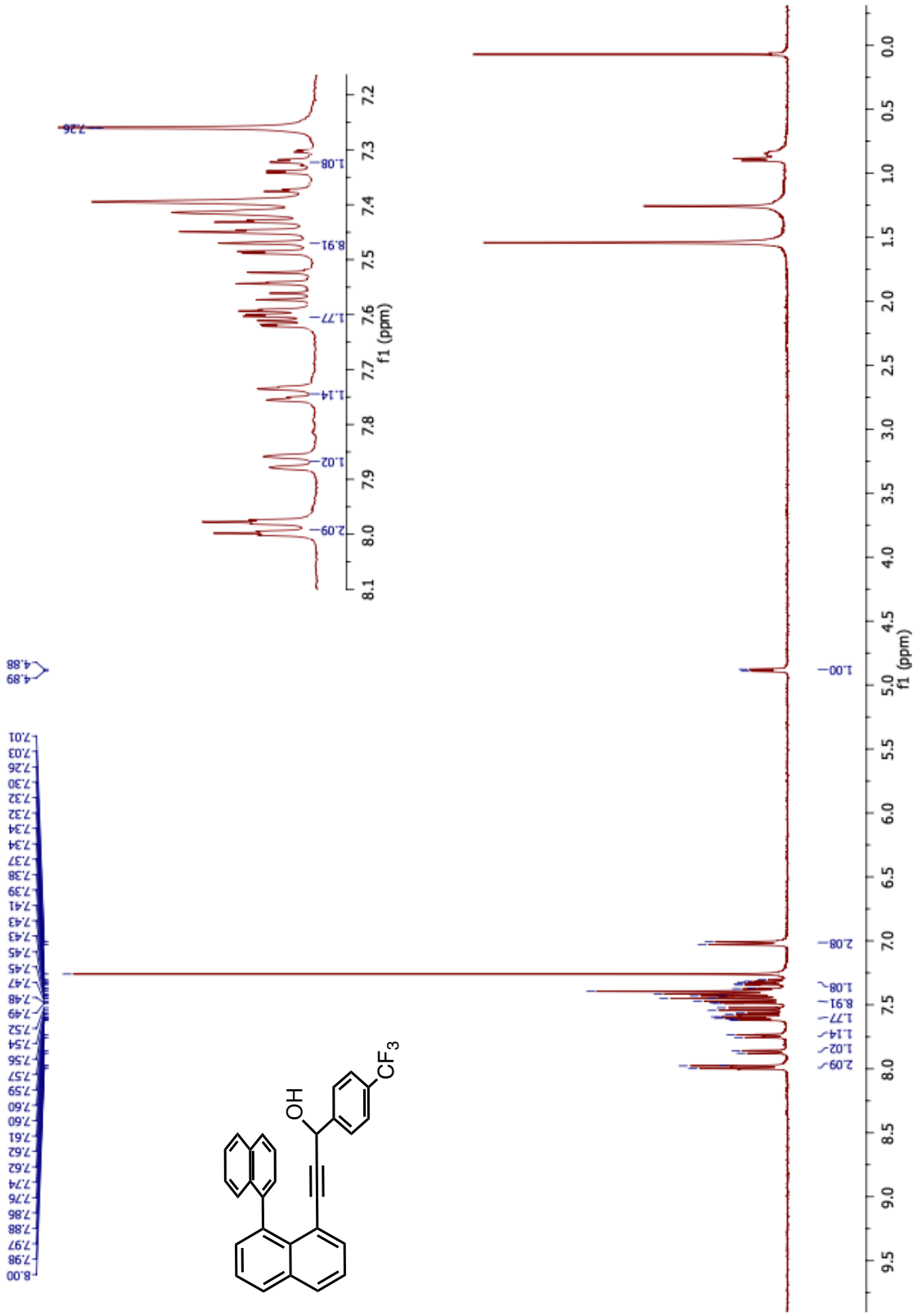

Figure 55. ^{1}H-NMR spectrum of compound **7** in $CDCl_3$

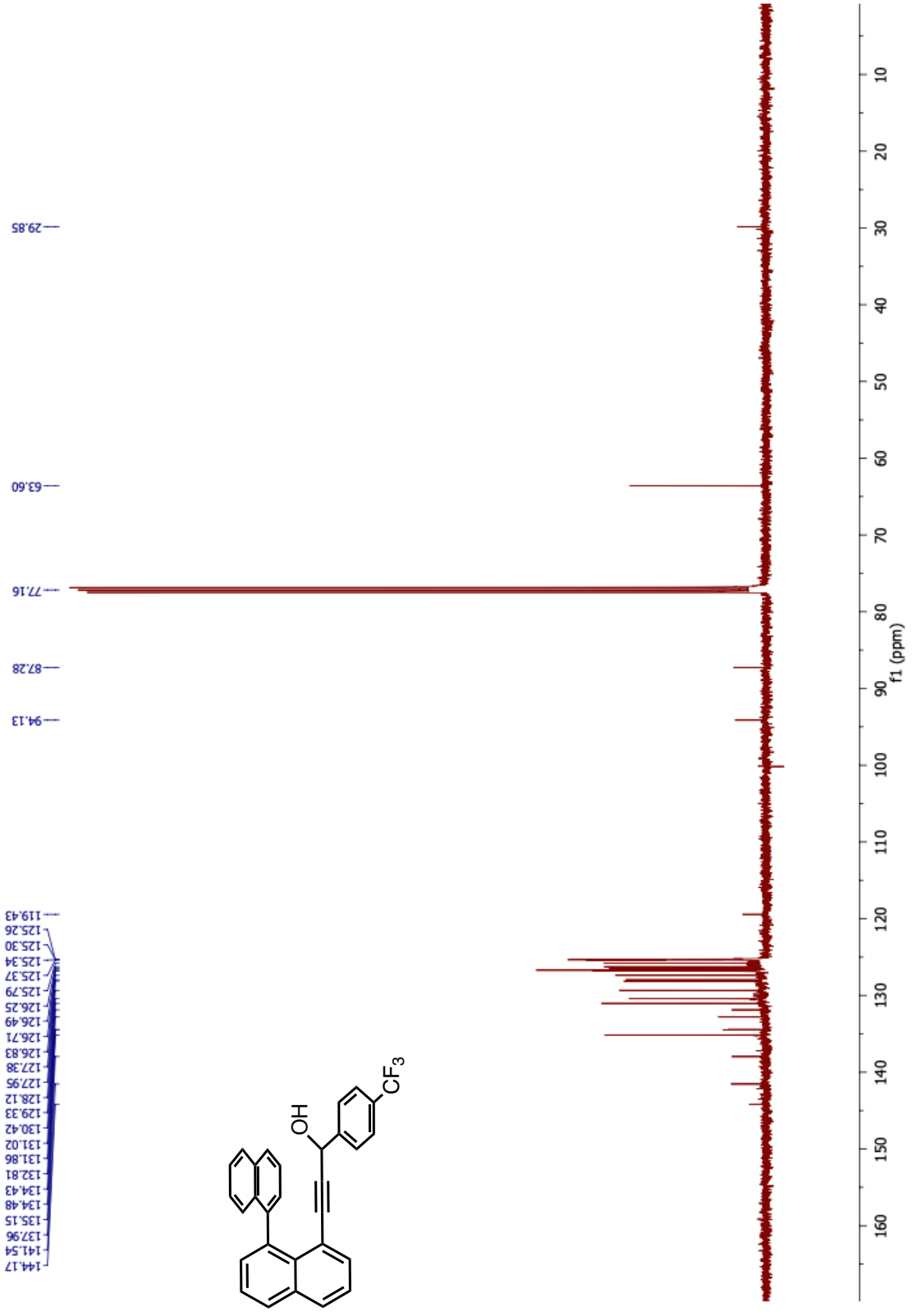

Figure 56. ^{13}C-NMR spectrum of compound **7** in $CDCl_3$

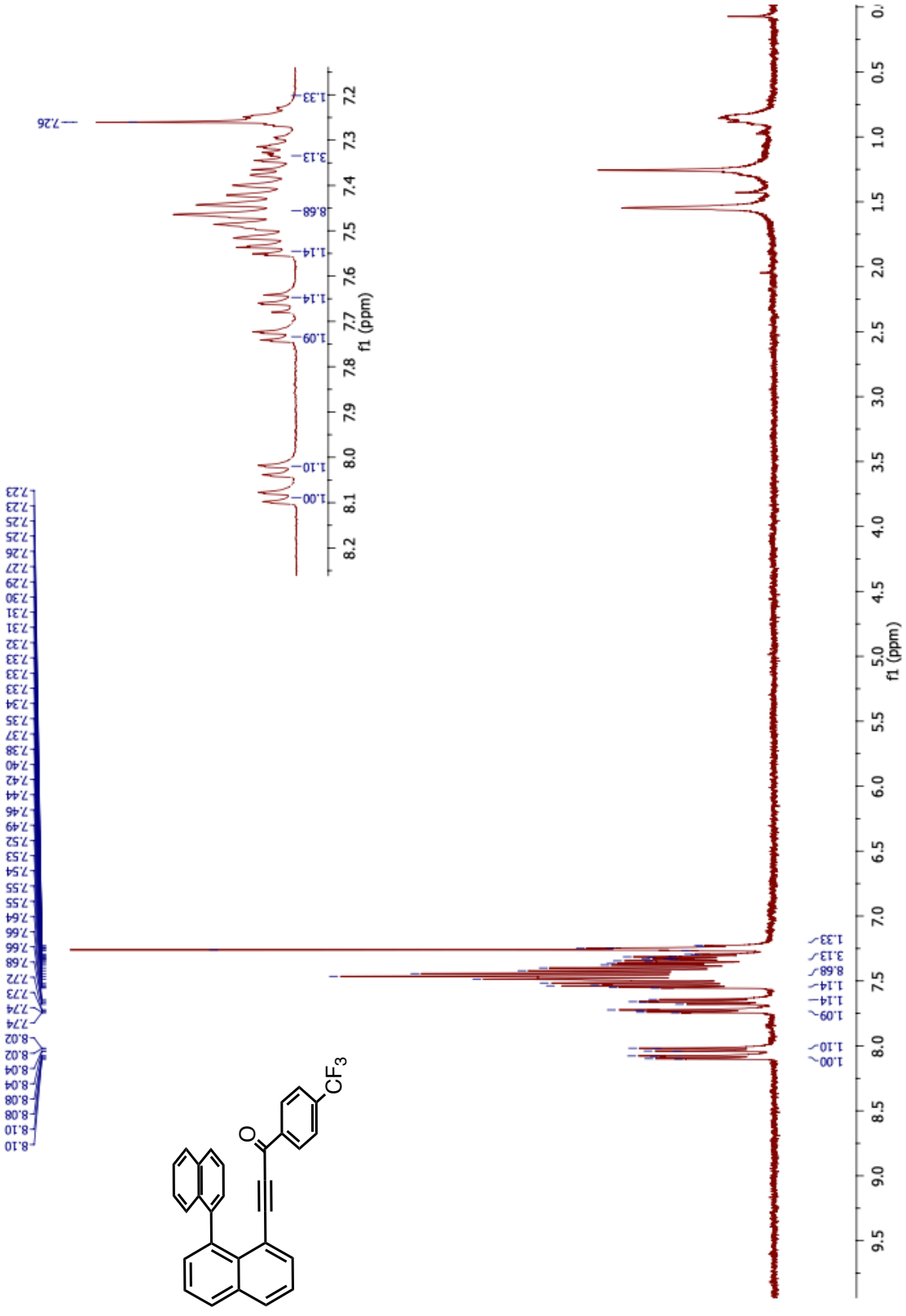

Figure 57. ^{1}H-NMR spectrum of compound **5d** in $CDCl_3$

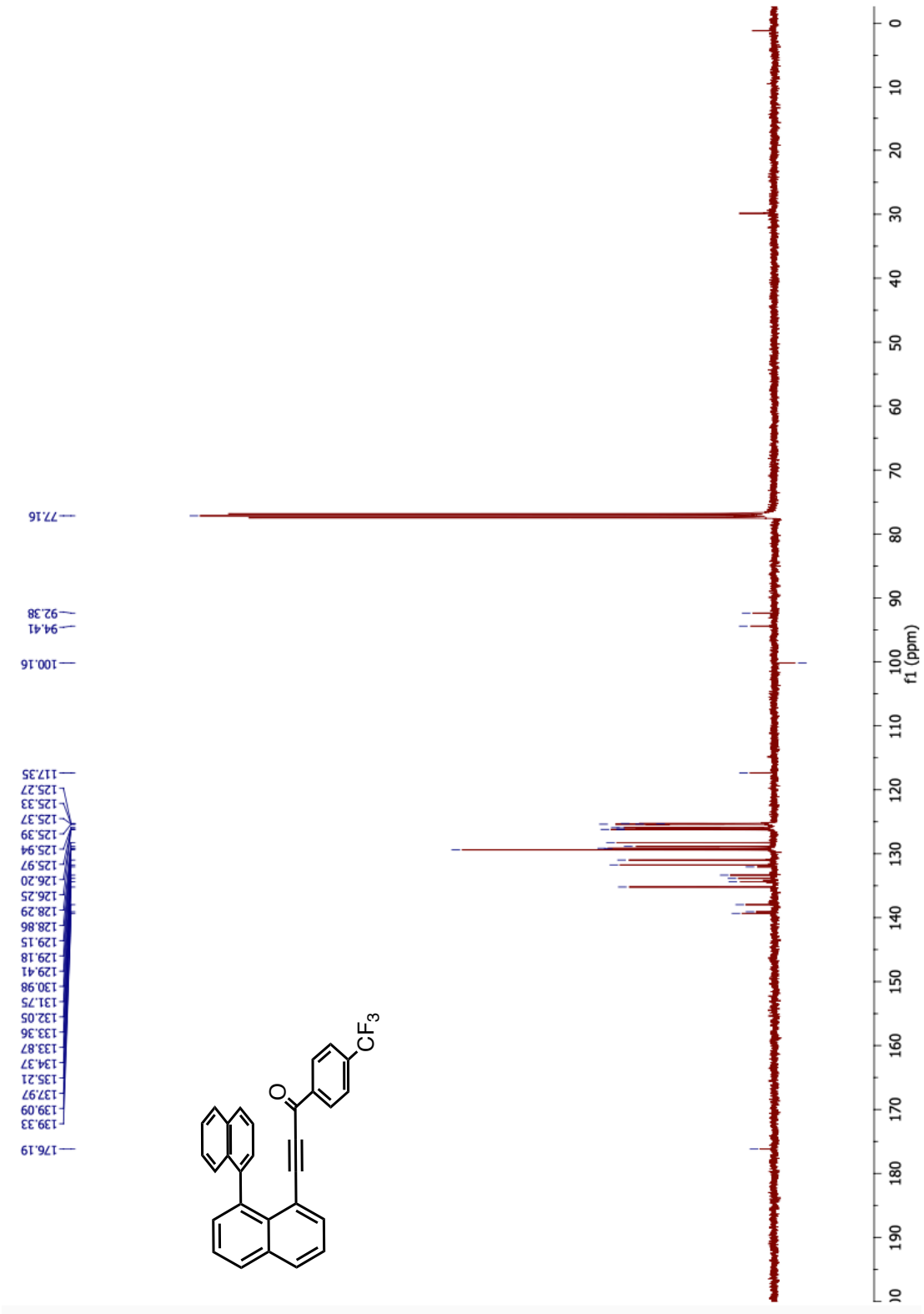

Figure 58. ^{13}C-NMR spectrum of compound **5d** in $CDCl_3$

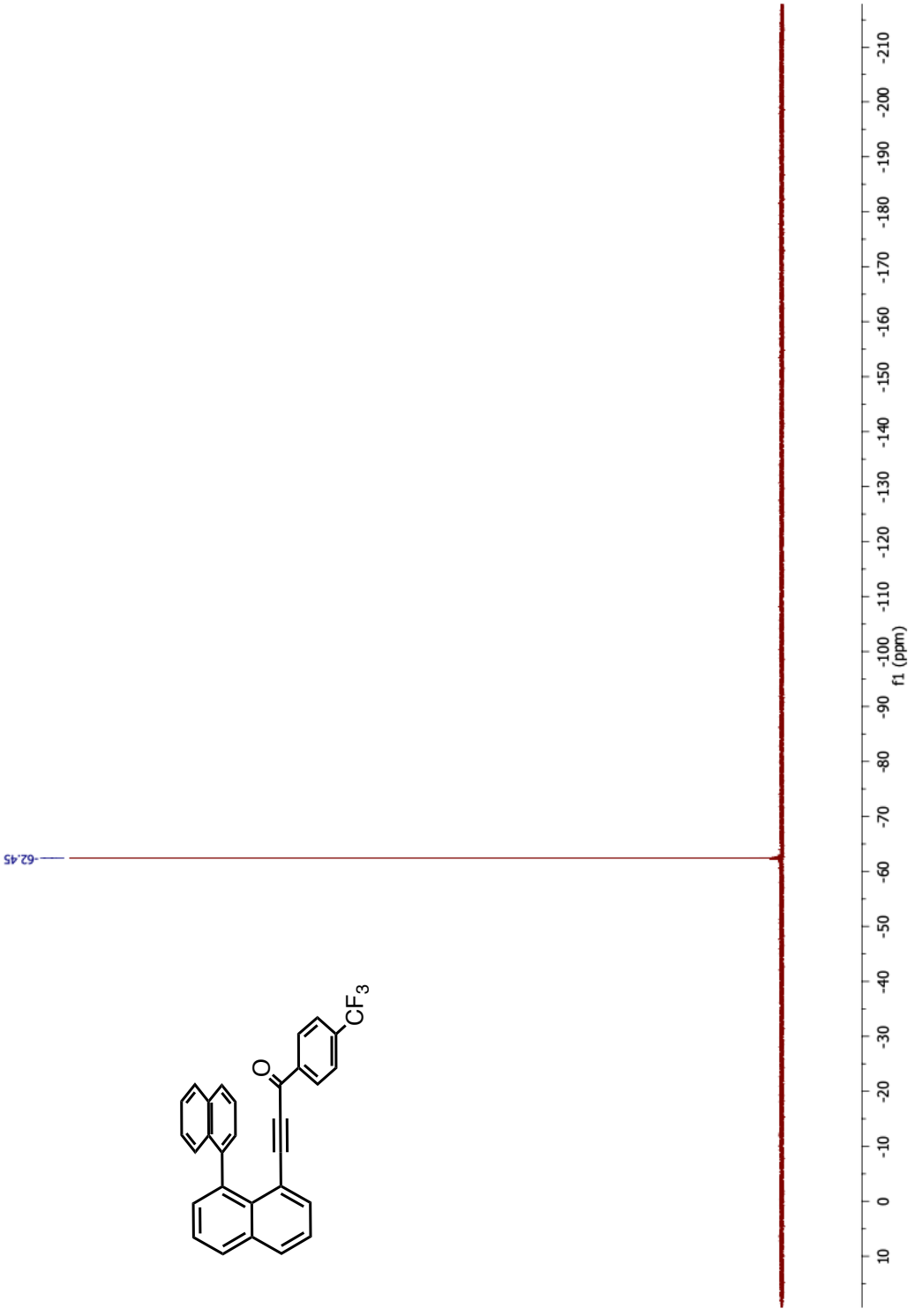

Figure 59. ^{19}F-NMR spectrum of compound **5d** in $CDCl_3$

4.2.UV-Vis Absorption Data

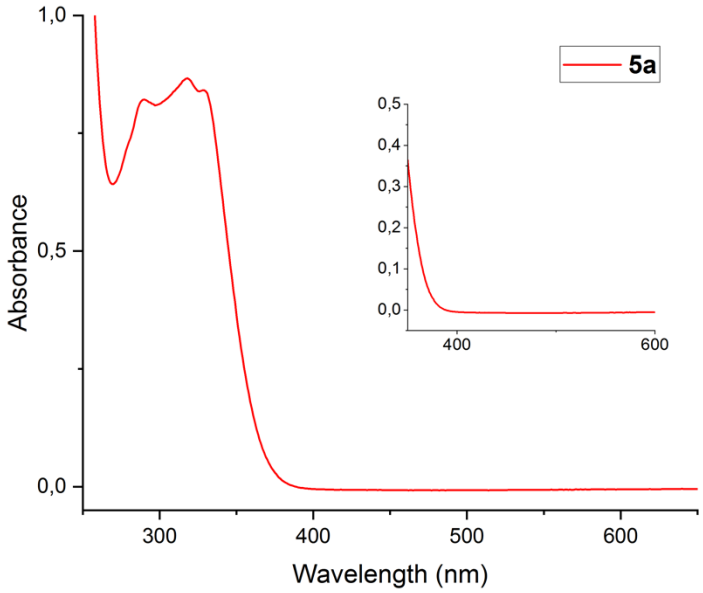

Figure 60. UV-Vis Absorption Spectrum of compound **5a** in DCM (10^{-2} M)

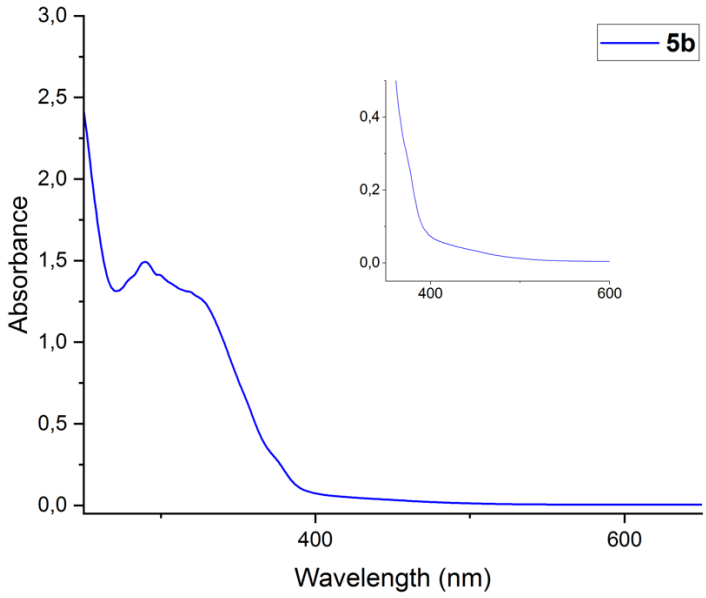

Figure 61. UV-Vis Absorption Spectrum of compound **5b** in DCM (10^{-2} M)

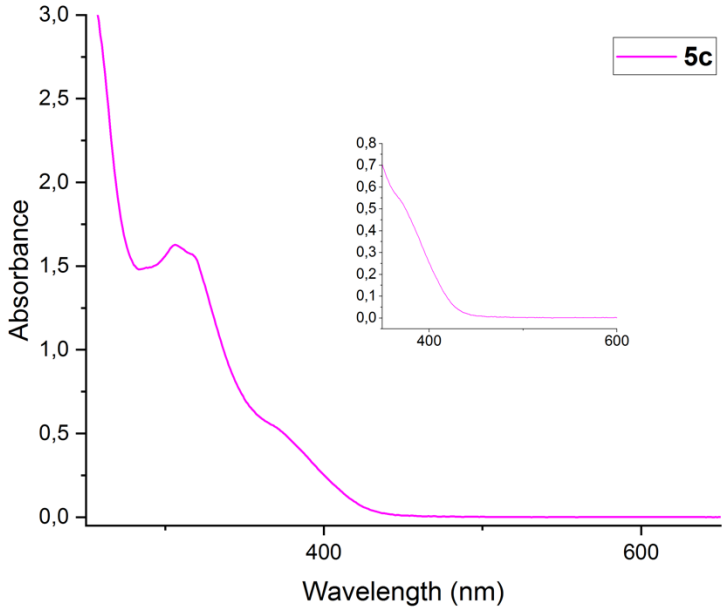

Figure 62. UV-Vis Absorption Spectrum of compound **5c** in DCM (10^{-2} M)

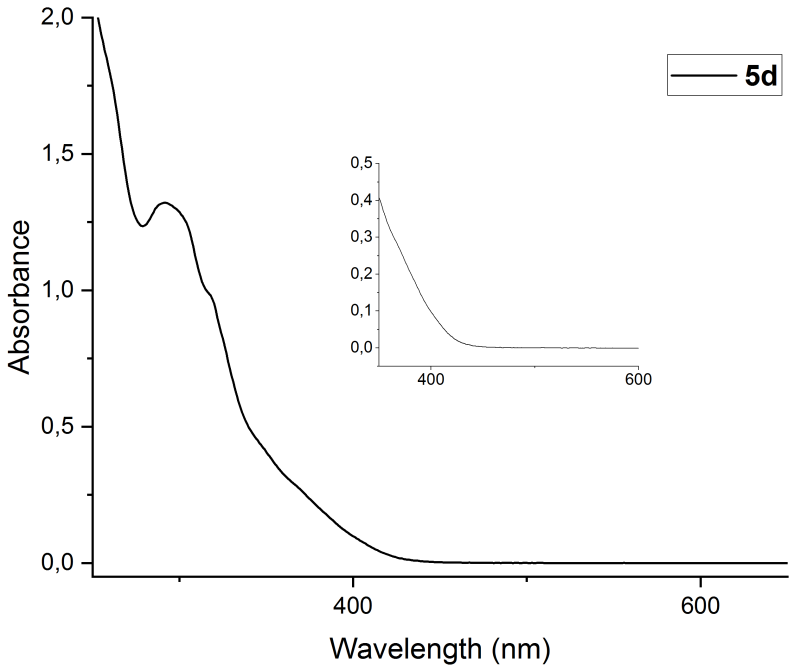

Figure 63. UV-Vis Absorption Spectrum of compound **5d** in DCM (10^{-2} M)

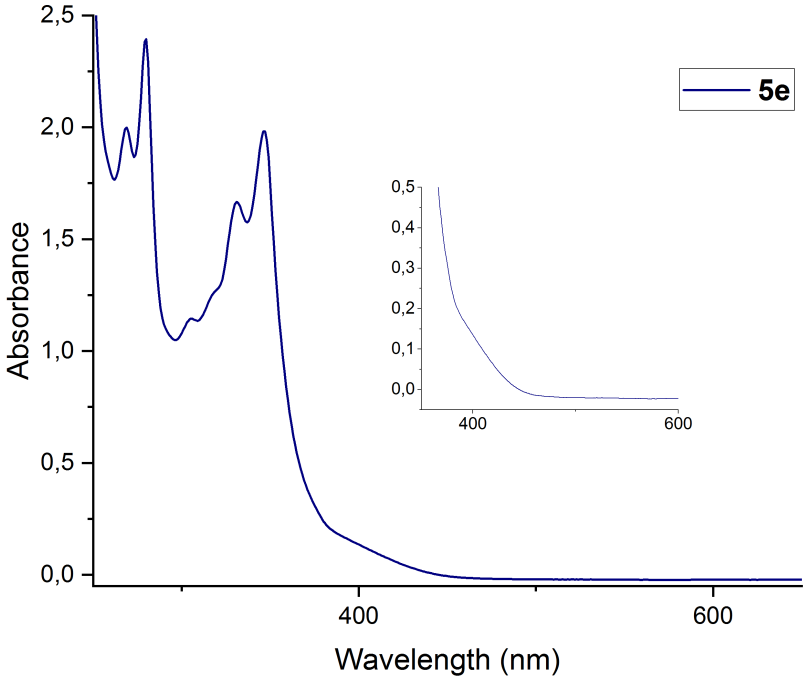

Figure 64. UV-Vis Absorption Spectrum of compound **5e** in DCM (10^{-2} M)

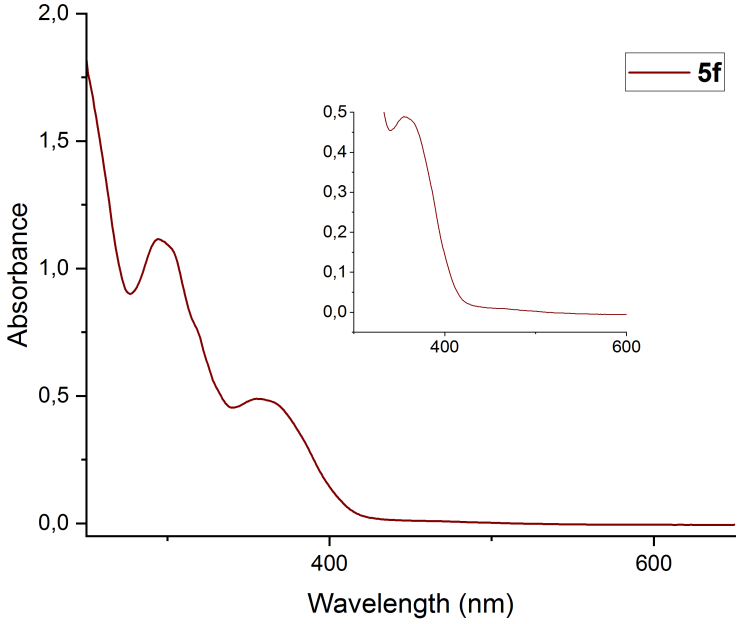

Figure 65. UV-Vis Absorption Spectrum of compound **5f** in DCM (10^{-2} M)

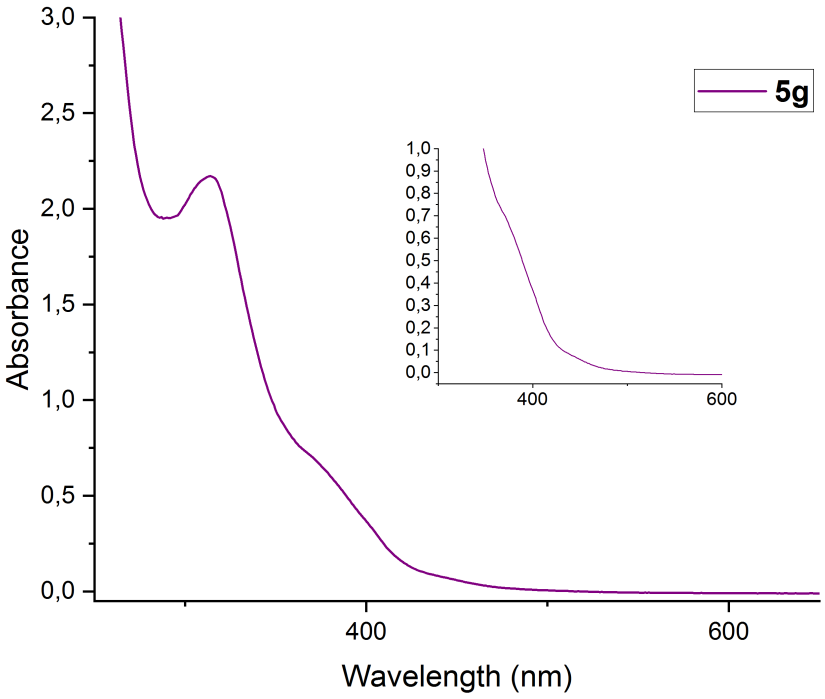

Figure 66. UV-Vis Absorption Spectrum of compound **5g** in DCM (10^{-2} M)

5. REFERENCES

1. Hoorens, M. W. H.; Szymanski, W.; Browne, W. R.; Feringa, B. L. Iminothioindoxyl as a Molecular Photoswitch with 100 nm Band Separation in the Visible Range. *Nat. Commun.* **2019**, *10* (1), 2390. https://doi.org/10.1038/s41467-019-10251-3.
2. Lakowicz, J. R. *Principles of Fluorescence Spectroscopy*, 3rd ed.; Springer US: Boston, MA, 2006.
3. Frackowiak, D. The Jablonski Diagram. *J. Photochem. Photobiol., B* **1988**, *2* (3), 399–414. https://doi.org/10.1016/1011-1344(88)80017-2.
4. Gupta, V. P. *Principles and Applications of Quantum Chemistry*; Academic Press: Cambridge, MA, 2015.
5. Peng, X.; Song, F.; Lu, E.; Wang, Y.; Zhou, W.; Fan, J.; Gao, Y. Heptamethine Cyanine Dyes with a Large Stokes Shift and Strong Fluorescence: A Paradigm for Excited-State Intramolecular Charge Transfer. *J. Am. Chem. Soc.* **2005**, *127*(12), 4170–4171. https://doi.org/10.1021/ja0421096.
6. Della Ciana, L. Photophysical Properties of Polypyridyl Carbonyl Complexes of Rhenium(I). *J. Chem. Soc., Dalton Trans.* **1991**, (S), 849–858. https://doi.org/10.1039/DT9910000849.
7. Guenther, B. D.; Steel, D., Eds. *Encyclopedia of Modern Optics*, 2nd ed.; Academic Press: Oxford, 2018.
8. Pan, Y. Y.; Huang, J.; Wang, Z. M.; Zhang, S. T.; Yu, D. W.; Yang, B.; Ma, Y. G. Accurate Description of Hybridized Local and Charge-Transfer Excited-State in

Donor–Acceptor Molecules Using Density Functional Theory. *RSC Adv.***2016**, *6* (110), 108404–108410. https://doi.org/10.1039/C6RA21374H.

9. Foster, R. Electron Donor–Acceptor Complexes. *J. Phys. Chem.* **1980**, *84* (17), 2135–2141. https://doi.org/10.1021/j100452a001.

10. Hou, Y.; Zhang, X.; Chen, K.; Liu, D.; Wang, Z.; Liu, Q.; Abdi, A.; Barbon, A. Charge Separation, Charge Recombination, Long-Lived Charge Transfer State Formation and Intersystem Crossing in Organic Electron Donor/Acceptor Dyads. *J. Mater. Chem. C* **2019**, *7* (39), 12048–12074. https://doi.org/10.1039/C9TC03540K.

11. Baharfar, M.; Hillier, A. C.; Mao, G. Charge-Transfer Complexes: Fundamentals and Advances in Catalysis, Sensing, and Optoelectronic Applications. *Adv. Mater.* **2024**, *36* (42), 2406083. https://doi.org/10.1002/adma.202406083.

12. Wasielewski, M. R. Self-Assembly Strategies for Integrating Light Harvesting and Charge Separation in Artificial Photosynthetic Systems. *Acc. Chem. Res.* **2009**, *42* (12), 1910–1921. https://doi.org/10.1021/ar9001735.

13. Thompson, D. W.; Ito, A.; Meyer, T. J. $[Ru(bpy)_3]^{2+*}$ and Other Remarkable Metal-to-Ligand Charge Transfer (MLCT) Excited States. *Pure Appl. Chem.* **2013**, *85* (7), 1257–1305. https://doi.org/10.1351/PAC-CON-12-09-04.

14. Xue, Q.; Xie, G. Thermally Activated Delayed Fluorescence beyond Through-Bond Charge Transfer for High-Performance OLEDs. *Adv. Opt. Mater.* **2021**, *9* (14), 2002204. https://doi.org/10.1002/adom.202002204.

15. Atkins, P. W.; De Paula, J. *Physical Chemistry: Thermodynamics, Structure, and Change*, 10th ed.; Oxford University Press: Oxford, 2014.

16. Marcus, R. A. Chemical and Electrochemical Electron-Transfer Theory. *Annu. Rev. Phys. Chem.* **1964**, *15* (1), 155–196. https://doi.org/10.1146/annurev.pc.15.100164.001103.

17. Sichula, V. A. *Flavins and Their Analogues as Natural and Artificial Catalysts*; Doctoral Dissertation, Bowling Green State University, 2011.

18. Mulliken, R. S. Molecular Compounds and Their Spectra. II. *J. Am. Chem. Soc.* **1952**, *74* (3), 811–824. https://doi.org/10.1021/ja01123a067.

19. Wu, L.; Wu, F.; Sun, Q.; Shi, J.; Xie, A.; Zhu, X.; Dong, W. A TTF–TCNQ Complex: An Organic Charge-Transfer System with Extraordinary Electromagnetic Response Behavior. *J. Mater. Chem. C* **2021**, *9* (9), 3316–3323. https://doi.org/10.1039/D0TC05832A.

20. Takeda, M.; Umemoto, K.; Nohara, T.; Tozawa, K.; Matsui, J.; Masuhara, A. Micro/Nano Crystal Composed of Tetrathiafulvalene–Tetracyanoquinodimethane Prepared Using a Charge Transfer-Induced Reprecipitation Method. *J. Electrochem. Soc.* **2019**, *166* (9), B3131–B3136. https://doi.org/10.1149/2.0131909jes.

21. Sun, L.; Zhu, W.; Wang, W.; Yang, F.; Zhang, C.; Wang, S.; Di, C.; Hu, W. Intermolecular Charge-Transfer Interactions Facilitate Two-Photon Absorption in

Styrylpyridine–Tetracyanobenzene Cocrystals. *Angew. Chem., Int. Ed.***2017**, *56* (27), 7831–7835. https://doi.org/10.1002/anie.201703036.

22. Ko, Y. H.; Kim, E.; Hwang, I.; Kim, K. Supramolecular Assemblies Built with Host-Stabilized Charge-Transfer Interactions. *Chem. Commun.* **2007**, (13), 1305–1315. https://doi.org/10.1039/B614196G.

23. Grabowski, Z. R.; Rotkiewicz, K.; Siemiarczuk, A. Dual Fluorescence of Donor–Acceptor Molecules and the Twisted Intramolecular Charge Transfer (TICT) States. *J. Lumin.* **1979**, *18–19*, 420–424. https://doi.org/10.1016/0022-2313(79)90062-X.

24. Wang, C.; Chi, W.; Qiao, Q.; Tan, D.; Xu, Z.; Liu, X. Twisted Intramolecular Charge Transfer (TICT) and Twists beyond TICT: From Mechanisms to Rational Designs of Bright and Sensitive Fluorophores. *Chem. Soc. Rev.* **2021**, *50*(22), 12656–12678. https://doi.org/10.1039/D1CS00563C.

25. Wei, X.; Yang, X.; Feng, Y.; Ning, P.; Yu, H.; Zhu, M.; Zhang, Y.; Meng, X. A TICT Based Two-Photon Fluorescent Probe for Cysteine and Homocysteine in Living Cells. *Sens. Actuators, B* **2016**, *231*, 285–292. https://doi.org/10.1016/j.snb.2016.03.029.

26. Kumari, N.; Jha, S.; Bhattacharya, S. Colorimetric Probes Based on Anthraimidazolediones for Selective Sensing of Fluoride and Cyanide Ion via Intramolecular Charge Transfer. *J. Org. Chem.* **2011**, *76* (20), 8215–8222. https://doi.org/10.1021/jo2009792.

27. Meng, X.; Lang, X.; Cao, Z. Structure Evolution of Organic Luminescent Molecules Utilizing Through-Space Charge Transfer Mechanism. *Chem. Asian J.* **2025**, *20* (7), e202401488.

https://doi.org/10.1002/asia.202401488.

28. Liang, H.; Lu, M.; Mahmood, Z.; Li, Z.; Chen, Z.; Chen, G.; Liu, H.; Ji, S. Efficient Intersystem Crossing and Long-Lived Charge-Separated State Induced by Through-Space Intramolecular Charge Transfer in a Parallel Geometry Carbazole–BODIPY Dyad. *Angew. Chem.* **2023**, *135* (44), e202312600. https://doi.org/10.1002/ange.202312600.

29. Tang, X.; Cui, L. S.; Li, H. C.; Gillett, A. J.; Auras, F.; Qu, Y. K.; Zhong, C.; Liao, L. S. Highly Efficient Luminescence from Space-Confined Charge-Transfer Emitters. *Nat. Mater.* **2020**, *19* (12), 1332–1338. https://doi.org/10.1038/s41563-020-0735-6.

30. Kumar, S.; Franca, L. G.; Stavrou, K.; Crovini, E.; Cordes, D. B.; Slawin, A. M. Z.; Zysman-Colman, E. Investigation of Intramolecular Through-Space Charge-Transfer States in Donor–Acceptor Charge-Transfer Systems. *J. Phys. Chem. Lett.* **2021**, *12* (11), 2820–2830. https://doi.org/10.1021/acs.jpclett.1c00526.

31. Bahl, A.; Grahn, W.; Stadler, S.; Feiner, F.; Bourhill, G.; Bräuchle, C.; Jones, P. G. Novel, Blue-Transparent Frequency Doublers Based on 1,8-Di(hetero)arylnaphthalenes. *Angew. Chem., Int. Ed. Engl.* **1995**, *34* (13–14), 1485–1488. https://doi.org/10.1002/anie.199514851.

32. Qu, Y. K.; Zhou, D. Y.; Zheng, Q.; Zuo, P.; Che, Z. L.; Liao, L. S.; Jiang, Z. Q. Linearly Arranged Multi-π-Stacked Structure for Efficient Through-Space Charge-Transfer Emitters. *Angew. Chem., Int. Ed.* **2024**, *63* (38), e202408712. https://doi.org/10.1002/anie.202408712.

33. Marini, A.; Muñoz-Losa, A.; Biancardi, A.; Mennucci, B. What Is Solvatochromism? *J. Phys. Chem. B* **2010**, *114*(51), 17128–17135. https://doi.org/10.1021/jp108650r.

34. Fromherz, P. Monopole–Dipole Model for Symmetrical Solvatochromism of Hemicyanine Dyes. *J. Phys. Chem.***1995**, *99* (18), 7188–7192. https://doi.org/10.1021/j100018a046.

35. Laage, D.; Thompson, W. H.; Blanchard-Desce, M.; Hynes, J. T. Charged Push−Pull Polyenes in Solution: Anomalous Solvatochromism and Nonlinear Optical Properties. *J. Phys. Chem. A* **2003**, *107* (31), 6032–6046. https://doi.org/10.1021/jp027482t.

36. Lee, S. Y.; Yasuda, T.; Yang, Y. S.; Zhang, Q.; Adachi, C. Luminous Butterflies: Efficient Exciton Harvesting by Benzophenone Derivatives for Full-Color Delayed Fluorescence OLEDs. *Angew. Chem., Int. Ed.* **2014**, *53* (25), 6402–6406. https://doi.org/10.1002/anie.201402992.

37. Zhang, T.; Xiao, Y.; Wang, H.; Kong, S.; Huang, R.; Au, V. K. M.; Huang, W. Highly Twisted Thermally Activated Delayed Fluorescence (TADF) Molecules and Their Applications in Organic Light-Emitting Diodes (OLEDs). *Angew. Chem., Int. Ed.* **2023**, *62* (39), e202301896. https://doi.org/10.1002/anie.202301896.

38. Mei, Y.; Liu, D.; Li, J.; Wang, J. Accelerating PLQY and RISC Rates in Deep-Blue TADF Materials with the Acridin-9(10H)-one Acceptor by Tuning the Peripheral Groups on Carbazole Donors. *J. Mater. Chem. C* **2022**, *10* (43), 16524–16535. https://doi.org/10.1039/D2TC03136C.

39. Brouwer, A. M. Standards for Photoluminescence Quantum Yield Measurements in Solution (IUPAC Technical Report). *Pure Appl. Chem.* **2011**, *83* (12), 2213–2228.

https://doi.org/10.1351/PAC-REP-10-09-31.

40. Calikyilmaz, E.; Karaoglu, G.; Demir, M.; Şahin, O.; Ulgut, B.; Akdag, A.; Türkmen, Y. E. Intramolecular Through-Space Charge Transfer between Benzofuran and Ynone Groups on a Naphthalene Spacer. *Chem. Commun.* **2024**, *60* (5), 550–553. https://doi.org/10.1039/D3CC05109A.

41. Heravi, M. M.; Zadsirjan, V. Recent Applications of Selected Name Reactions in the Total Synthesis of Alkaloids. In *Name Reactions Applied in Total Synthesis of Alkaloids*; Academic Press: Amsterdam, 2021; pp 107–152. https://doi.org/10.1016/B978-0-12-824021-2.00002-9.

42. Meringdal, J. W.; Menche, D. Suzuki–Miyaura (Hetero-)Aryl Cross-Coupling: Recent Findings and Recommendations. *Chem. Soc. Rev.* **2025**, *54* (12), 5746–5765. https://doi.org/10.1039/D4CS00940K.

43. Algar, W. R.; De Jong, C. A.; Maxwell, E. J.; Atkins, C. G. Demonstration of the Spectrophotometric Complementary Color Wheel Using LEDs and Indicator Dyes. *J. Chem. Educ.* **2016**, *93* (1), 162–165. https://doi.org/10.1021/acs.jchemed.5b00520.

44. Molčanov, K.; Kojić-Prodić, B. Towards Understanding π-Stacking Interactions between Non-Aromatic Rings. *IUCrJ***2019**, *6* (2), 156–166. https://doi.org/10.1107/S2052252519000809.

45. Janiak, C. A Critical Account on π–π Stacking in Metal Complexes with Aromatic Nitrogen-Containing Ligands. *J. Chem. Soc., Dalton Trans.* **2000**, (21), 3885–3896. https://doi.org/10.1039/B003010O.

46. Cheng, J.; Kang, C.; Zhu, W.; Luo, X.; Puah, C. M.; Chen, K.; Jiang, H. N-Methylformamide–Benzene Complex as a Prototypical Peptide N–H···π Hydrogen-

Bonded System: Density Functional Theory and MP2 Studies. *J. Org. Chem.* **2003**, *68* (19), 7490–7495. https://doi.org/10.1021/jo034539e.

47. Neese, F.; Wennmohs, F.; Becker, U.; Riplinger, C. The ORCA Quantum Chemistry Program Package. *J. Chem. Phys.* **2020**, *152* (22), 224108. https://doi.org/10.1063/5.0004608.

48. Becke, A. D. Density-Functional Thermochemistry. III. The Role of Exact Exchange. *J. Chem. Phys.* **1993**, *98* (7), 5648–5652. https://doi.org/10.1063/1.464913.

49. Lee, C.; Yang, W.; Parr, R. G. Development of the Colle–Salvetti Correlation-Energy Formula into a Functional of the Electron Density. *Phys. Rev. B* **1988**, *37* (2), 785–789. https://doi.org/10.1103/PhysRevB.37.785.

50. Weigend, F.; Ahlrichs, R. Balanced Basis Sets of Split Valence, Triple Zeta Valence and Quadruple Zeta Valence Quality for H to Rn: Design and Assessment of Accuracy. *Phys. Chem. Chem. Phys.* **2005**, *7* (18), 3297–3305. https://doi.org/10.1039/B508541A.

51. Barone, V.; Cossi, M. Quantum Calculation of Molecular Energies and Energy Gradients in Solution by a Conductor Solvent Model. *J. Phys. Chem. A* **1998**, *102* (11), 1995–2001. https://doi.org/10.1021/jp9716997.

52. Garner, A.; Wilkinson, F. Quenching of Triplet States by Molecular Oxygen and the Role of Charge-Transfer Interactions. *Chem. Phys. Lett.* **1977**, *45* (3), 432–435. https://doi.org/10.1016/0009-2614(77)85091-4.

53. Ahmadli, D.; Sahin, Y.; Calikyilmaz, E.; Şahin, O.; Türkmen, Y. E. Rapid Access to Hydroxyfluoranthenes via a Domino Suzuki–Miyaura/Intramolecular Diels–Alder/Ring-Opening Reactions Sequence. *J. Org. Chem.* **2022**, *87* (9), 6336–6346. https://doi.org/10.1021/acs.joc.2c00134.

54. Zhang, Y.; Lai, W.; Zhang, L.; Gao, X.; Qiu, G.; Zhou, H. The Copper-Catalyzed Synthesis of (Z)-2H-Naphtho[1,8-bc]thiophenes with Solid Emission. *Org. Biomol. Chem.* **2021**, *19* (8), 1827–1834. https://doi.org/10.1039/D0OB02379F.